Observation-Based Estimates of Present-Day and Future Climate Change Impacts on Heavy Rainfall in Harris County

John W. Nielsen-Gammon
Regents Professor, Dept. of Atmospheric Sciences, Texas A&M University
Texas State Climatologist

May 17, 2020
Final Report

Update June 23, 2020

OSC Report 2020-02

Contents

Executive Summary

This report describes the results of an extreme value analysis of precipitation in and around Harris County, Texas, in order to determine whether the newly-promulgated NOAA Atlas 14 rainfall design values are valid in a changing climate. The analysis in this report is based on the original NOAA Atlas 14 data set as well as a set of composite stations for the Gulf and Southeast Coasts. As of this writing, this report and its findings have not yet been peer-reviewed.

- The recent upward trend in extreme precipitation in the Houston area has contributed to extreme rainfall design values in the area that far exceed those of comparable locations. This is in part due to some stations not having a sufficiently lengthy set of observations and in part due to southeast Texas receiving more than its fair share of storms. *We assess that the design values of 100-year rainfall amounts would be 7% smaller if a longer period of record was available at all observation locations.*
- Coastal southeast Texas has the largest single-day and multi-day return values anywhere along the Gulf and Atlantic coasts for return periods of 100 years or more. This is in part due to some recent storms that could have occurred anywhere along the Gulf coast concentrating their activity around Houston. There is no known factor that would make storms such as Harvey more likely to happen in Texas than elsewhere along the northern Gulf Coast. *We assess that extreme rainfall risk in Southeast Texas should consider storms from a broader portion of the Gulf Coast, decreasing return values by an additional 1%-18%, with the larger values applying to the larger return periods.*
- A robust upward trend in extreme precipitation is present across the southern and southeastern United States. The trend is larger in southeast Texas, but we have no reason to expect that climate change would cause trend variations on such a small scale. *Using averaged trends across areas near the Gulf Coast, we assess the best estimate of the climate-driven trend in southeast Texas to be 11%-15% over the past 60 years, with the remainder of the observed trend caused by regionally unusual storms (like Harvey) that are not likely to recur in the same places.*
- The three factors listed above effectively cancel each other out for 2-year return values. *We assess that the present-day nonstationary return values are approximately equal to the stationary estimates of NOAA Atlas 14 for 2-year return periods.*
- Because of the three factors listed above, the NOAA Atlas 14 100-year and 500-year return values generally overestimate the present-day and near-term future extreme rainfall risk in and around the Houston area. *We assess that for 100-year return periods, current nonstationary values are still about 10-12% below the NOAA Atlas 14 values*.
- The historic upward trend is very likely to continue with global warming. *Because of this, we assess that NOAA Atlas 14 return values underestimate the intensity of all future 2-year rainfall events in the Harris County area. We also assess that, depending on the rate of future warming, the nonstationary 100-year return values will exceed the NOAA Atlas 14 values around the middle of the 21st century.*

1. Introduction and Scope

The purpose of this report is to provide a statistical analysis of historic records of extreme rainfall amounts and trends in Harris County in the context of observations in neighboring areas and more general past analyses of extreme rainfall trends, with the goal of estimating the appropriate baseline and trend for current and future extreme rainfall amounts. This report was sponsored by the Harris County Flood Control District (HCFCD); the opinions contained in this report are those of the author.

The issue of probabilities of current and future extreme rainfall has grown in importance due to a succession of recent extreme rainfall events in and around Harris County, including the Memorial Day Flood (2015), the Tax Day Flood (2016), Hurricane Harvey (2017), and Tropical Storm Imelda (2019). In 2018, the National Oceanic and Atmospheric Administration (NOAA), released Volume 11 of NOAA Atlas 14 (Perica et al. 2018, henceforth "NOAA Atlas 14"), which contains the latest official estimates of extreme rainfall amounts for design purposes. Some of the largest 100-year rainfall amounts in the state of Texas are found in Harris County in the newest analysis, and the 1-day 100-year value is about 4" larger than the previous estimate in Technical Paper No. 40 (Hershfeld 1961). This begs the question of whether the higher estimated values of extreme rainfall represent a long-term trend that should be expected to continue.

Several analyses and projections of extreme precipitation in the United States indicate that an upward trend should be expected due to climate change and that such a trend is already underway. Assuming these analyses and projections are correct, it is unclear whether increased extreme rainfall frequency or intensity should be expected beyond what has occurred in Harris County recently or, on the other hand, whether recent extreme rainfall events represent a statistical fluke that won't become a realistic expectation for many years.

To address these issues, this report analyzes extreme rainfall using the same quality-controlled extreme rainfall dataset used by NOAA Atlas 14, with additional analyses of observations from the entire Gulf Coast and adjacent southeast Atlantic Coast. The report evaluates evidence for the existence of a long-term trend in extreme rainfall frequency and intensity. The report considers to what extent the large Atlas 14 estimates, calculated under the assumption of a stationary climate with unchanging extreme rainfall risk, are caused by or affected by an underlying long-term trend. The report also considers evidence on whether such an underlying trend in extreme rainfall in Harris County is caused or affected by urbanization, coastal proximity, and climate change, or is merely a statistical artifact of random weather events. Lastly, considering all these potential influences, the report estimates the actual present-day and future risk of extreme rainfall.

It is hoped that this report will inform flood protection and infrastructure management decisions and provide Harris County with an improved understanding of extreme rainfall risk. However, this report is not intended to be a substitute for NOAA Atlas 14 for assessment of current and future floodplain extent for regulatory or insurance purposes. The author of this

report was an external reviewer of NOAA Atlas 14 Volume 11 and is satisfied that the underlying methods were sound, were applied appropriately, and reviewer comments were appropriately considered in the finalization of Volume 11. While we believe this new report to be accurate, it relies on scientific research methods rather than firmly established engineering procedures and has not undergone peer review. A version of this report is planned to be submitted to a scientific journal for peer review.

Note on June 23, 2020 update: The June 23 update corrects the assignment of certain counties to the MS4 and GA2 regions (Appendix B), with minor changes to the figures in Fig. 5. The values of some numbers in Table 8.6 change by 0.1%, but other tables are unaffected. Figures 8.1 and 8.2 are also changed by this correction; in addition for Figs. 8.1 and 8.2 the assignment of pooled regions to coastal and inland categories has been slightly amended. Graphics depicting the identification of coastal and inland categories have been added to Figure 5.11. Finally, an incorrect figure in the original report (Fig. 5.10) was replaced with the correct figure; the original discussion applies to the correct figure.

2. Data

This report includes analyses of two data sets, and each data set is processed in two different ways prior to analysis. This results in four distinct sets of observations, referred to in this report as "raw", "ext", "ful", and "qcd".

2.1 Raw and ext data for Texas

The raw data is the same data set used by NOAA Atlas 14, downloaded from the Hydrometeorological Design Studies Center. This data set has been extensively screened and quality-controlled; for details, see Perica et al. (2018).

The raw data consists of annual block maxima of precipitation for durations ranging from 15 minutes to 60 days. This report analyzes durations of 6 hours, 1 day, and 4 days, but analyses for other durations can easily be generated using the same software.

Each block maximum is designated with a particular date of occurrence in the raw data set. It appears that the dates provided in the data set are the starting dates of the block maxima, while each observation is assigned to its block year according to the ending date of the block. For example, a four-day heavy rainfall event that begins on December 30, 1991 and ends on January 2, 1992 would appear in the data set dated as December 30, 1991 but would be the block maximum for the year 1992 instead of 1991. This report follows the same convention, assigning block maxima to the year of the end of the event.

The NOAA Atlas 14 data set runs through 2017, except that some 2018 data from South Texas were included in the analysis. For internal consistency, this report excludes the 2018 data.

The creation of the ext (short for "extended") data was motivated by the fact that many of the stations in Harris County used for NOAA Atlas 14 were HCFCD or airport stations with a relatively short period of record. In order to improve the robustness of estimates of extreme rainfall trends, all missing block maxima were replaced by block maxima from nearby stations. The resulting data set covers the period 1895-2017 for durations of one day or longer and 1941-2017 for durations of less than one day; the choice of starting year was guided by the availability of widespread data.

Because of spatial variations in expected extreme rainfall magnitudes, rainfall data is not directly interchangeable across stations. A station that normally receives more rainfall will typically have larger block maxima, and the use of block maxima from one station to fill the early part of the data record of another station can artificially influence the apparent extreme rainfall trend. To avoid this problem, the replacements were made in such a way that the stations used to fill missing data are centered around the location of the station with missing data. For details and examples, see Appendix A.

The NOAA Atlas 14 data set only includes stations within Texas. The actual Volume 11 analysis made use of data from stations beyond the Texas border, but such data was not included in the published data archive and data from other volumes does not extend as far as 2017.

2.2 Ful and qcd data for the Gulf and Southeast coastal regions

In order to place the southeast Texas extreme precipitation into the context of larger scale weather and climate patterns, a second data set is created for the entire Gulf Coast and southeast Atlantic Coast. For this regional-scale data set, data was selected to maximize the length of the period of record while maintaining a roughly even spatial distribution of stations.

To accomplish these goals, composite stations were created for each county as follows: For each year, stations in a given county with no more than 31 missing days were identified. If only one station met that criterion, data from that station were used to determine that year's block maximum. If more than one station met that criterion, data from the station with the longest period of record were used to determine that year's block maximum. If no station met that criterion, no block maximum was calculated for that county for that year.

This method of creating composite stations assumes that all stations in a given county are in a sufficiently similar meteorological setting that they are approximately interchangeable. Because the purpose of this data set is to analyze regional-scale patterns and trends, exact interchangeability is not necessary as long as any inherent differences are random from county to county.

The data for this analysis was obtained from the Applied Climate Information System (ACIS), a data set maintained by NOAA's Regional Climate Centers and synchronized with the National Centers for Environmental Information database. The data presented in this report was downloaded on February 10, 2020. Most, but not all, of this data has undergone automated quality control by the National Centers for Environmental Information (Menne et al., 2012). The automated quality control is designed to be lenient, so that data is erroneously flagged as incorrect only 1-2% of the time.

The ful data set was generated from the full ACIS data using the methods described above. The qcd data set is the result of an additional three-part screening process applied to the ful data set to eliminate erroneous extreme values.

The first part of the screening process was designed to eliminate false outlier extreme precipitation events. First, suspicious three-day block maximum data were flagged if their block maximum values exceeded the values reported in overlapping periods by any neighboring stations by a factor of two or more or if the values were low outliers compared to the population of block maximum values. Next, each flagged case was investigated to determine whether the data should be considered to be accurate. This step involved examination of original observer forms, radar observations, data from neighboring stations, and other weather information. A quality control flag was assigned to each case on the basis of this examination:

"bad" if the data record is clearly erroneous; "suspicious" if there is evidence in addition to the buddy check that suggests that the data record is erroneous, "probably good" if there are no apparent problems with the original observer form and no other evidence that the data record is erroneous, and "good" if there is affirmative evidence that the data record is correct. Any "bad" or "suspicious" observations affecting the 01d and 04d block maxima in any month were removed from the qcd data set. Through this mechanism, a total of 16 data points were dropped.

The second part of the screening process was designed to eliminate false reports of a lack of extreme precipitation. First, a check was made for unusually low three-day block maxima outliers. Then, the observations from any such stations were compared to those from neighboring stations. Through this process, one station in Alabama was identified that was falsely underreporting precipitation for several years. Through this mechanism, a total of 5 data points were dropped.

The third part of the screening process was designed to eliminate snowfall reports being incorrectly recorded as water equivalent precipitation. Since a ten-inch snow accumulation typically contains about one inch of water when melted, four inches of snow (say) reported as four inches of precipitation would overestimate the actual precipitation amount by roughly a factor of ten. Snow accumulation is reported to the nearest inch or tenth of inch while water equivalent is typically reported to the nearest hundredth of an inch, so snow reports are suggested when the precipitation report has no tenths or hundredths digit. To check for this, all instances of no tenths or hundredths digit were counted and compared for extreme events occurring in winter versus the other three seasons. Three states (North Carolina, South Carolina, and Louisiana) had anomalously high wintertime counts of round precipitation totals. Each of those reports were then checked against the reported temperatures. If temperatures remained well above freezing, the precipitation must have fallen as rain. If not, the reports were checked against the original observer forms and against neighboring reports. As a result of this check, three precipitation reports were judged to be faulty and were dropped from the data set, and an additional report was found to be faulty for separate reasons and was also dropped. Another case in Texas of snow reported as water equivalent was flagged and dropped during the first part of the screening process.

2.3 Durations

This report presents results for durations of six hours (06h), one day or 24 hours (01d), and four days (04d). The 06h block maxima are not available for ful and qcd data because the underlying data set is daily.

3. Methods

3.1 Outline of NOAA Atlas 14 procedure

The NOAA Atlas 14 Volume 11 procedure for estimating return values is stated as follows (Perica et al. 2018; numbers in parentheses refer to sections in the report):

Data processing
1. Data collection (4.2)
2. Block maxima extraction (4.3)
3. Station screening (4.4)
4. Outlier screening (4.5.1)
5. Addition of extreme events (4.5.2)
6. Identification of unconstrained extreme events (4.5.3)
7. Application of correction factor for constrained observations (4.5.3)
8. Duration consistency check (4.5.4)

Statistical analysis
9. Calculate L-moment statistics at each station (4.6.2)
10. Calculate GEV distributions using local L-location and L-scale and regional averages of higher-order L-moment ratios (4.6.2, 4.6.3)
11. Smooth GEV probabilities across durations (4.6.3)
12. Convert to partial duration series probabilities (4.6.4)
13. Estimate confidence intervals (4.6.5)

Spatial analysis
14. Create detailed maps of mean annual maximum precipitation (4.8.1)
15. Create maps of longer return period precipitation and confidence intervals by applying spatial analysis of precipitation ratios with additional dynamic smoothing (4.8.2)

3.2 Data processing for this report

Except for step 7, all data processing steps are incorporated into the posted Atlas 14 data set and thus into raw and ext. We apply step 7 to all four data sets used here prior to calculating return frequencies and values by multiplying the data values by the same correction factors as were used in NOAA Atlas 14. For the durations relevant to this report (6h, 1d, and 4d), the correction factors are 1.01, 1.11, and 1.02, respectively.

The purpose of the step 7 correction is to statistically account for the fact that, for example, maximum 24-hour rainfall events will not necessarily begin and end at the exact daily observation times and will instead often be spread out across two daily rainfall totals. Thus daily observations tend to underestimate the peak 24-hour rainfall totals. Similar considerations apply when sub-daily precipitation is evaluated using stations that record rainfall totals every hour.

The unconstrained estimates in step 6 had been converted to the equivalent constrained estimates within the archived data set by dividing by the appropriate correction factor. Applying the step 7 correction factor to the entire data set restores those estimates to their original unconstrained values.

For ful and qcd, station screening involved elimination of all composite stations with fewer than 30 years of block maxima. Outlier and error screening was as described in section 2.2. The data was not enhanced with additional unconstrained extreme events; this includes not adding the additional unconstrained extreme events from raw into ful and qcd. The same step 7 correction factors were applied to ful and qcd. No duration consistency check was necessary, since the 04d totals were calculated directly from 01d values.

3.3 Statistical and spatial analysis for this report

For emulation of NOAA Atlas 14, Step 9 (calculation of L-moments) is performed for this report using the lmoments3 software package (Hollebrandse et al. 2015). Step 13 follows the same procedure as NOAA Atlas 14, using 1000 bootstrap samples. Most new calculations in this report use the climextRemes software package, in the form of a Python wrapper to R routines (Paciorek et al., 2018). The climextRemes package has been used by Risser and Wehner (2017) to analyze climate change impacts on Hurricane Harvey's rainfall. Analysis software is written in Python within Jupyter notebooks. A three-parameter Generalized Extreme Value (GEV) distribution is assumed to provide an appropriate characterization of the probability distribution under conditions of stationarity and nonstationarity throughout the analysis domain; after testing of several candidate distributions, NOAA Atlas 14 chose to use a GEV distribution throughout Texas.

Steps 10, 11, 14, and 15 of the statistical and spatial analysis used in NOAA Atlas 14 are not described in sufficient detail to be exactly reproduced, and this report does not attempt to do so. These four steps collectively have the effect of producing appropriately spatially smooth estimates of return values across Texas. We present results in two ways: first, as individual station-based estimates, and second, as estimates derived from aggregated data. The individual estimates will inherently be noisier than the NOAA Atlas 14 values, but it is instructive to see the underlying single-station values so that the effect of smoothing on the resulting maps can be discerned. For the purposes of NOAA Atlas 14, smoothing is appropriate, and the smoothing applied to NOAA Atlas 14 improved the robustness of the results.

This report uses two forms of aggregation: pooling and averaging. For pooling, the individual observations from various stations in a region are treated as a single set of observations to be fitted by a single GEV distribution. We apply this form of aggregation to the ful and qcd data, aggregating the individual county composite observations into regions of approximately ten counties each. Harris County is part of a nine-county region that also includes Orange, Jefferson, Hardin, Liberty, Chambers, Galveston, Fort Bend, and Brazoria Counties. Regions are defined a priori to encompass common extreme rainfall environments, for example by

separating more coastal stations from more inland stations. Testing and implementing other forms of pooling (Requena et al., 2019) was beyond the scope of this study. A complete list of the counties comprising each region is given in the Appendix.

Averaging is performed on the return values produced by the GEV analysis for individual stations. Averaging is applied to stations in and around Harris County to represent the three hydrologic regions defined by Yung (2019). Stations were assigned to each region based on location. Stations along the border between regions were assigned to the region with fewer stations to provide similar numbers of stations for each region. Selected stations outside Regions 1 and 3 but with similar 1-day 100-yr precipitation amounts were added to Regions 1 and 3 to improve robustness. However, stations 41-5196 and 60-0011 turn out to be extreme event outliers compared to other stations in southeast Texas, so they were dropped from Region 3 so that the stations used for Region 3 were more representative of the area. A map of the stations ultimately used for each region is shown in Figure 3.1.

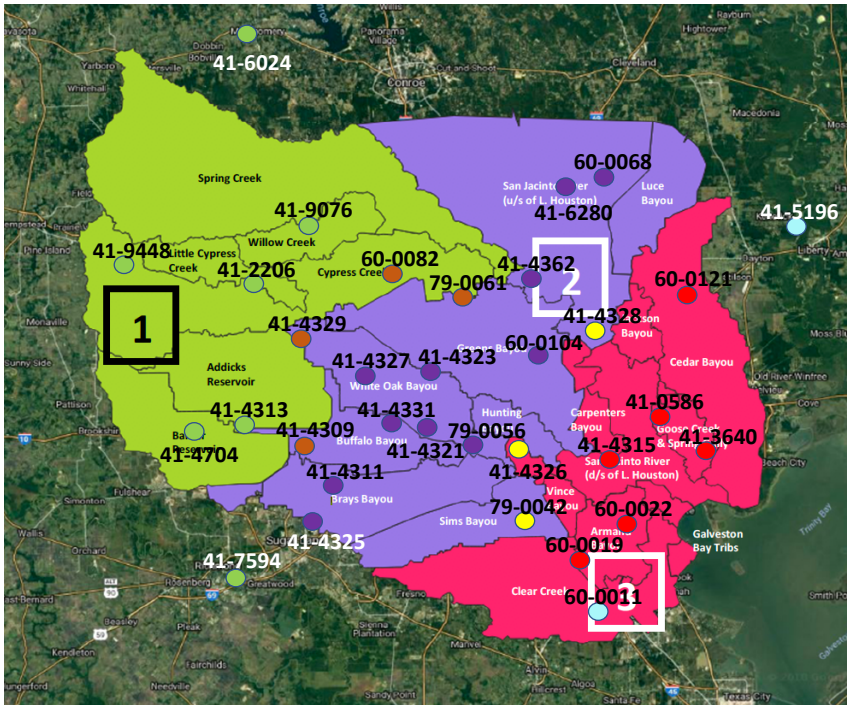

Figure 3.1: Stations used in NOAA Atlas 14 and assigned to the three hydrologic regions of the Harris County area. Green: Region 1. Brown: Border stations assigned to Region 1. Purple: Region 2. Yellow: Border stations assigned to Region 3. Red: Region 3. Light blue: Outlier stations dropped from Region 3. Map background: Yung (2019).

The conversion to partial duration series probabilities (step 12) is performed here using the same method as NOAA Atlas 14. For engineering applications, one desires to know the amount of precipitation that has a certain probability of being exceeded in any given year. Annual block maximum data can exceed a particular value at most once in any given year. Since instances of two or more exceedances in a given year are missed, the probability of exceeding a particular value is systematically underestimated. In practice, this is dealt with by adjusting the return

period to obtain an appropriately larger return value. To obtain a two-year return value, for example, the return value for annual exceedances is evaluated at a return period of 2.5415 years.

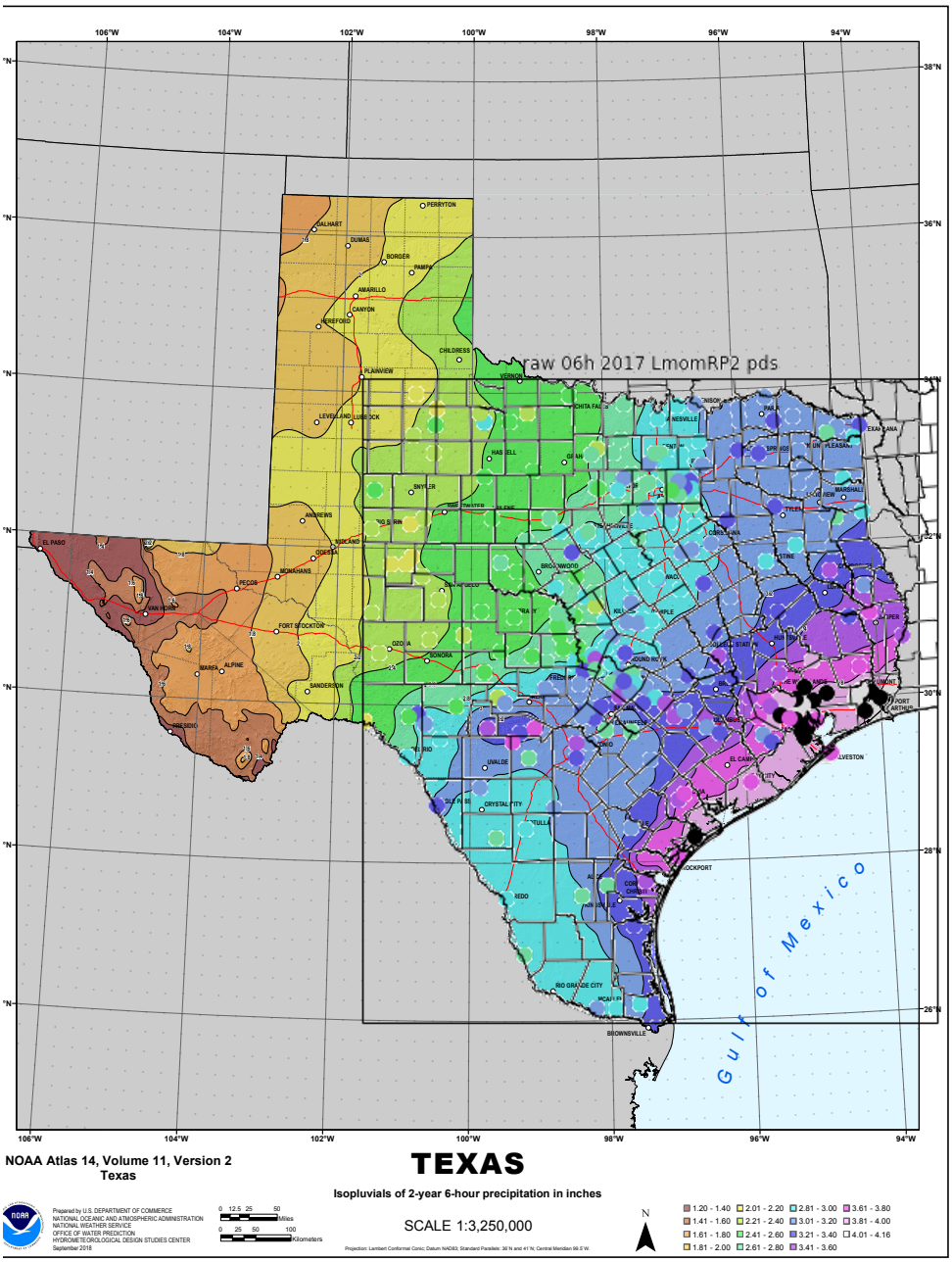

Figure 3.2: Station-by-station 2-year return values for 6-hour precipitation calculated for this report, overlaid on corresponding NOAA Atlas 14 map. Black is greater than 4.2".

To check whether the procedures have been properly implemented and to illustrate the variability of extreme precipitation thresholds across stations, we overlay our calculated return values onto NOAA Atlas 14 maps. In these figures, each station is represented by a colored dot, with colors assigned according to return values using the same color table as the underlying NOAA Atlas 14 maps. Black dots represent values beyond the maps' color scales.

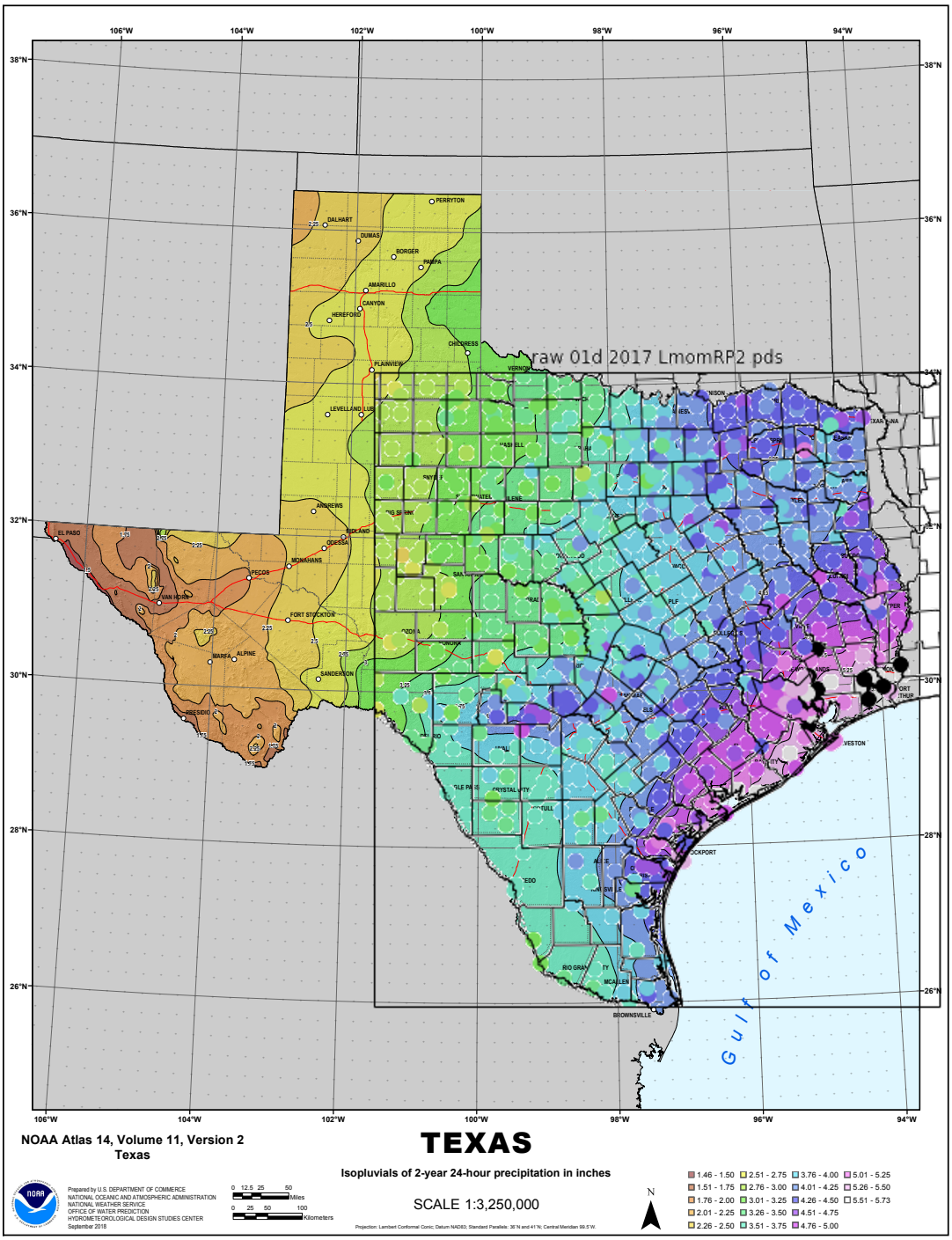

Figure 3.3: Station-by-station 2-year return values for 1-day precipitation calculated for this report, overlaid on corresponding NOAA Atlas 14 map. Black is greater than 5.75".

The 2-year return values for individual stations (Figs. 3.2 and 3.3) match the NOAA Atlas 14 pattern well. There are about as many stations with higher values as lower values, consistent with the NOAA Atlas 14 map intended to be a fairer representation of the smoother underlying extreme rainfall probabilities for future events. There are a few interesting deviations. In

particular, the band of higher return values along the Balcones Escarpment from Austin to Del Rio is more prominent in the individual station values, suggesting the possibility that the local topography is locally enhancing extreme rainfall to an even greater extent than is depicted on the NOAA Atlas 14 maps.

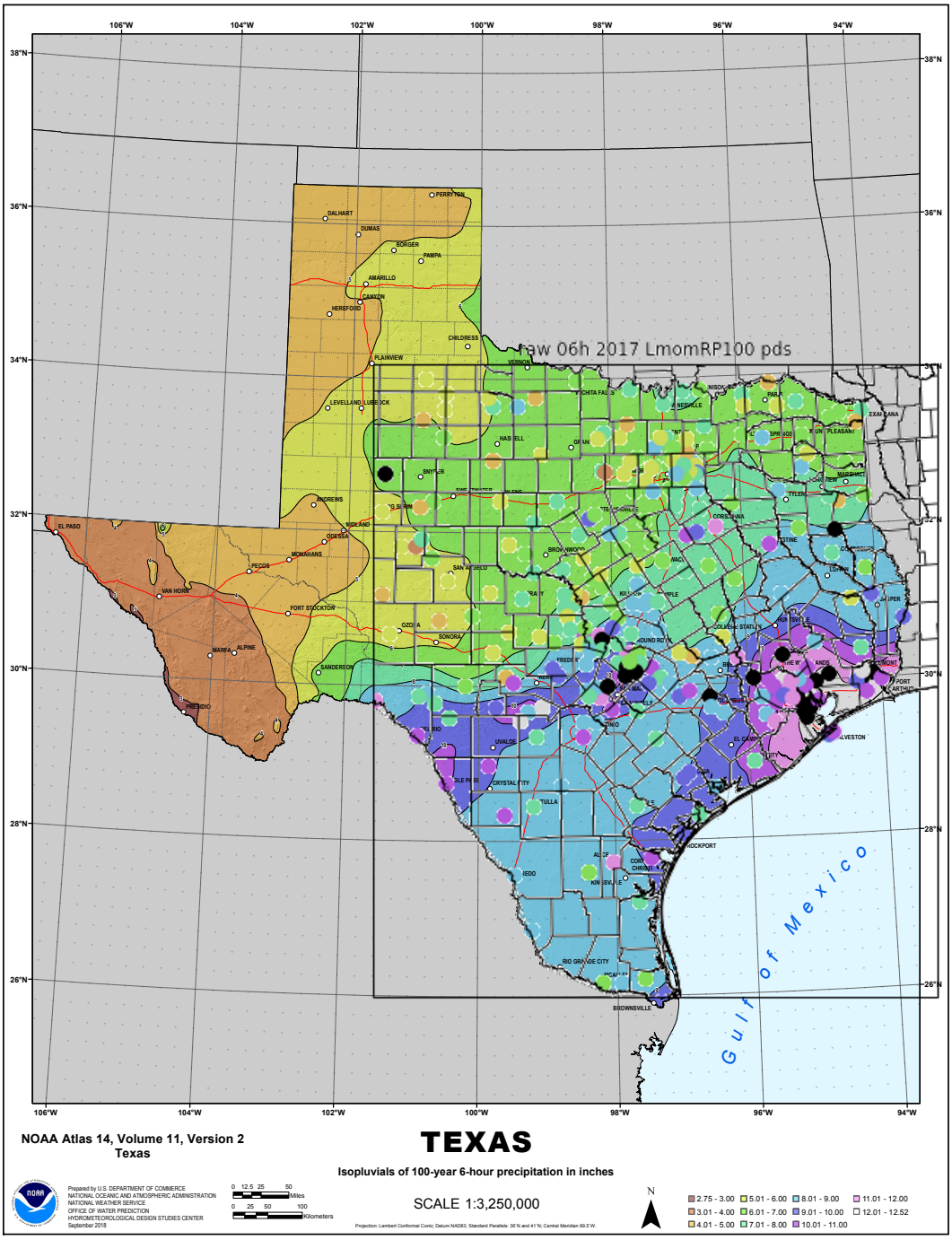

Figure 3.4: Station-by-station 100-year return values for 6-hour precipitation calculated for this report, overlaid on corresponding NOAA Atlas 14 map. Black is greater than 13.0".

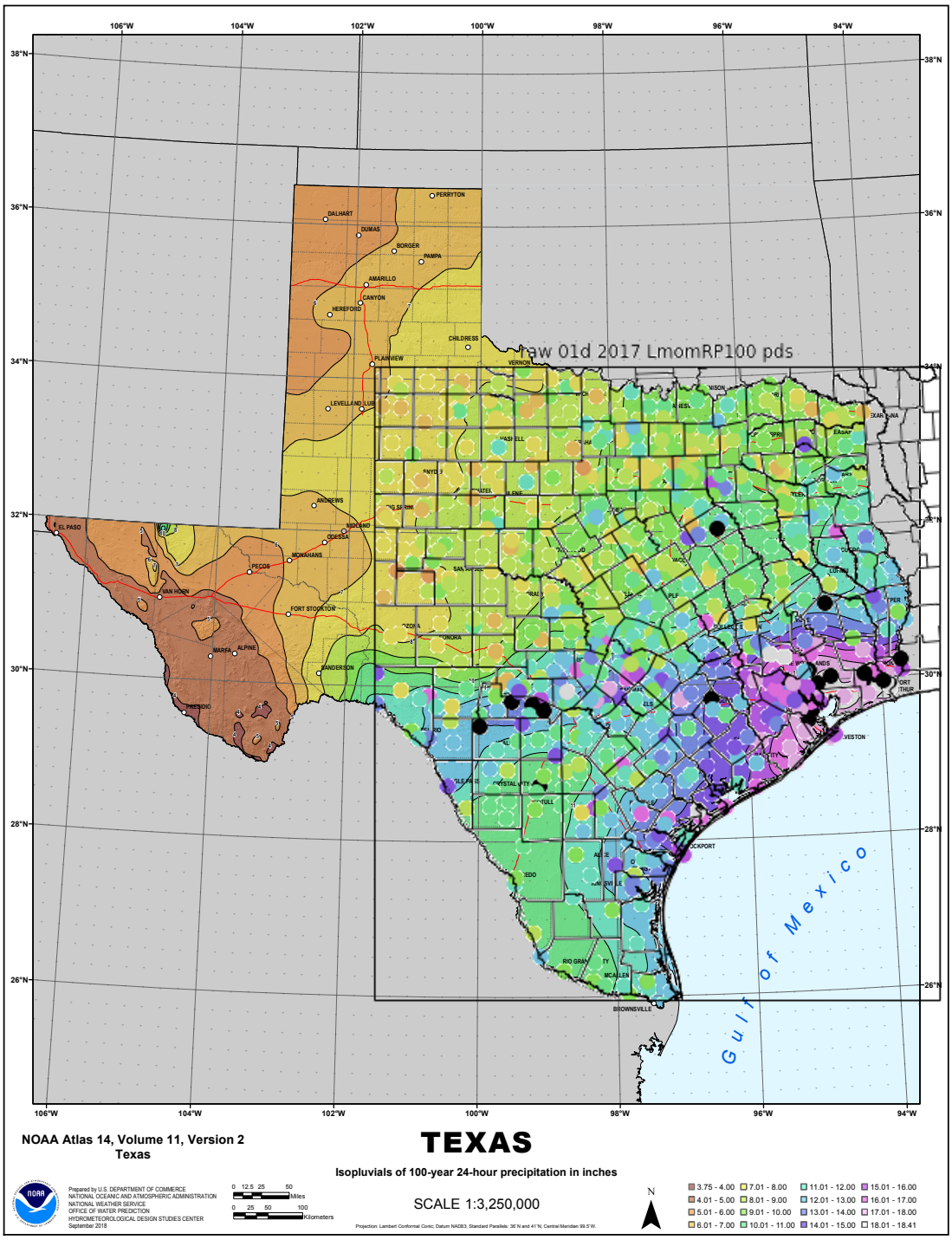

Figure 3.5: Station-by-station 100-year return values for 1-day precipitation calculated for this report, overlaid on corresponding NOAA Atlas 14 map. Black is greater than 19.0".

As would be expected, the 100-year station-based return values are even noisier than the 2-year station-based return values. Nevertheless, the overall pattern of station values is consistent with the smoother NOAA Atlas 14 pattern, indicating that the individual station data processing steps have been properly reproduced here.

3.4 L-moments and Maximum Likelihood Estimation

There are various techniques available for estimating the parameters of probability distributions from data. NOAA Atlas 14 uses the L-moment method (Hosking and Wallis, 1997), which has become quite popular for spatial analysis of rainfall extremes. However, there are no established methods for calculating nonstationary or time-dependent statistics using L-moments. Except for the emulation of NOAA Atlas 14 presented above, we use maximum likelihood estimation (MLE) as implemented by the climextRemes software package.

Various studies have assessed the reliability of MLE for stationary and nonstationary hydrologic time series. For stationary time series, the L-moment method tends to be more robust for sample sizes less than about 100, primarily because it is less influenced by outliers (Martins and Stedinger, 2000). For nonstationary time series, a semi-Bayesian method has been developed for MLE that constrains the GEV shape parameter to physically plausible values and avoids the outlier problem (El Adlouni et al., 2007). As with stationary series, the performance of ordinary MLE suffers at smaller sample sizes.

In this study, we use ordinary MLE but take precautions to avoid instability associated with small sample sizes. We make use of the ext data rather than the raw data whenever possible, which extends the data record for local stations to provide 123 data points for 1-day and 4-day rainfall and 77 data points for 6-hourly rainfall (section 2.1). For the ful and qcd data, we rely on combined pooled regional data sets, which typically contain several hundred data points but with some dependence among the pooled data.

We now compare return value estimates based on L-moments and MLE to determine whether MLE introduces a bias in return value estimates when considered against NOAA Atlas 14. The percentage differences in 2-year and 100-year return values for 1-day rainfall are shown in Figs. 3.6 and 3.7, respectively.

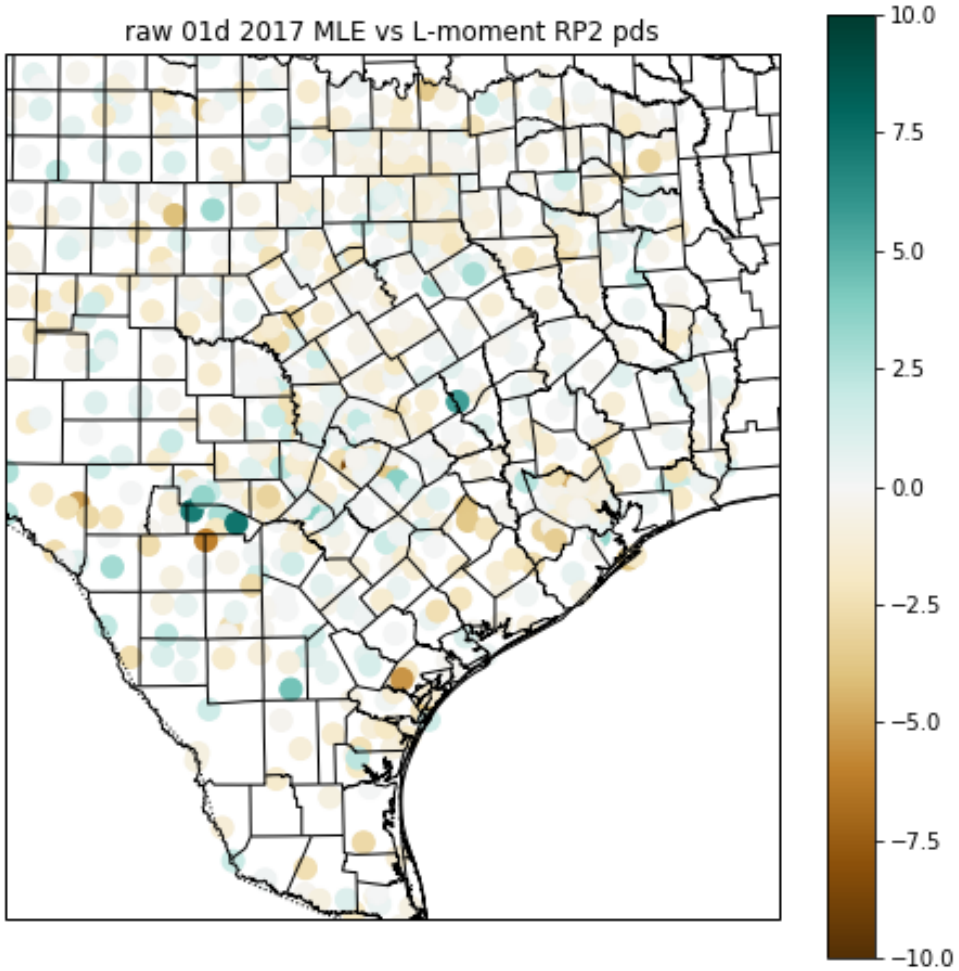

Figure 3.6: Percentage difference between MLE and L-moment estimates of 2-year return value for 1-day precipitation. Positive percentages indicate that the MLE estimate is higher.

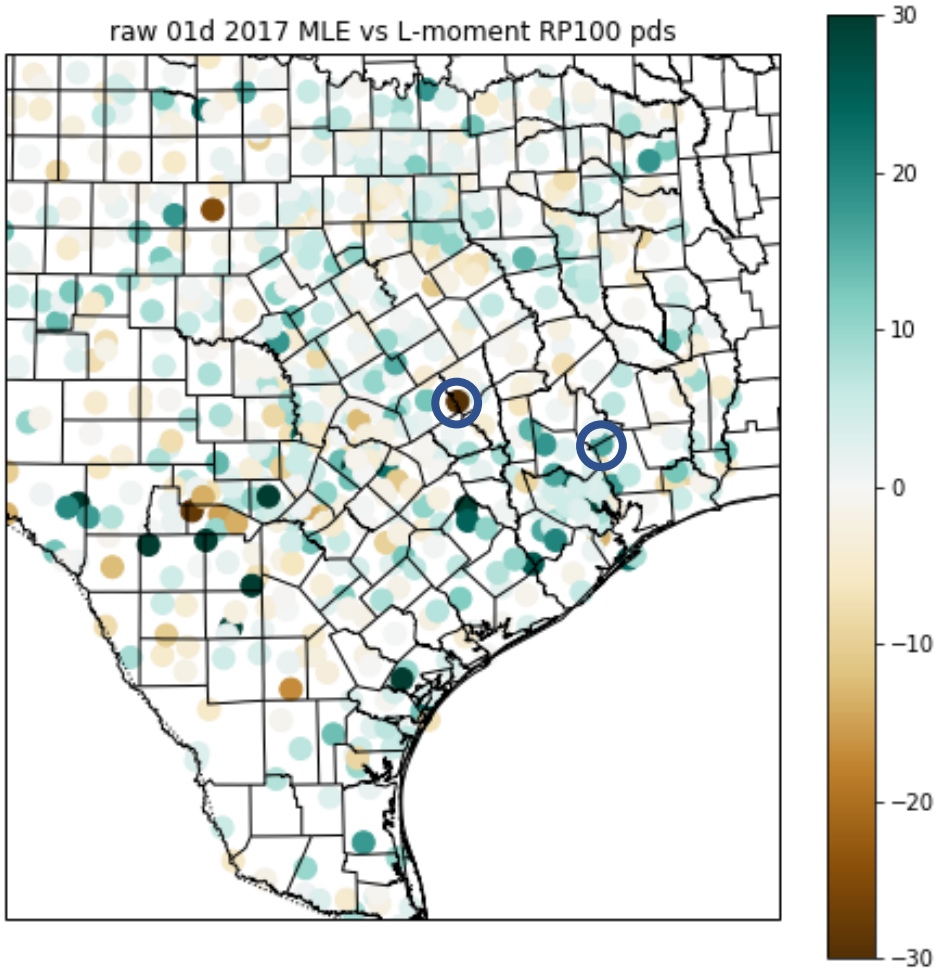

Figure 3.7: Percentage difference between MLE and L-moment estimates of 100-year return value for 1-day precipitation. Positive percentages indicate that the MLE estimate is higher. The circled stations are Valley Junction (41-9280, brown) and Cleveland (41-1810, green).

There is a slight tendency for the 2-year return values to be smaller with MLE, and conversely the 100-year return values tend to be larger with MLE. This is true for Harris County (2-year values about 1% smaller, 100-year values about 3% larger) as well as the entire plotted domain. More specifically, almost all stations have a 2-year return value difference that is the opposite sign of the 100-year return value difference, indicating a difference in the shape of the GEV fits to the observed distributions.

In order to investigate how the different GEV fits are produced by different patterns of data, we focus on two stations in southeast Texas with large but opposing differences between the L-moment and MLE estimates: Valley Junction and Cleveland (see Fig. 3.7 for locations). For both stations, we plot the observed cumulative distribution of 1-day block maximum precipitation values, the L-moment and MLE GEV fits to the observed cumulative distribution, and the 90% bootstrapped confidence intervals for the GEV fits. Figure 3.8 shows most of the cumulative distribution, while Figure 3.9 focus on the extreme upper tail. The distributions are shown and calculated without adjustment for constrained observations or partial duration series (see Sections 3.2 and 3.3).

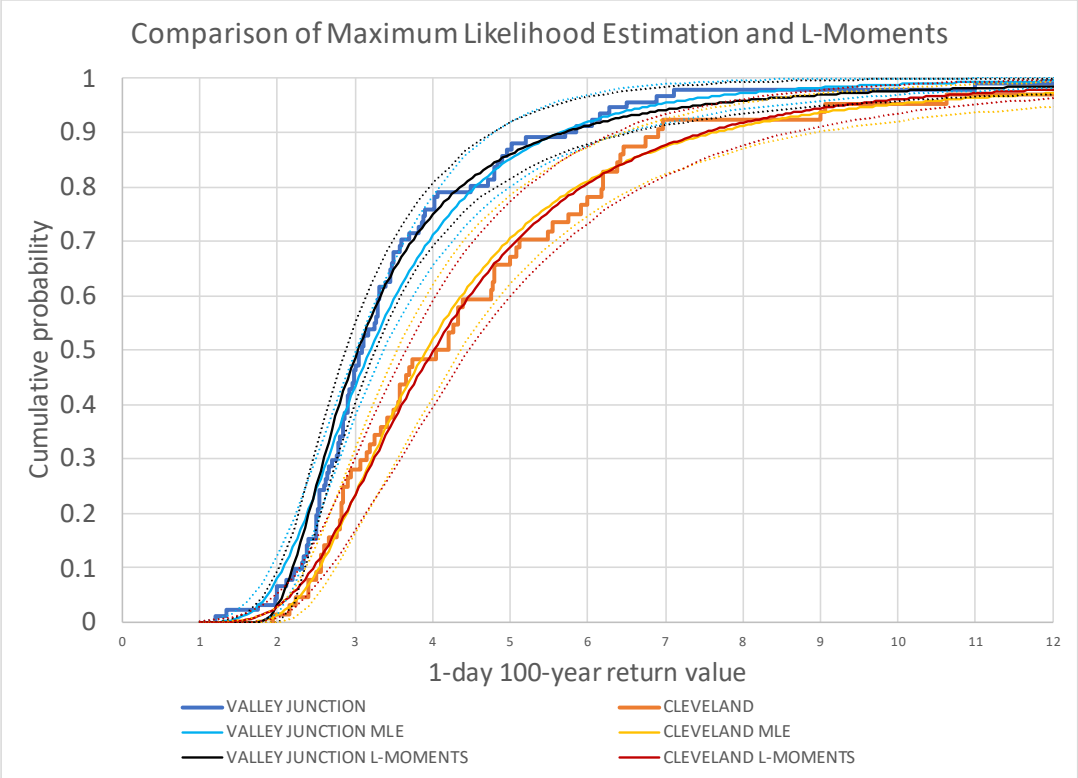

Figure 3.8: Plot of observed cumulative distribution of annual maximum 1-day precipitation amounts, along with L-moment and MLE GEV fits (solid) and 90% bootstrapped confidence intervals for the fits (dotted).

Return values may be read directly from such figures. For example, a cumulative probability of 0.5 corresponds to a 2-year return value for annual exceedances. The Valley Junction observed data hits the 0.5 cumulative probability line at about 3", meaning that the 2-year return value is 3". The L-moment method produces a GEV fit with a 2-year return value of 3" as well, while the MLE method yields a 2-year return value of about 3.2". In this instance, the MLE fit has systematically higher values than the L-moment fit near the middle of the distribution, and the

L-moment fit tends to more closely match the data. At Cleveland, the MLE fit has systematically lower values near the middle of the distribution, and the L-moment fit appears to more closely match the data as well. At both stations, the sign of the difference changes near probabilities of 0.2 and 0.85, so that the tails have an oppositely signed difference than the middle of the distributions.

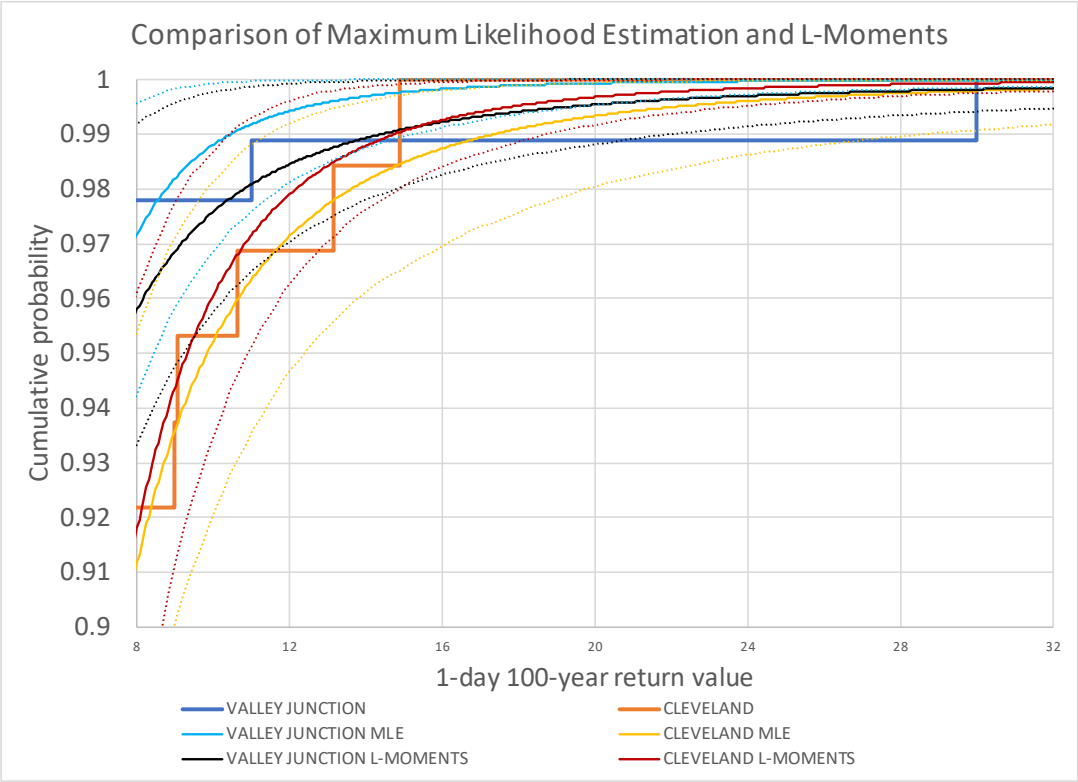

Figure 3.9: Plot of observed cumulative distribution of annual maximum 1-day precipitation amounts, along with L-moment and MLE GEV fits (solid) and 90% bootstrapped confidence intervals for the fits (dotted). Only return values above 8" are shown.

At the upper end of the distribution, the two sets of observations have strikingly different observed distributions. Valley Junction has only two observed annual maximum daily rainfall totals over 8" after the adjustments described in sections 3.2 and 3.3 are applied: a remarkable 30.0" on June 30, 1899 during the Hearne (Brazos River) flood, and 11.0" on May 13, 2004. Cleveland, by contrast, has five observed annual maximum daily rainfall totals over 8": 10.63" on July 30, 1954, 9.06" on May 19, 1989, 13.17" on October 17, 1994, 9.00" on November 18, 2004, and 14.90" on August 28, 2017. Neither station has an extreme tail that resembles a GEV distribution, with Valley Junction having a single extreme outlier and Cleveland having several extreme events clustered around similar amounts. The differences in return values for the two fits are large, with the 100-year return value (cumulative probability 0.99) about 4" larger with

L-moments than with MLE at Valley Junction and about 2" smaller with L-moments than with MLE at Cleveland.

We cannot know whether any of these fits accurately reflects the future chances of extreme rainfall. But based on meteorological experience, a 30" one-day event seems much more likely to occur in the future near Cleveland than near Valley Junction. (Tropical Storm Imelda came close to achieving this in 2019.) In that context, it is remarkable that the L-moment fits for the two stations cross, so that according to the L-moment fits the chance of a one-day rainfall exceeding 15" in a given year are larger at Valley Junction than at Cleveland. On the other hand, according to the MLE fits, the chance of a one-day rainfall exceeding 15" in a given year are several times as large at Cleveland than at Valley Junction. At the extreme tail, for these two stations, the MLE fits appear to better reflect the difference in underlying probabilities of extreme rainfall.

To investigate to what extent the difference in fits is driven solely by the extreme outlier 30" rainfall event at Valley Junction, we repeat the above analysis with the 30" event removed from the Valley Junction record and added to the Cleveland record.

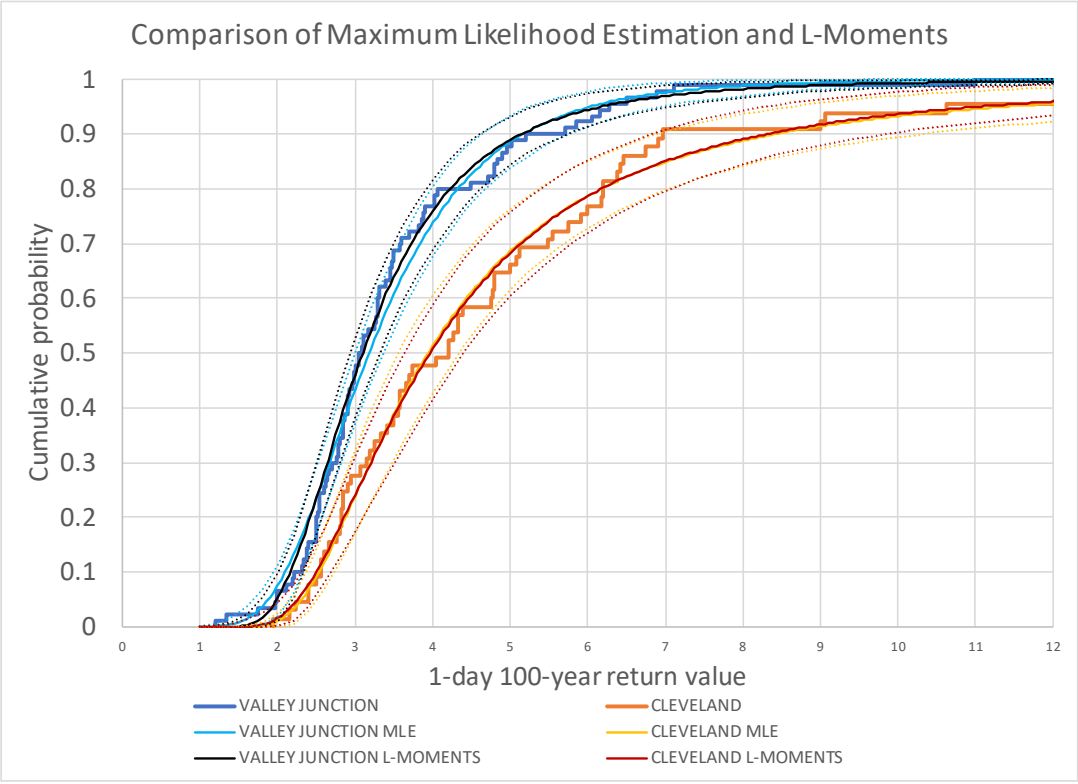

Figure 3.10: As in Fig. 3.8, but with an extreme outlier rainfall event removed from Valley Junction and added to Cleveland. See text for details.

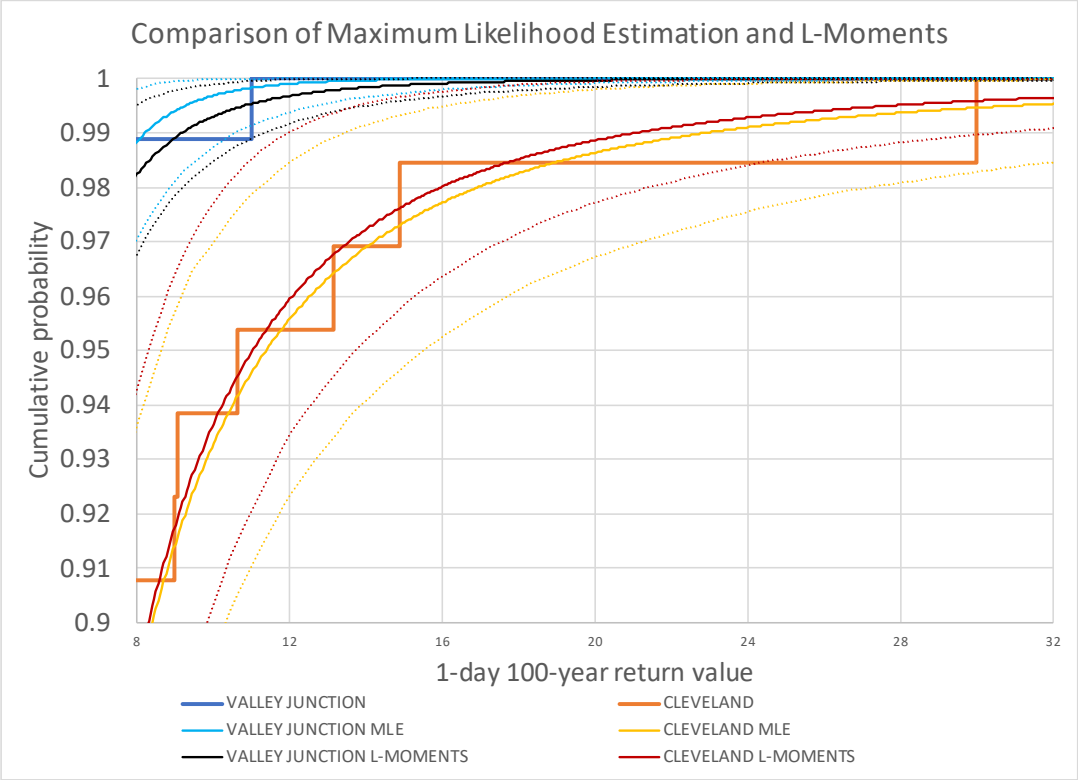

Figure 3.11: As in Fig. 3.9, but with an extreme outlier rainfall event removed from Valley Junction and added to Cleveland. See text for details.

The change in assignment of the outlier makes both observed distributions more closely resemble GEV distributions. As a result, the L-moment and MLE fits for Cleveland become almost identical, and the fit difference for Valley Junction becomes half as large. It appears that the remaining differences in the Valley Junction fits may be driven by two or three observations at the lower tail, which likewise do not conform to a GEV distribution.

As would be expected, differences arise between L-moment and GEV fits when the underlying data does not fit a GEV distribution well. In these two examples, the L-moment fit seemed better behaved near the middle of the distribution, while the MLE fit seemed better behaved near the tails of the distribution. Neither is clearly superior overall. Most importantly, the MLE approach is suitable for representing the stationary extreme value distributions observed in Texas and thus is interpreted as being suitable for investigating nonstationarity.

3.5 Nonstationary Analysis

The same climextRemes package is used for nonstationary analysis of the block maxima. In nonstationary analysis, one or more of the GEV parameters are assumed to be a linear (or log-linear in the case of scale) function of one or more covariates, and the best GEV fit is determined iteratively via the MLE method.

The choice of covariate is arbitrary but should be driven by knowledge of the underlying physical processes causing a change in probability of extreme rainfall. One possible covariate is time (year), which is how trends are usually conceptualized, but rainfall is not physically affected by the year. Instead, temporal trends emerge because other factors that affect precipitation change over a long period of time.

With climate change, two basic drivers of extreme precipitation changes have been identified. The first is known as "thermodynamic" changes: in a given storm system, all else being equal, warmer air contains more water vapor and produces heavier rain when it rises. The relationship between temperature and water vapor capacity is approximately 7% per one degree Celsius change in temperature, or 4% per one degree Fahrenheit. The second is known as "dynamic" and represents changes in storm frequency due to changes in global and regional weather patterns. Dynamic changes are much more variable globally, but research suggests that the thermodynamic factor should be dominant in the central United States (Pfahl et al. 2017).

Given this, a logical covariate would be global mean temperature, regional mean temperature, or local temperature. However, on an interannual basis, wetter conditions during the warm season are associated with cooler temperatures, so the relationship between temperature and extreme precipitation probably changes sign depending on time scale. Also, modes of natural variability such as El Niño affect Texas precipitation and temperature simultaneously. Temporally-smoothed global or regional temperature may provide a more consistent relationship with extreme precipitation; global temperature was used by van Oldenborgh et al. (2017) in their study of Hurricane Harvey and regional temperature was used by Russell et al. (2019).

Another way of avoiding this problem is to use climate forcing. Variations in forcing tend to be much smoother than variations in temperature. However, volcanic forcing can be large on an interannual basis and is expected to affect precipitation differently than other types of forcing, which appear to have more consistent effects (Mascioli et al. 2016). Using a subset of forcing, such as the natural logarithm of atmospheric carbon dioxide concentrations (lnCO2), which is roughly proportional to the radiative forcing caused by carbon dioxide (Myrhe et al. 1998) may isolate the longer-term, climate-driven relationships. This covariate was used by Risser and Wehner (2017), along with a measure of El Niño.

Once one or more covariates has been chosen, the next step is to decide which parameters describing the GEV distribution should be allowed to depend on the covariates. As a general

rule, the higher-order moments require a greater amount of data in order to be reliably estimated; reliably estimating trends in the higher-order moments requires even greater amounts of data. Allowing everything to be covariate-dependent runs the risk of overfitting. Consider, for example, a station with 30 years of annual maxima. Any model with 30 imperfectly correlated parameters will fit the data perfectly, even if the model is absurd. (One could create a model that perfectly predicts the past 30 years of global temperatures based on the sales of 30 brands of beer. Such a model would likely produce a nonsense forecast for the 31st year, maybe even worse than the forecast one would make after drinking 30 bottles of beer.)

Generally, only location and scale parameters are allowed to vary. If they vary simultaneously, the distribution of extreme rainfall can expand or contract over time. If only the location parameter varies, the shape of the PDF would remain constant, that is, its width would not change even if the magnitude of extreme rainfall changes. If 100-year rainfall increases from 15" to 18", 2-year rainfall would increase, say, from 3" to 6". This seems unrealistic. A more plausible single-parameter model assumes a linear fit to the location parameter for the logarithm of precipitation. Under such a model, if the 100-year rainfall increases from 15" to 18", the 2-year rainfall would increase from 3" to 3.6".

To choose the most parsimonious models, this report applies the Akaike Information Criterion (AIC), which penalizes models with a greater number of parameters or with a poorer agreement with the data. Five different configurations are considered: stationary, a location parameter (describing the logarithm of precipitation) dependent on year or lnCO2, or two parameters (location and the logarithm of the scale parameter) dependent on year or lnCO2. Resulting delta-AIC values (differences from the lowest AIC for a given block maximum time series) are averaged for each station within a dataset. The lowest AIC value corresponds to the most parsimonious model, with the fewest number of parameters needed to fit the observed data.

Variable	Precip	ln(Precip)	ln(Precip)	Precip	Precip
Nonstationary Parameters	0	1	1	2	2
Covariate	n/a	year	ln(CO2)	year	ln(CO2)
mean d-AIC (ful)	1.83	1.52	**1.41**	2.56	2.42
mean d-AIC (ful pooled)	16.05	8.36	6.81	5.34	**3.02**

Table 3.1: Akaike Information Criterion analysis of candidate statistical models for stationary and nonstationary GEV models. Delta-AIC values are calculated for each block maximum time series and model and averaged across all stations. The models with the lowest AIC values are chosen as the most parsimonious description of the data.

A recent nonstationary extreme rainfall analysis of recent major rainfall events including Hurricane Harvey by Vu and Mishra (2019) tested twenty candidate statistical models, also using AIC to choose models. For each station and duration, they chose the model with the

lowest AIC value. We feel that this amounts to overfitting, as there is little physical justification for expecting the long-run precipitation values to be governed by different large-scale processes in different ways from one station to another. Here we take the opposite approach and choose the same model structure for all stations of a similar type.

For the ext station data, a single nonstationary parameter (the location parameter of the logarithm of precipitation dependent on the logarithm of carbon dioxide concentrations) produces on average the lowest AIC. For the pooled ful data, the logarithm of carbon dioxide affecting both the location and scale parameters produces on average the lowest AIC. Year performs more poorly than lnCO2 as a covariate for both data sets, while the stationary model tends to perform worst of all. Based on these AIC results, our nonstationary analysis of the annual maxima of individual stations uses a GEV fit to the logarithm of precipitation with a location parameter covarying with lnCO2, while our nonstationary analysis of pooled data uses a GEV fit to precipitation with both location and scale parameters covarying with lnCO2.

Historic lnCO2 values are based on the CMIP mid-year CO2 historical concentrations through 2005, and on annual average Mauna Loa concentrations up to the present day. Trend magnitudes are quantified as the percentage difference between the return values at CO2 levels corresponding to 1960 and 2020, with the mean CO2 for 2020 estimated using recent CO2 trends. Future projections are discussed in Section 10.

Graphical examples of the nonstationary analysis are shown in Figs. 3.12-3.15 for the qcd data set. The annual maximum return values are shown rather than the partial duration series return values for ease of interpretation: roughly half of the events are expected to be above the estimated 2-year return value, and for a 100-year period of record there would most likely be zero or one event above the estimated 100-year return value.

The solid lines show the MLE return value estimates at 2 years (brown) and 100 years (blue). The 50% and 95% confidence intervals are shown with darker and lighter shading, respectively. The confidence intervals are constructed using the bootstrap method with 10,000 draws. The proper interpretation of these confidence intervals is as follows: if you randomly picked 130 annual maximum events and their associated lnCO2 values out of this set, with some events randomly included multiple times and others not at all, and calculated the MLE nonstationary fit, the resulting return values would have a 50% (95%) chance of lying within the 50% (95%) confidence interval.

Figure 3.12 shows the time series of annual maxima for the Harris County composite station, which consists of the downtown Houston station (Houston WB City; COOP number 414305) through 1989 and Hobby Airport thereafter. This composite station managed to miss the more intense parts of the most notable extreme rainfall events of the past fifty years, such as Claudette 1979, October 1994, and Allison 2001. Even Hurricane Harvey, because of the timing of the event and the use of calendar days for daily rainfall totals, ended up producing relatively low single-day totals at Hobby compared to other stations in the area: 12.07" on Aug 26, 10.99" on Aug 27, and 9.41" on Aug 28. Because of this, most other stations in the area have much

higher calculated 100-year return values (see for example Figs. 3.13-3.14), and the NOAA Atlas 14 return value estimates for Harris County are much larger than the 100-year return values calculated from this time series.

This illustrates that the confidence intervals are not statements about the likelihood that the true return value lies within the confidence interval. Here, for reasons just given, evidence from surrounding stations indicates that the true return values likely lie well above the 50% confidence intervals, and probably above the 95% confidence intervals as well.

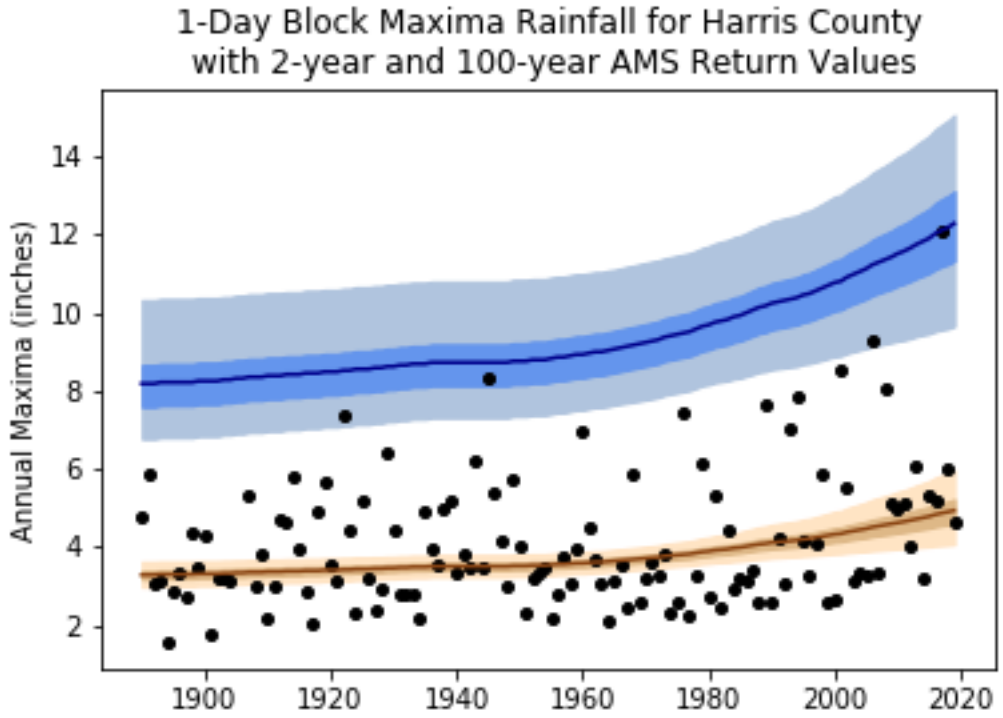

Figure 3.12: Annual maximum 1-day precipitation values for the Harris County composite station, along with nonstationary MLE fits and bootstrapped 50% and 95% confidence intervals.

The nonstationary analysis in Fig. 3.12 shows a very large trend in extreme precipitation at both the 2-year and 100-year return values. For the MLE fits, the 2-year and 100-year trends are coupled: with only one nonstationary parameter, the 2-year and 100-year trends must rise and fall by the same percentage. Because the analysis is nonstationary, the confidence intervals at the beginning and end of the period of record are wider than the confidence intervals near the middle of the period of record. This is due to uncertainty in the trend, which affects the extent to which the endpoints differ from the middle values.

Consistent with expectations, about half the points lie above the 2-year return value line. Note that the positive trend in the 2-year return values is consistent with the trend apparent visually in the run-of-the-mill annual maxima during the past 30 years. This serves to illustrate that the

trend in this area is not driven solely by one or two extreme events but is instead reflective of a trend in the overall event population.

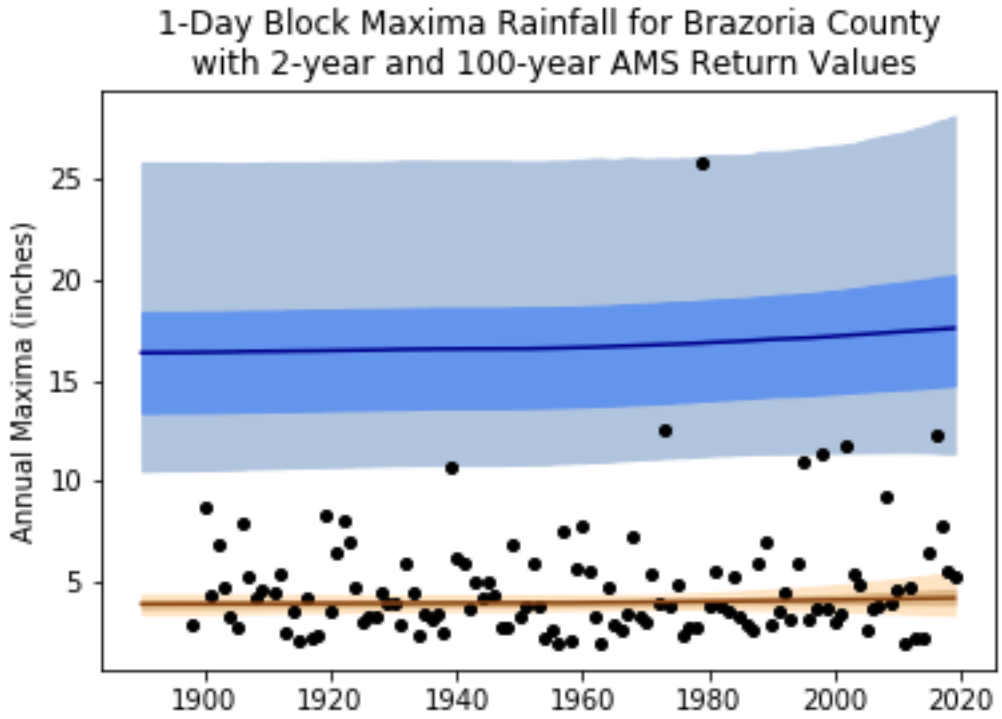

Figure 3.13: Annual maximum 1-day precipitation values for the Brazoria County composite station, along with nonstationary MLE fits and bootstrapped 50% and 95% confidence intervals.

Figure 3.13 shows the nonstationary GEV analysis for the composite Brazoria County station. Unlike the composite Harris County station, which had just one annual maximum 1-day precipitation value above 10 inches, the Brazoria County station had seven. The highlight is the 25.75 inches at Alvin from Tropical Storm Claudette in 1979. This outlier event results in wide confidence intervals for the 100-year return values, much wider than those at the Harris County composite. This reflects the fact that the bootstrap resampling will sometimes not include Claudette, sometimes it will, and sometimes it will even include two or more Claudettes. But since Claudette occurred while carbon dioxide values were relatively low, it doesn't influence the nonstationary trends, which are only weakly upward.

Figure 3.14 features the nonstationary GEV analysis for the composite Liberty County station. Liberty received one-day precipitation of 15 inches or greater three times in the past thirty years. The overall trend in the nonstationary fit is positive, and the confidence intervals for 100-year return values are narrower than for Brazoria because the historical record doesn't include an outlier.

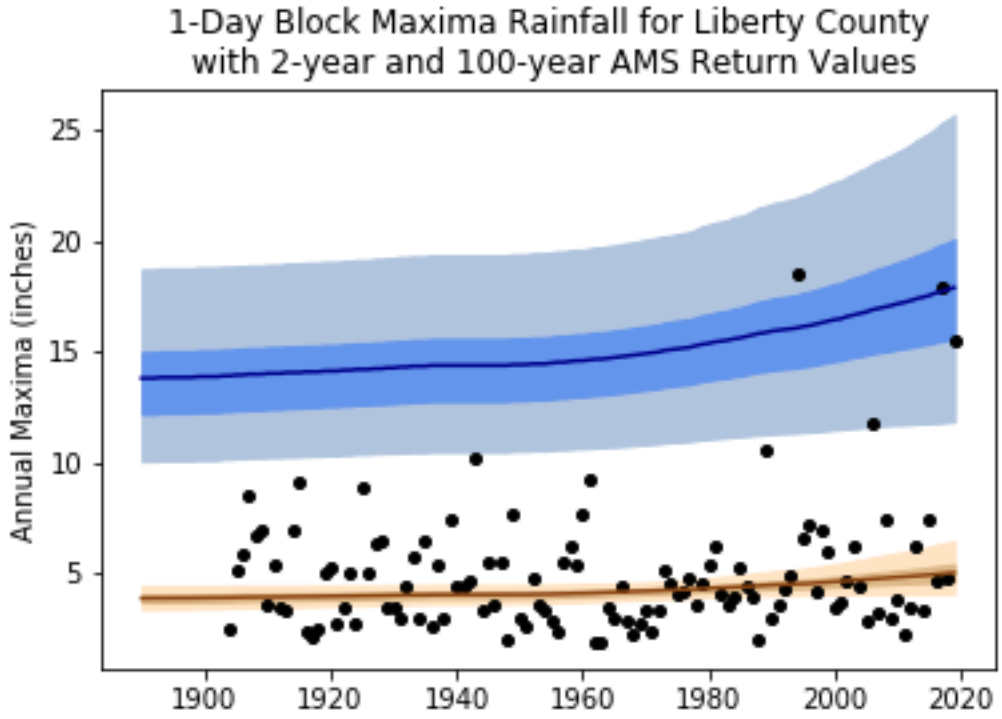

Figure 3.14: Annual maximum 1-day precipitation values for the Liberty County composite station, along with nonstationary MLE fits and bootstrapped 50% and 95% confidence intervals.

The overall nine-county composite for Southeast Texas (consisting of Orange, Jefferson, Hardin, Liberty, Chambers, Harris, Galveston, Fort Bend, and Brazoria Counties) is shown in Fig. 3.15. With a total of 924 data points, about 8-10 annual maxima ought to lie above the 100-year return value line. This provides a much stronger constraint on the 100-year return values than does data from a single composite station, and so the confidence intervals for the pooled composite are much narrower than for the individual composite stations in Figs. 3.12-3.14. The 2-year confidence intervals are so small as to be barely visible.

The regional composite fit has an upward trend at both 2-year and 100-year return periods. The overall shapes of the two return value curves are constrained to be similar because a single covariate (lnCO2) is used to represent nonstationarity. However, because the pooled composite fit allows both the location and scale parameters to be nonstationary, the 2-year and 100-year fits are not constrained to change by the same percentage. In this instance, differences in the percentage change are nonetheless too small to detect visually in Fig. 3.15.

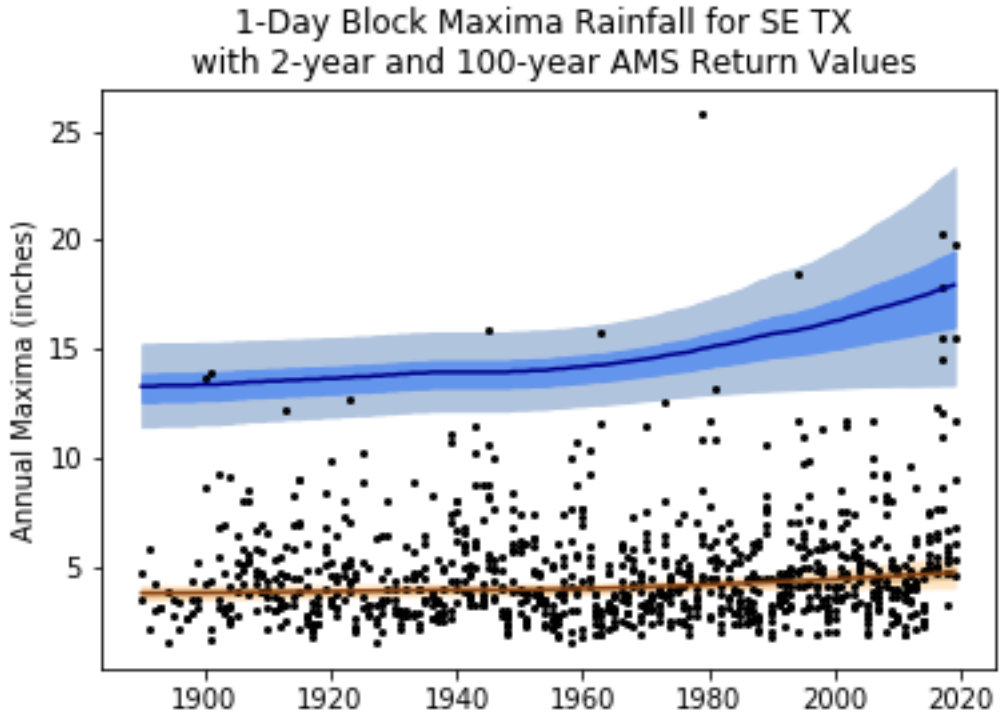

Figure 3.15: Annual maximum 1-day precipitation values for the nine-county Southeast Texas region, along with nonstationary MLE fits and bootstrapped 50% and 95% confidence intervals.

4. Previous Research on Harris County Extreme Rainfall Trends

The assessment of trends in extreme rainfall depends on several aspects of the analysis: the definition of extreme rainfall, the statistical model, the period of the data record, and the spatial aggregation. Longer periods of record, larger aggregation areas, and less stringent definitions yield more tightly constrained trends, but larger aggregation and less stringent definitions come at the expense of providing information specific to Harris County and relevant to HCFCD. Nonetheless, studies have consistently found observed upward trends in extreme rainfall in regions that include Texas.

The Fourth National Climate Assessment (Easterling et al. 2017) reported an increase of 13% over 115 years in the magnitude of 2-day, 5-year block maxima averaged over Texas, Oklahoma, and Kansas. More recently, Wright et al. (2019) examined trends in the number of exceedances of NOAA Atlas 14 design values across the United States for 47, 67, and 87-year periods ending in 2017. For a region spanning Texas, Oklahoma, Kansas, Arkansas, Louisiana, and Mississippi, the overall trend in 1-day exceedance counts over 67 years was 8% for 2-year events and 6% for 100-year events; 4-day exceedances were similar but were not statistically significant. Considering the United States east of 100 °W, Wright et al. (2019) found robust trends of 7-9% per decade for 2-year return thresholds and 8-21% per decade for 100-year return thresholds. Kunkel et al. (2020) examined trends in observed exceedance values in the same six-state region as Wright et al. (2019) and found trends of about 5% per decade, mostly not statistically significant. Sub-daily extreme precipitation in the southern and southeastern United States was examined by Brown et al. (2020), who did not aggregate beyond the station level and found few statistically significant trends, although those that were significant were mostly positive.

Hurricane Harvey inspired several studies into the changing probability of extremely heavy precipitation in the Houston area. All such papers have identified positive historic changes in certain aspects of very extreme rainfall in the Houston area (Risser and Wehner 2017, van Oldenborgh et al. 2017, Russell et al. 2019) or model projections of certain aspects of very extreme rainfall (van Oldenborgh et al. 2017, Emanuel 2017, Wang et al., 2017), even when Hurricane Harvey is omitted from the trend analysis. However, the quantitative results are very sensitive to choices of historic period, event definition, and other aspects of the problem. A recent attribution analysis of rainfall from Tropical Storm Imelda (September 2019) found a similarly positive trend for rainfall intensities commensurate with Imelda (van Oldenborgh et al. 2019). Unlike the more general studies of extreme rainfall trends in the previous paragraph, the Harvey-related studies tend to examine the connection between climate change metrics and extreme precipitation rather than simply assuming a linear trend over time.

As Fischer and Knutti (2016) describe, global climate models were predicting, and climate scientists were expecting, a global and regional increase in extreme precipitation intensity even before an observed trend was detectable. Given the early success of primitive climate models, studies with modern global climate models provide indications of what to expect, and why, as the observed record continues to grow and the climate continues to change. Extreme

precipitation is expected to increase in general in both dry and wet regions of the globe (Donat et al., 2016). Subdaily rainfall is also observed and expected to generally increase, possibly more rapidly than daily or multi-day durations (Westra et al., 2014). Models also robustly predict that the change in frequency of extreme precipitation will be larger for the more extreme events (Pendergrass and Hartmann, 2014; Fischer and Knutti, 2016; Feng et al., 2019; Giorgi et al., 2019). There is tentative evidence that the change in frequency of extreme precipitation may also be larger for shorter precipitation durations (Zhang et al., 2017).

Models have been used to investigate more local characteristics of possible future extreme rainfall trends. Sanderson et al. (2019) analyzed extreme precipitation projections for the Gulf Coast region using quantile mapping and found projected increases of 3-day 100-year precipitation events of 3% to 9% per degree Celsius of global warming, but with large variability among models. Li et al. (2019) identified upward trends in precipitation intensity for global climate model output downscaled to the Clear Creek watershed. Global or regional climate models do not simulate precipitation at such a small scale; relating such model output to local precipitation extremes involves making assumptions about the relationship between local extreme precipitation and larger-scale precipitation that may or may not be sound (Li et al. 2020).

One aspect of the observed and simulated increase in extreme precipitation is the simple principle that warmer air can contain more water vapor and thus produce a greater amount of precipitation, all else being equal. However, large-scale weather patterns, such as jet stream locations and preferred tropical cyclone tracks, can also change with a warming climate, and the enhanced precipitation production can also affect the structure and intensity of individual storms, in turn altering the storm's ability to produce extreme precipitation (Pfahl et al. 2017; Chen et al. 2019). Studies indicate that the simple principle is also the dominant one in most of the United States, but such conclusions are tentative since changes in weather patterns and storm structure are much more uncertain.

An occasionally important weather phenomenon for extreme rainfall along the Gulf Coast is the tropical cyclone. About 10%-15% of the annual maximum daily precipitation along the upper Texas coast is attributable to tropical cyclones (Villarini and Smith 2013; Aryal et al. 2018; Dhakal and Jain 2019), with the Houston area at greater risk than most other Texas coastal areas (Zhu et al. 2013) and widespread extreme precipitation being a particular threat (Kunkel and Champion, 2019). There is general agreement among experts that the precipitation rates associated with tropical cyclones are increasing globally due to climate change (Knutson et al. 2020), and that climate change has increased the odds of Harvey-like precipitation along the Texas Gulf Coast (Knutson et al., 2019). A recent study of observed tropical cyclone precipitation in China is consistent with this upward trend (Liu and Wang, 2020). Tropical cyclones have been observed to be more likely to stall along the North American coast in recent years, but it is unclear whether that trend should be expected to continue (Hall and Kossin, 2019). Because tropical cyclone precipitation is both rare and extreme, accurate assessment of extreme precipitation may require treating tropical cyclone precipitation separately from other types of precipitation (Chin et al. 2019).

Taken together, recent scientific studies and assessments are unanimous that extreme rainfall has been increasing in general in the Texas area and should be expected to continue to increase. Given that trend, how much spatial variation should be expected in the magnitude of the climate-driven trend?

Considerable variation might be expected where changes in weather patterns alter the effect of topographic variations on extreme weather. For example, in areas with large topographic relief, where changes in large-scale wind direction can influence the relative prevalence of upslope or downslope conditions on either side of a mountain range. Likewise, locations whose extreme precipitation has a large influence from tropical cyclones might see different trends than other locations if climate change affects the frequency or intensity of tropical cyclones differently from extreme rainfall in general.

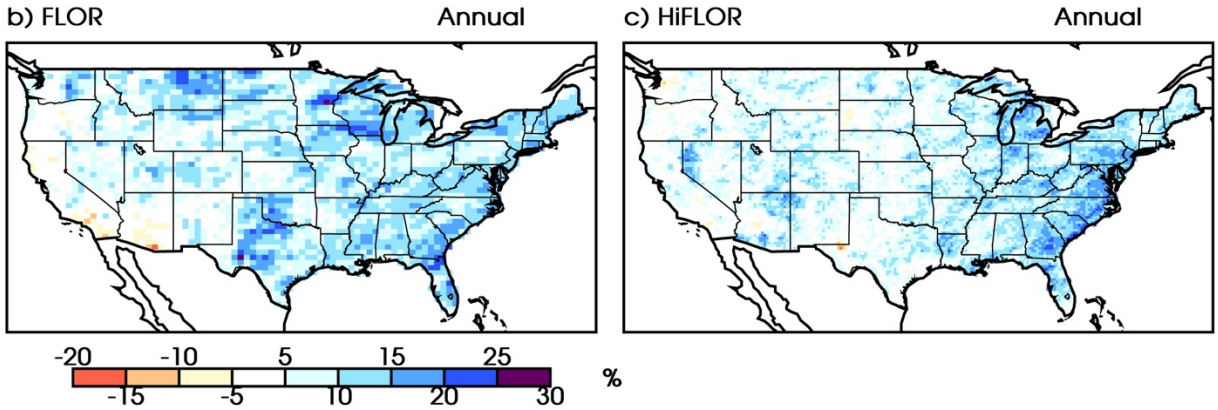

Figure 4.1: Relative increase in the amount of the 1-day annual returning precipitation event between 100-yr simulations with climate forcings corresponding to the year 1990 and simulations with doubled CO2. Panel b uses the FLOR model with 1/2 degree lat-lon resolution, while panel c uses the HiFLOR model with 1/4 degree lat-lon resolution. Reproduced from Figure 5 of van der Weil et al. (2016). Copyright 2016 American Meteorological Society.

Van der Wiel et al. (2016) examined CO2-driven changes in annual maximum 1-day rainfall in the United States with three separate models of varying spatial resolution. The simulations of local changes in extreme rainfall are shown in Fig. 4.1 for the two higher-resolution models. Both models depict spatial variations in maximum 1-day rainfall over spatial scales smaller than typical Gulf Coast states. However, it is notable that, despite identical experimental conditions, the locations of maximum precipitation change are often opposite in the two simulations. For example, FLOR simulates large changes in western Texas, with a secondary maximum in the Coastal Bend area; while HiFLOR has the maximum extreme precipitation changes in between these two areas. FLOR has greater extreme precipitation change in Mississippi than in Alabama or Louisiana; HiFLOR has less extreme precipitation change in Mississippi than in Alabama or Louisiana. The only patterns that might be reliable are the overall tendency for extreme precipitation increases and the greater increases in general in the eastern US than the western US. Those patterns are also found in the lowest-resolution simulation and in 1-day rainfall with

five year return periods (not shown). Since changes in weather and climate patterns are similar across the two models, we conclude that the details of spatial extreme rainfall changes at the state or sub-state scale are produced by the random occurrence of extreme events at different specific locations.

A similar tendency (greater extreme precipitation trends in the eastern US and increased precipitation overall) were also found by Wright et al. (2019). The robustness of these findings and agreement with observations leads us to treat trends that are consistent across several states as robust and possibly driven by climate change, while localized trend variations are likely to lack a large-scale climate driver and would instead be produced by clusters of individual events that inevitably happen more over a given period of time in one place than another. Projections of future trends should rely on multi-state consistent trends unless there is a local topographic or similar influence that would cause a different location-specific response to climate change or that would separately drive a trend in extreme precipitation.

5. Regional Amounts and Trends

5.1 Regional return values

The pooled one-day stationary 100-yr rainfall amounts for the coastal and near-coastal southeastern United States are shown in Figs. 5.1 and 5.2. The two figures are nearly indistinguishable, indicating that the differences between the ful and qcd data sets are of little consequence. Henceforth, all regional plots will use the qcd data.

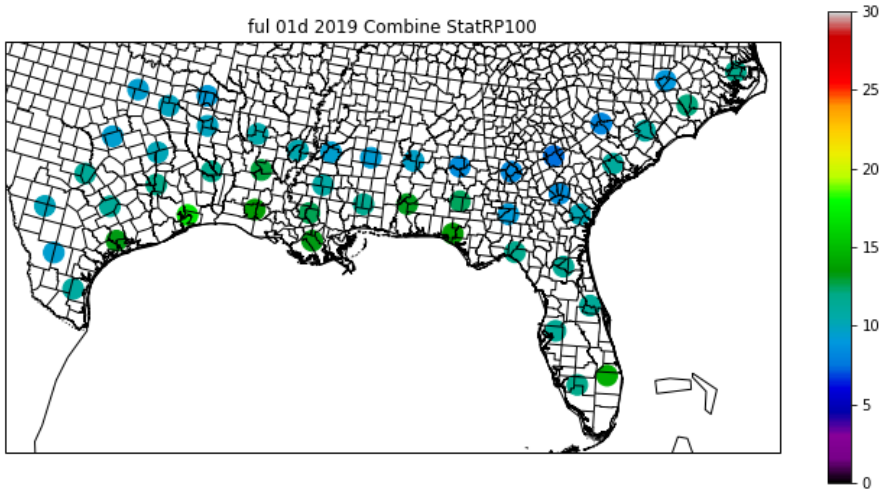

Figure 5.1: Pooled 1-day 100-year rainfall amounts (inches), ful data, stationary model.

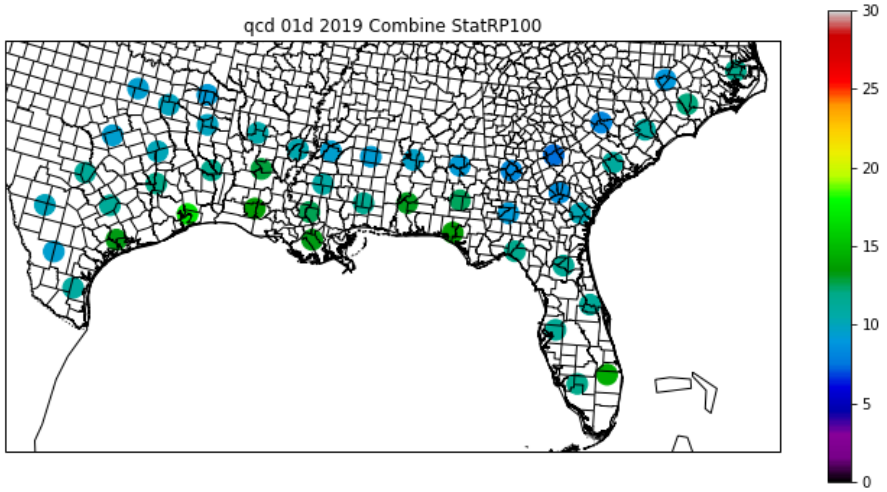

Figure 5.2: As in Fig. 5.1 but for qcd data.

The region including Harris County features the largest one-day 100-yr rainfall amount by far, 16.92" for the qcd data and 16.86" for the ful data. The 100-year amounts on either side of that region along the coast are over 3" smaller. The next largest value is 14.35" for the qcd data and 14.31" for the ful data in southeastern Florida. The 100-year rainfall amounts also generally decrease with distance from the coast.

The 16.92" seems anomalous. One could hypothesize that this particular region of Texas is especially susceptible to the combination of upper-level weather disturbances traveling eastward over northern Mexico and deep moisture along the western margin of the Bermuda High, but then one would expect heavily elevated precipitation totals in the next row of regions farther inland. Instead, the inland values are only a few tenths of an inch higher than their neighbors, and the largest inland pooled value is in Louisiana.

Another possible explanation for the 16.92" is Hurricane Harvey and the other recent extreme rainfall events listed earlier. To determine whether these events are responsible for the elevated 1-day 100-yr amount, the data is truncated at the end of 2014 and a similar analysis is performed. The result, in Fig. 5.3, is a reduction of the 100-yr rainfall amount by 1.40" and a similarly-sized reduction in the extent to which the value in coastal southeast Texas exceeds those of its neighbors. So while recent extreme rainfall events did contribute to the high 100-yr rainfall amount seen in Fig. 1 in southeast Texas, they are not the sole cause.

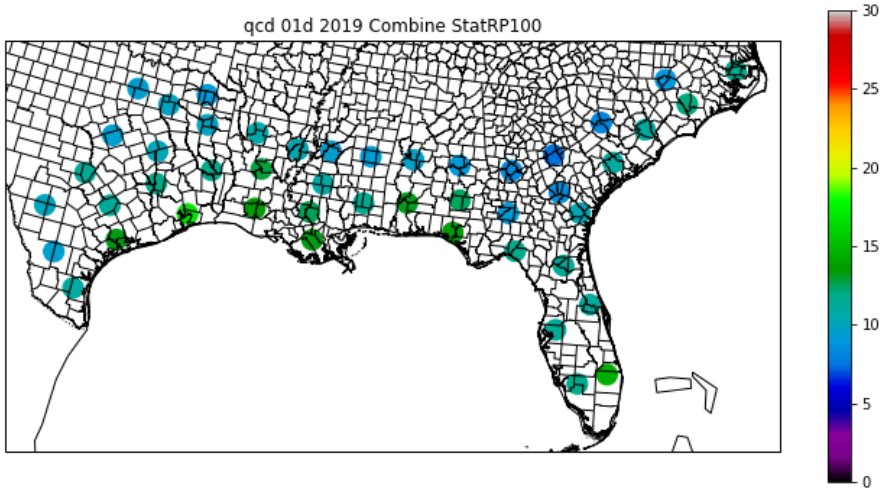

Figure 5.3: Pooled 1-day 100-year rainfall amounts (inches), qcd data through 2014, stationary model.

The percentage difference in 100-yr rainfall amounts for periods ending in 2014 and 2019 is shown in Fig. 5.4. While the estimates increased by 9% in parts of southeast Texas, other substantial increases in the estimated 100-yr rainfall amount occur elsewhere. In particular, the parts of Louisiana most affected by the 2016 flood increase by 4% to 5%, and parts of North

and South Carolina affected by Joaquin, Florence, Matthew, and Dorian saw a 6% to 11% increase in the estimated 100-yr rainfall amount.

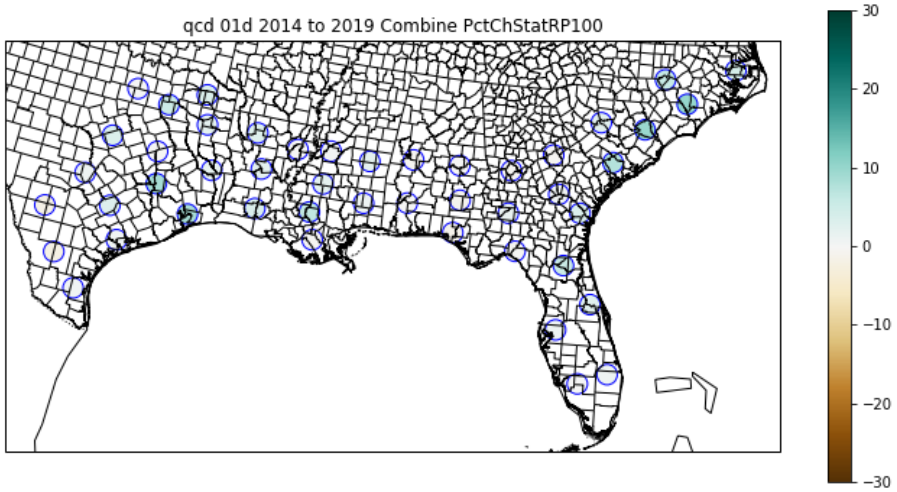

Figure 5.4: Percentage increase in stationary estimate of 1-day 100-year return value due to data in years 2015-2019.

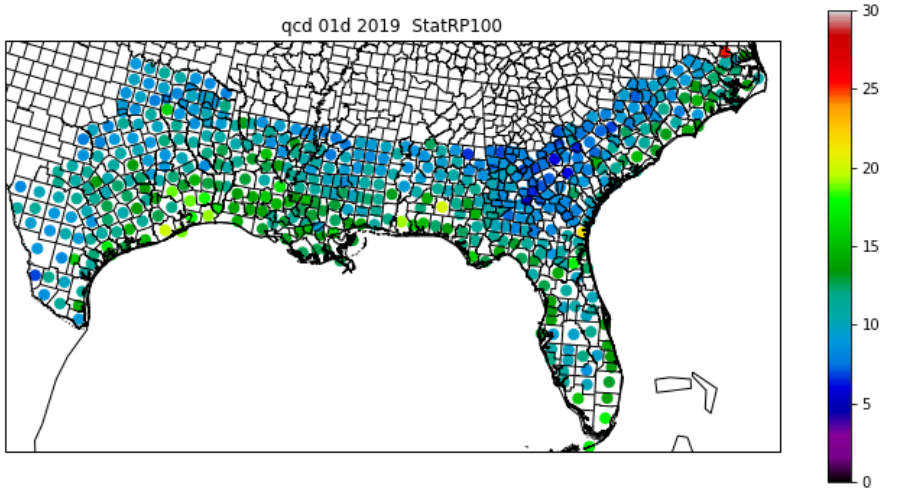

Figure 5.5: Composite station 1-day 100-year rainfall amounts (inches), qcd data, stationary model.

The 1-day 100-year return values for the individual composite stations (Fig. 5.5) are somewhat noisier than the pooled values (Fig. 5.2). This county-level data emphasizes the high values near the coast. Some additional details of structure are more apparent as well. There appears

to be a tendency of the Louisiana Delta and Florida to provide a bit of protection against heavy rainfall for southern Mississippi and Georgia, respectively.

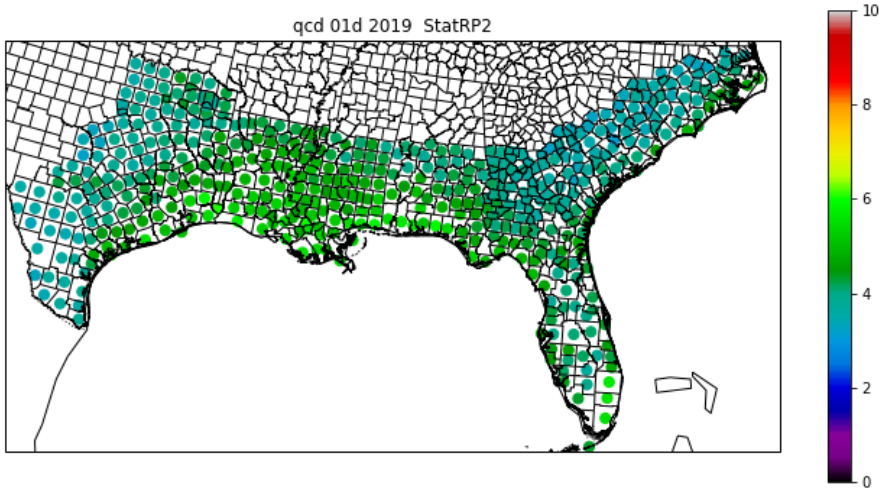

Figure 5.6: Composite station 1-day 2-year rainfall amounts (inches), qcd data, stationary model

The 2-year return values (Fig. 5.6) are considerably smoother than the 100-year return values (Fig. 5.5) at the individual county level, reflecting the smaller uncertainty near the middle of the GEV cumulative distribution. The pooled value for the region including Harris County is 5.17"; this is exceeded slightly by coastal Louisiana and nearly equaled by southeastern Florida. This return value is only about 5% larger than the average of the two surrounding coastal regions, whereas the 100-year return value was about 20% larger than the average. This indicates that southeast Texas is unusual in the context of very large return periods but not smaller return periods.

5.2 Regional trends

The trend in rainfall amounts (Fig. 5.7), expressed as the percentage change in expected 100-year return values between 1960 and 2020, shows a large trend for coastal southeast Texas, with a 27% increase in the maximum likelihood amount over the 60-year period. Larger increases are found in parts of Louisiana and North Carolina, as well as farther inland in eastern and northeastern Texas. Of the pooled trends, 40 out of 47 are positive. Across the entire region, the average best-fit increase is 13.2%.

Note that the 1960 return value is not calculated from the data up to the year 1960. It, like the 2020 return value, is based on the entire data set, assuming that certain characteristics of the probabilities are smoothly changing according to the temporal pattern of the CO2 radiative forcing, with the sign and magnitude of the change dictated by the entirety of the data.

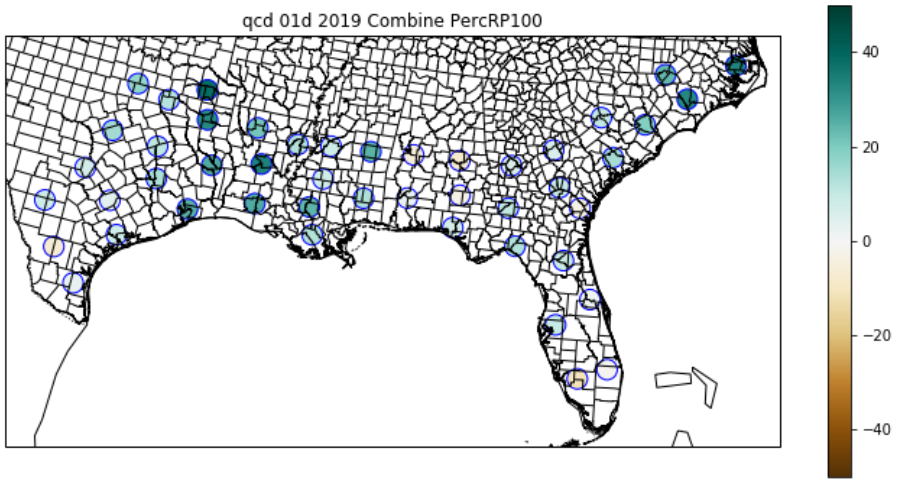

Figure 5.7: Percentage changes in nonstationary pooled estimates of 1-day 100-year return values between 1960 and 2020, qcd data.

Are these trends statistically significant? Collectively, they are. If one assumes that the observed trends represent spatial variations of an underlying average trend, the confidence interval for the estimated average trend depends on the extent to which individual weather events simultaneously lead to block maxima in multiple regions. If the extreme events in each region are independent of those in the others, the underlying trend and 95% confidence interval would be 13.2% +/- 3.7%. If a high degree of interdependency is assumed, such that there are effectively only six independent regions, the underlying trend would be 13.2% +/- 10.2%. We choose an intermediate value, 12, as our best estimate of the number of effective degrees of freedom, which yields 13.2% +/- 7.2%.

Trends exist in the 2-year return periods as well. Figures 5.8 and 5.9 compare the county-level trends in 100-year and 2-year return periods. The trends have more station-to-station variability than the stationary return values. Also notice that the pattern of trends is identical in Figures 5.8 and 5.9. This is because, with only one nonstationary parameter in the GEV fit, all return values are constrained to change simultaneously by similarly proportional amounts. If there is a difference in the trends of 2-year and 100-year return values, it is necessary to turn to the pooled GEV fit with two nonstationary parameters. A nonstationary shape parameter literally allows the shape of the extreme value distribution to change with time (or with ln(CO2)).

The pooled 2-year return value trends (Fig. 5.10) turn out to be slightly smaller and considerably smoother than the pooled 100-year return value trends (Fig. 5.7), even at the state scale. The mean 2-year trend is 11.3%, slightly smaller than the 100-year trend, while the standard deviation of the trends is only 8.0% compared to 12.8% for the 100-year trends. The smaller standard deviation implies a narrower confidence interval as well, making the overall

trend estimate for our preferred number of degrees of freedom 11.3% +/- 4.5%. The trend in Harris County's region is 20.2%, tenth-largest among all regions.

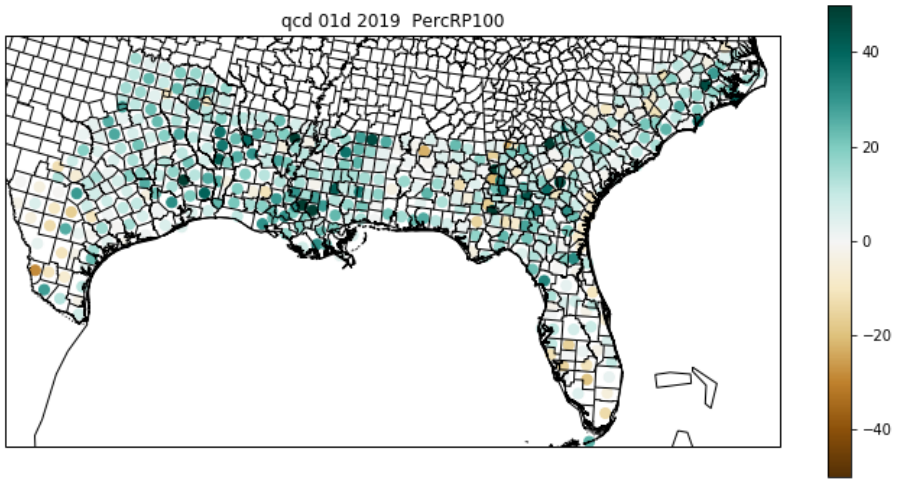

Figure 5.8: Percentage changes in nonstationary composite station estimates of 1-day 100-year return values between 1960 and 2020, qcd data.

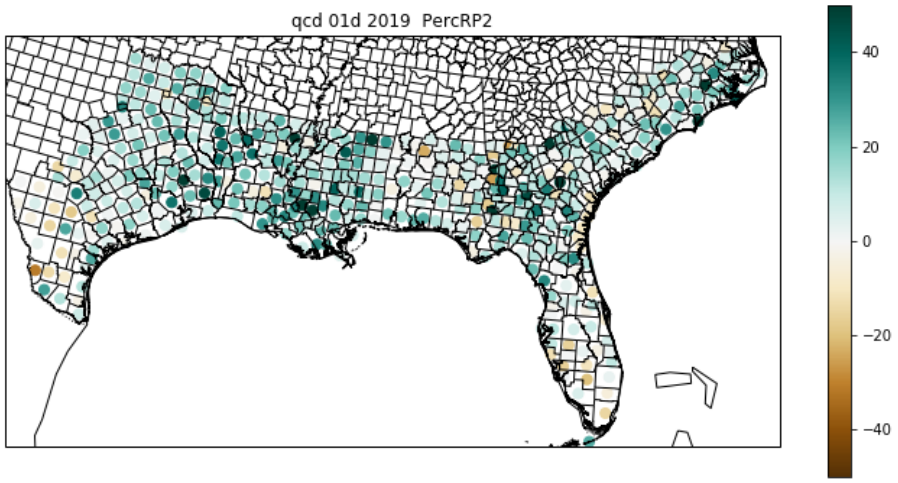

Figure 5.9: As in Fig. 5.8, but for 2-year return values.

If heavy rainfall over the past five years has increased the stationary return value estimates, it should also have increased the estimated trend magnitudes. Figure 5.11 shows the difference in estimated trend magnitudes using only data through 2014 compared to using the full data set. The change in the trend in southeast Texas is very large: 3.8% using data through 2014, and 27.1% using data through 2019. The trend in the region immediately to the northwest,

which includes Waller and Washington Counties, is even larger. Somewhat smaller changes in the trend estimates are found in the Carolinas. Averaged across the entire region, though, there is a 5% difference: 8.1% +/- 6.7% using data through 2014, compared to 13.2% +/- 7.2% using data through 2019. The change in the trend estimates is within the confidence interval for the trend estimates.

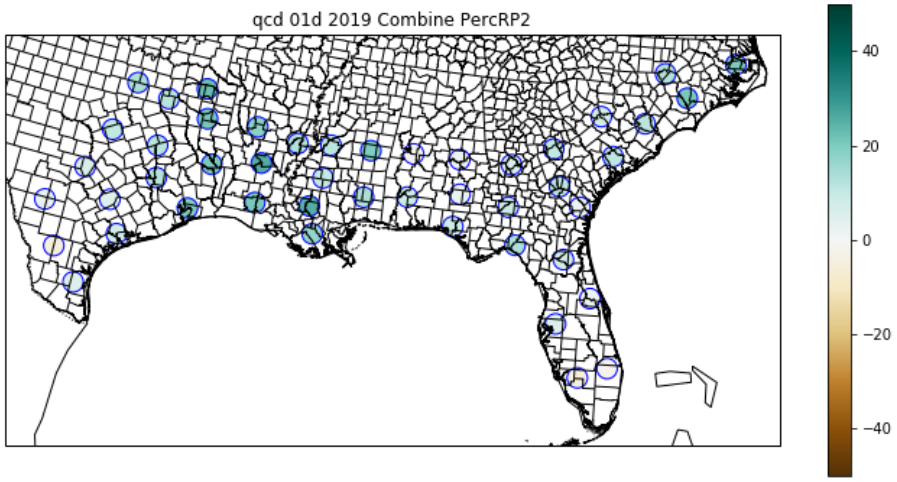

Figure 5.10: Percentage changes in nonstationary pooled estimates of 1-day 2-year return values between 1960 and 2020, qcd data.

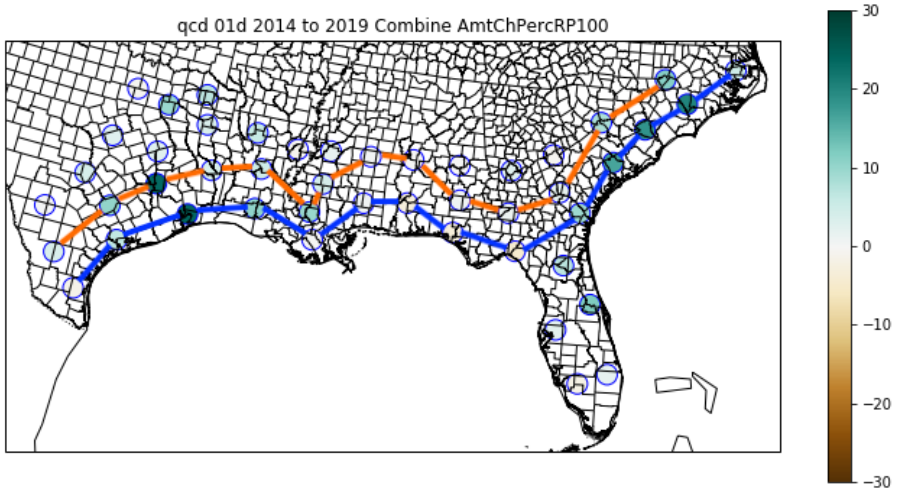

Figure 5.11: Difference in nonstationary pooled trend estimates of 1-day 100-year return values between estimates using data through 2014 and through 2019, qcd data. Blue and orange lines identify pooled coastal and inland stations, respectively, for Figs. 8.1 and 8.2.

The combination of a large stationary return value and a large trend produces an especially large estimate of the nonstationary 100-year return value for the year 2020 in southeast Texas: 20.06". The next highest pooled value is 16.53" in the adjoining coastal region of Louisiana. The adjoining Texas coastal region to the southwest has a pooled value of 14.16". The adjoining inland regions in Texas have pooled values of 13.25" and 14.11". The corresponding 2-year nonstationary return values for 2020 are 6.02" for southeast Texas, 6.11" to the east, 5.05" to the southwest, and 5.30" and 4.80" in the adjoining inland regions. In the 2-year context, southeast Texas is somewhat higher than most of its neighbors but is not an outlier.

In summary, coastal southeast Texas has a 1-day 100-year rainfall amount that is considerably higher than its neighbors. While recent heavy rain in the Houston area contributed somewhat to that anomalous value, the recent rain had a much larger influence on the nonstationary trend fit. Compared to other regions, the recent extreme rainfall events have helped to elevate the return values in coastal southeast Texas and, because most of those events were recent, they also have had an outsized effect on the local extreme rainfall trend analysis.

6. Stationary Analysis for Harris County

Figure 6.1 shows the 1-day 100-year amount for eastern Texas, based on the MLE GEV fit to the NOAA Atlas 14 data. Each dot represents one of the stations used in the NOAA Atlas 14 analysis. Aside from a different color scheme, the map is similar to that in Fig. 3.5, since the MLE method produces similar GEV fits to the L-moments method used in NOAA Atlas 14 and demonstrated in Section 3.

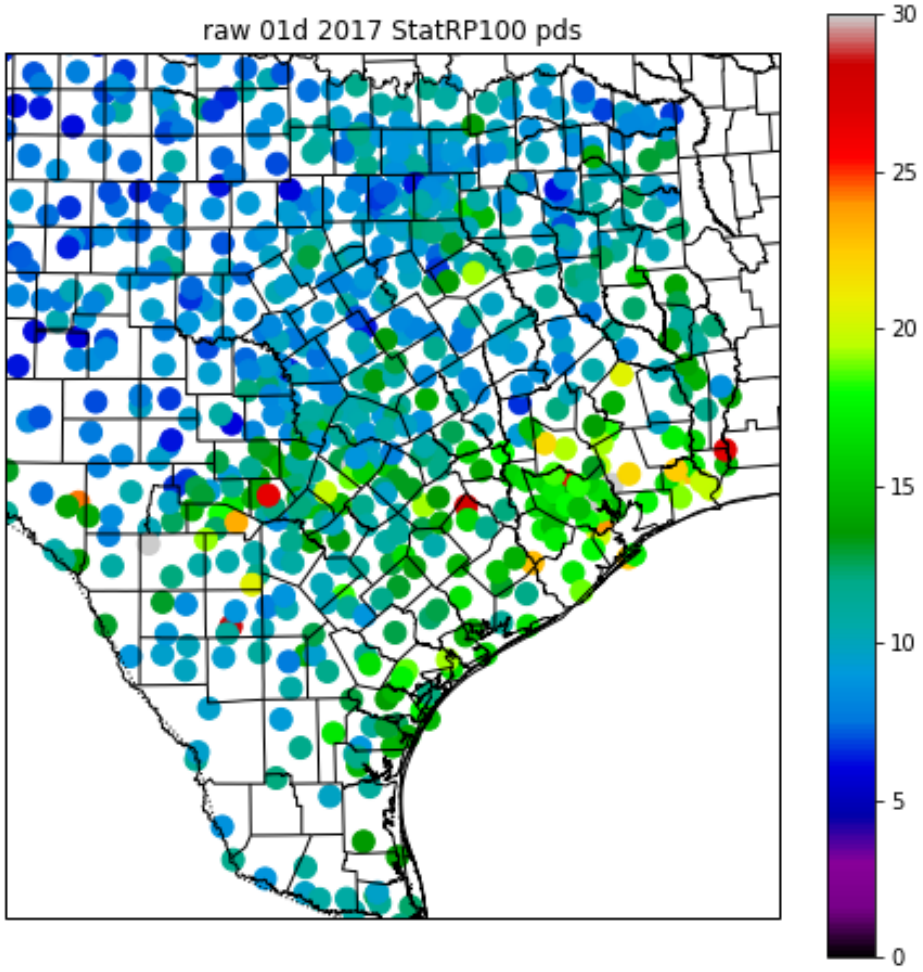

Figure 6.1: 1-day 100-year stationary return values, raw data

In addition to being noisier than the NOAA Atlas 14 map (Fig. 3.5), the raw 1-day 100-year return periods are also noisier than the composite county station data (Fig. 5.5). The reason for

this is the improved robustness of the county composites, which piece together data from multiple individual stations to obtain as long a period of record as possible.

The purpose of the ext data is to reproduce that statistical robustness with the NOAA Atlas 14 data set. Figure 6.2 shows the corresponding return values for the ext data set. As intended, the ext data set does not have the extreme outliers of the raw data set and there is much more consistency in return values from station to station.

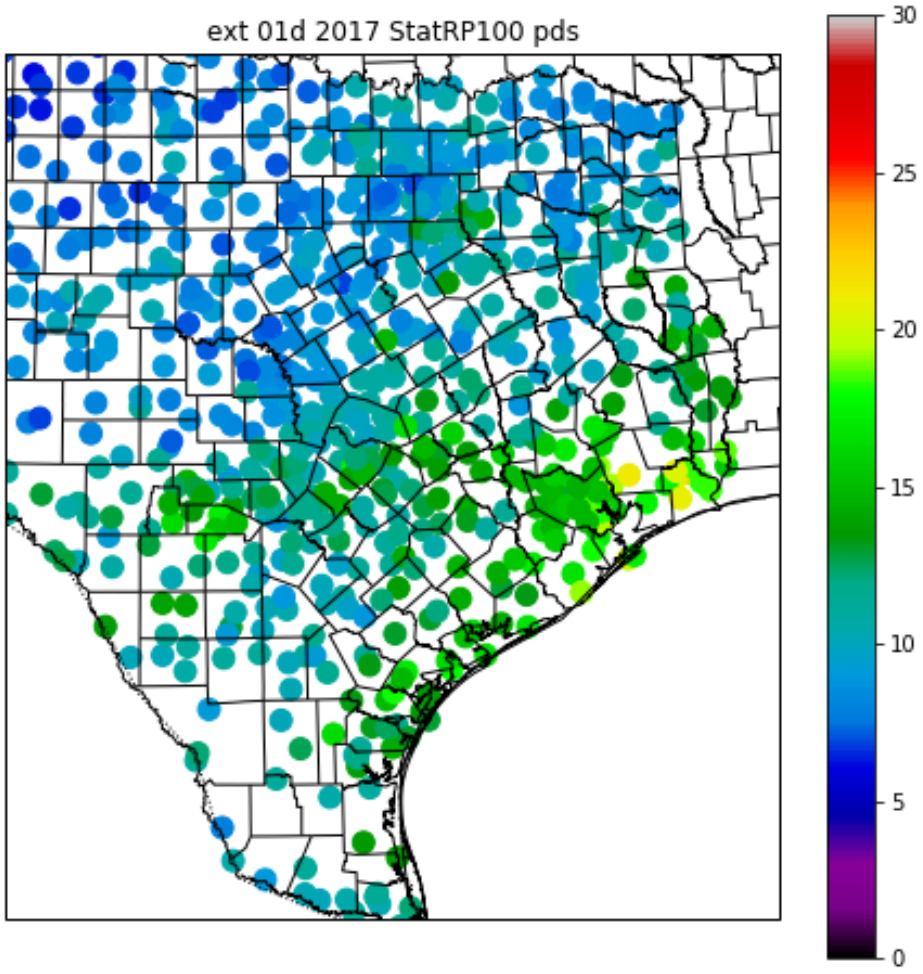

Figure 6.2: *1-day 100-year stationary return values, ext data*

Figures 6.3 and 6.4 show closeups of southeast Texas. The closeups make it possible to discern each of the 25 or so stations in Harris County. The closeup reveals that some stations have a historical data record that implies a 1-day 100-yr return amount of 30" or more. The median

value of return values in Harris County appears to be around 16".5, in line with the median for NOAA Atlas 14. So the GEV fit here is a reasonable reproduction of the NOAA Atlas 14 statistical analysis.

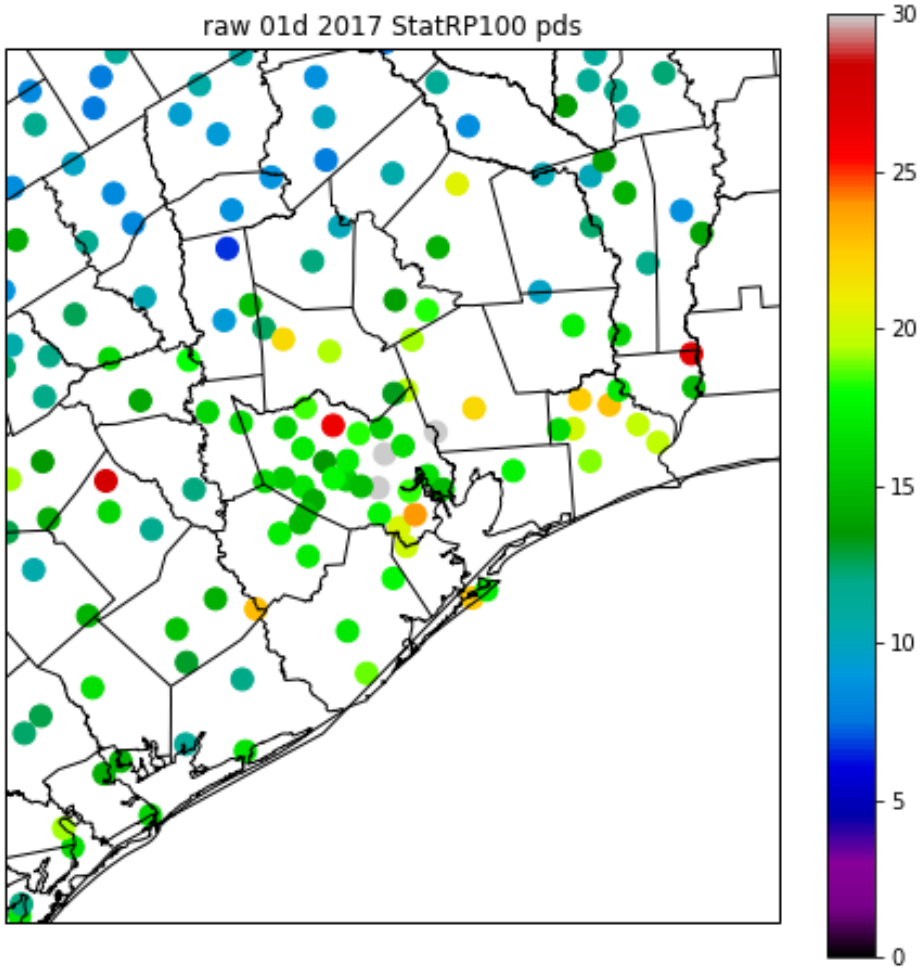

Figure 6.3: 1-day 100-year stationary return values, raw data, southeast Texas

A GEV analysis of the period of record of the stations used by NOAA Atlas 14 in the Houston area includes three stations whose 1-day 100-year return value is literally off the charts: greater than 30". When the period of record for each station is extended back to 1895 using neighboring stations, all such 1-day 100-year return values reduce to 20" or less.

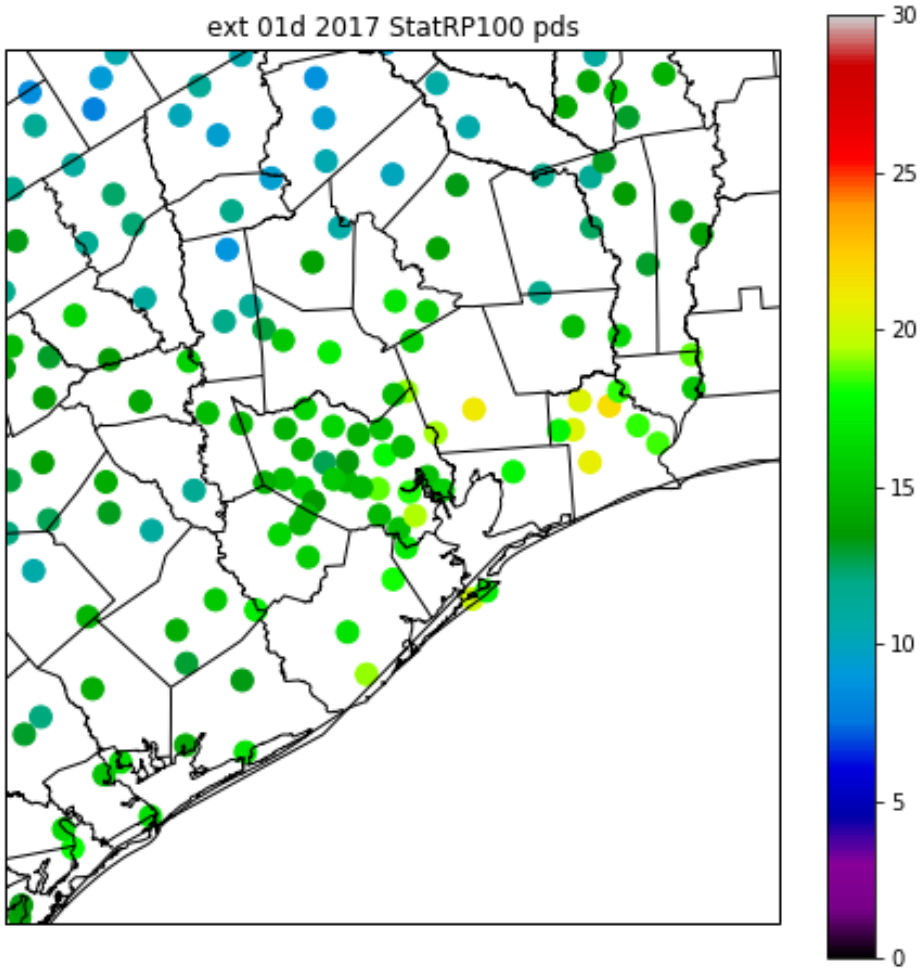

Figure 6.4: 1-day 100-year stationary return values, ext data, southeast Texas

Figure 6.5 shows the difference between the raw and ext 1-day 100-year stationary return values. The map is a patchwork of positive and negative differences, depending on whether rainfall in the distant past was especially heavy. The positive changes northeast of Austin may be at least partially attributable to the extreme rainfall events in 1899 and 1921. Conversely, Harris County did not have many epochal rainfall totals early in the climate data record (at least, compared to more recent rainfall events), so extending the data record tends to reduce the extreme precipitation estimates.

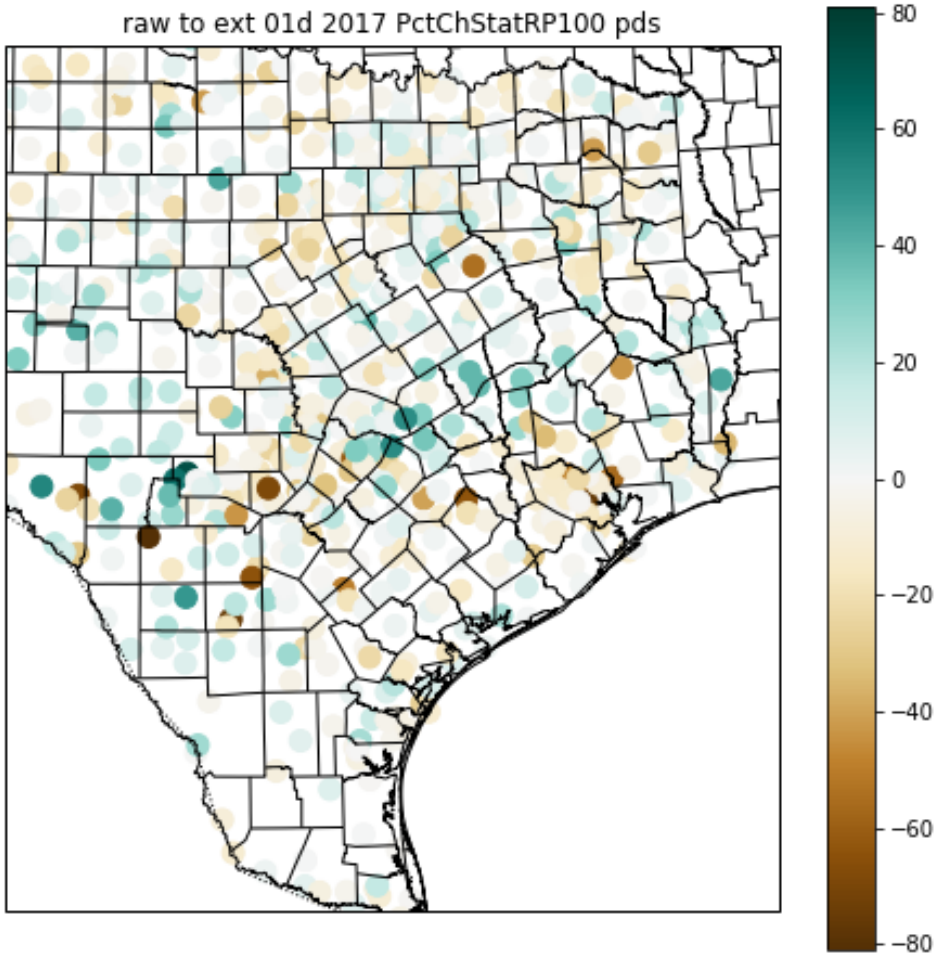

Figure 6.5: Difference in 1-day 100-year stationary return values, raw vs ext data. Positive differences correspond to higher ext values.

Figure 6.6 shows the difference within Southeast Texas. Harris County receives a larger downward adjustment to its 1-day 100-year stationary value than any other county in the area, with the largest adjustments at precisely those stations that had the largest 1-day 100-year stationary return value in the raw data set. Had NOAA Atlas 14 been based on the ext data set, its return values would have been smaller in the Harris County area. Note that the difference would be smaller than Fig. 6.6 suggests, since NOAA Atlas 14 is smoothed and the change in return value estimates would be smoothed too. But to the extent that the ext data produces smoother return value estimates, its resulting return values should approximate what NOAA Atlas 14 would have deduced from the ext data.

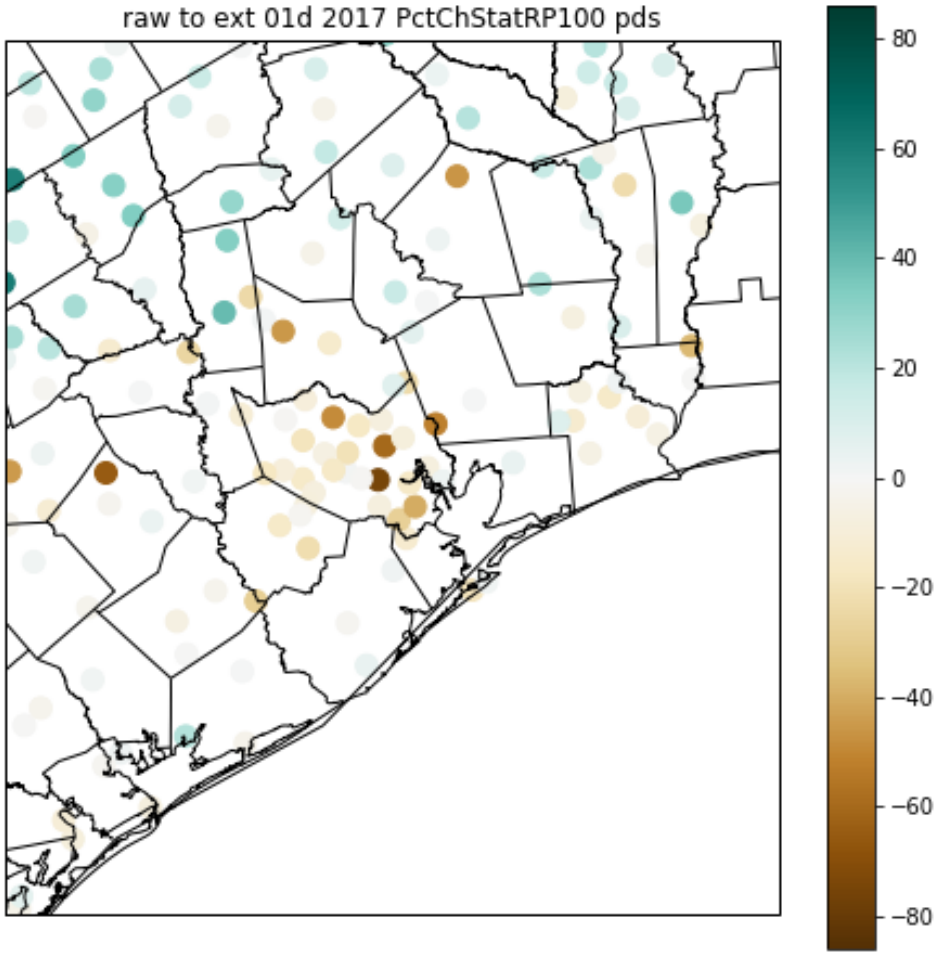

Fig. 6.6: *Difference in 1-day 100-year stationary return values for southeast Texas, raw vs ext data. Positive differences correspond to higher ext values.*

Figures 6.7 through 6.9 show the ext return values for other durations or return periods. In all cases, including Fig. 6.4, the Harris County values seem representative of the broader geographical context. We therefore interpret the ext return values averaged across each of the three regions of Harris County as the approximate return values that NOAA Atlas 14 would have estimated if it had used the ext technique to extend the period of record of each time series.

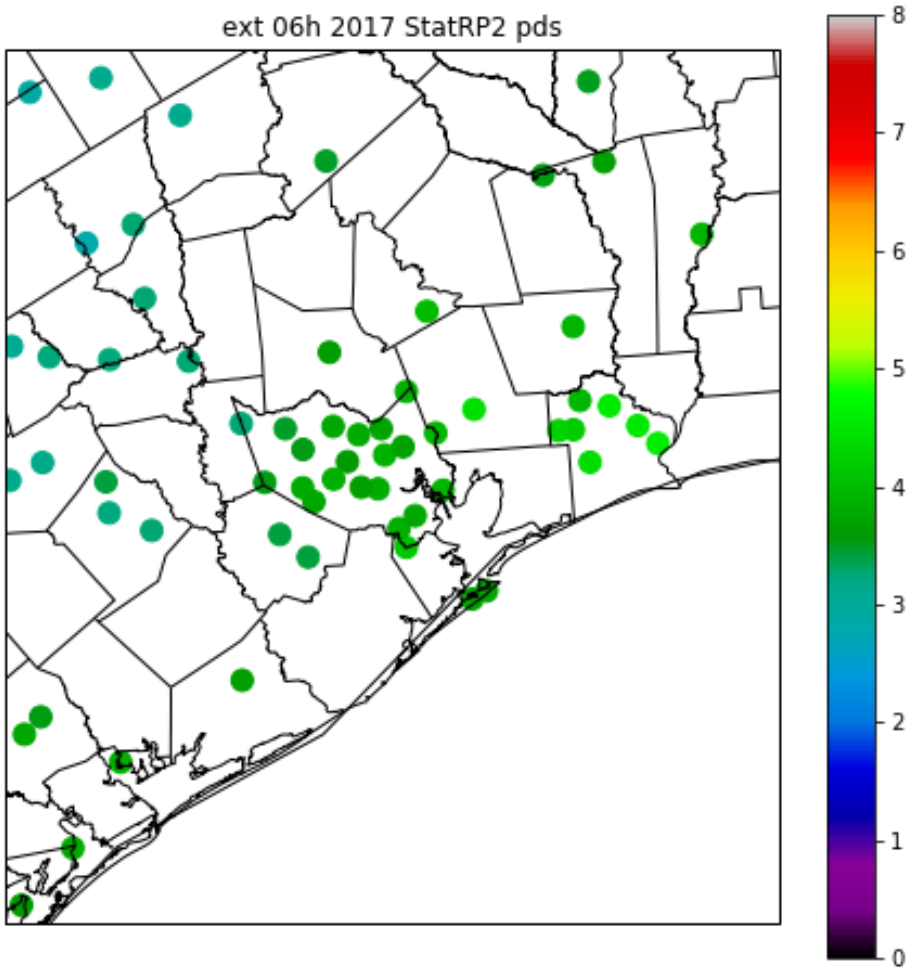

Figure 6.7: 6-hour 2-year stationary return values, ext data, southeast Texas

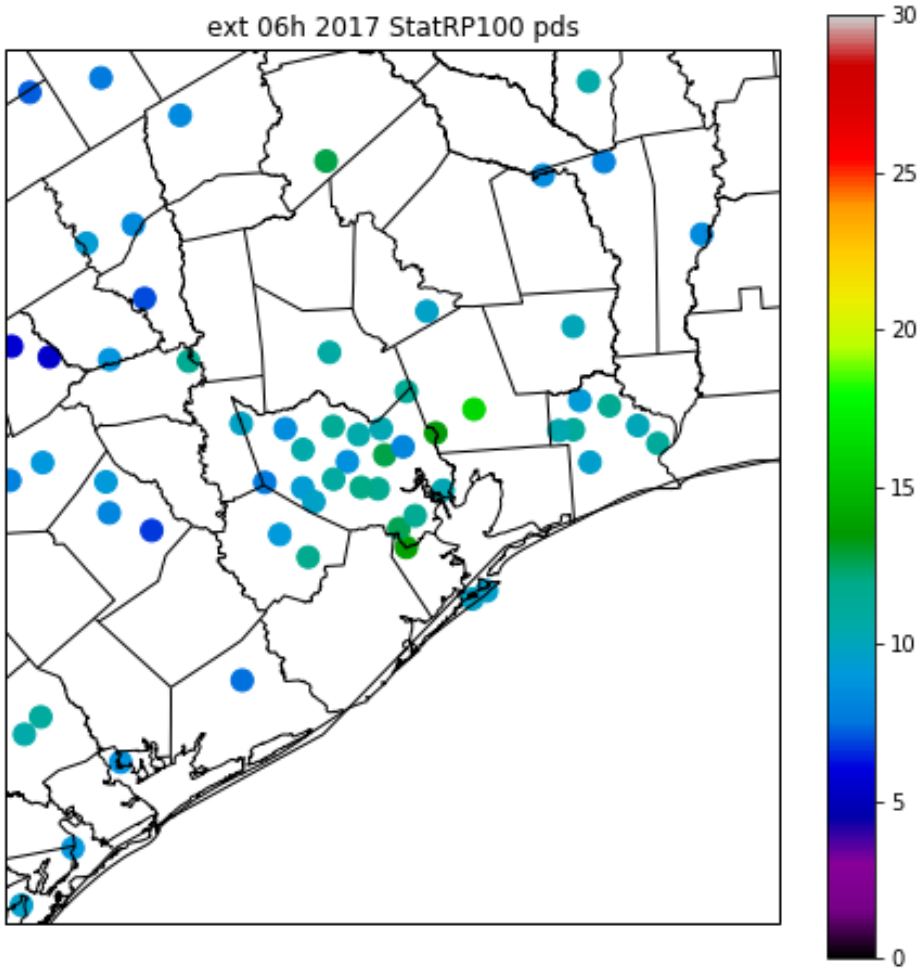

Figure 6.8: 6-hour 100-year stationary return values, ext data, southeast Texas

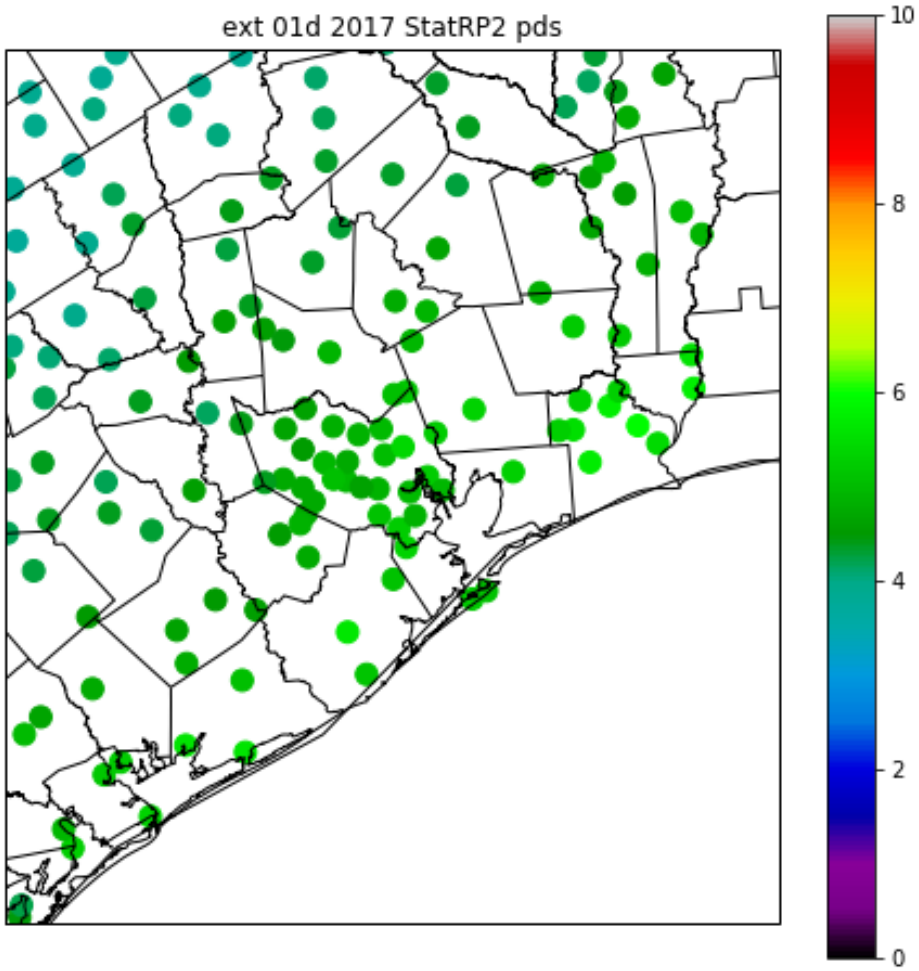

Figure 6.9: 1-day 2-year stationary return values, ext data, southeast Texas

Table 6.1 compares the NOAA Atlas 14, raw, ext, and qcd return values. In all cases, the ext values are lower than the raw values. Also, in ten out of twelve cases, the raw values are higher than the NOAA Atlas 14 values, and in all twelve cases, the ext values are lower than the NOAA Atlas 14 values. At the one-day time scale, the qcd pooled data provides an additional point of comparison. Since Harris County is slightly farther inland than the average location within the region, the true pooled values would be expected to be slightly higher than the true Harris County values. We find that the qcd pooled values are close to the NOAA Atlas 14 values at the 2-year return period and tend to exceed it at the 100-year return period, implying that NOAA Atlas 14 is an overestimate of return values relative to the qcd benchmark.

Region	Dataset	6-h 2-year	1-d 2-year	6-h 100-year	1-d 100-yr
1	**Atlas 14**	**3.58**	**4.83**	**10.7**	**16.3**
1	raw stat	3.67	4.86	10.77	17.27
1	ext stat	3.58	4.63	9.58	15.03
2	**Atlas 14**	**3.75**	**5.11**	**11.3**	**16.9**
2	raw stat	4.06	5.09	11.45	15.89
2	ext stat	3.79	4.92	10.58	14.99
3	**Atlas 14**	**3.87**	**5.30**	**12.5**	**18.0**
3	raw stat	4.11	5.48	15.61	19.26
3	ext stat	3.85	5.10	11.09	16.73
SE TX	qcd stat	n/a	5.17	n/a	16.86

Table 6.1: Comparison of stationary return values for the three watershed regions of Harris County.

The apparent explanation for the tendency of ext data to yield smaller stationary return values in the Harris County area lies in the fact that many of the Harris County stations have shorter, recent record periods. Section 5 illustrated that there is an observed long-term upward extreme precipitation trend in the region, and also illustrated that the Harris County area has received a large increment of extreme rainfall over the past few years. Both of those factors would lead to stations with a short, recent period of record having a larger estimated return value than a station with a longer period of record. NOAA Atlas 14 weighted longer periods of records more heavily, which would have reduced but not eliminated the bias.

The results in this section also imply that a more robust stationary analysis than NOAA Atlas 14 would have yielded smaller return values. On average, the difference between the Atlas 14 and ext return values is 0.2% for 6-h 2-year values, -3.9% for 1-d 2-year values, -9.4% for 6-h 100-year values, and -8.7% for 1-d 100-year values. The grand mean difference is -5.5%.

This does not mean that NOAA Atlas 14 overestimates the return values that should be expected today by 5.5%. If there is a long-term trend, stations with a shorter, more recent period of record will be sampling from a climate more similar to the present-day climate and thus will yield extreme rainfall estimates that are closer to the present-day reality. The artificially enhanced 100-yr precipitation estimates over Harris County may mean that the precipitation estimates for Harris County are closer to the actual rainfall risk compared to county-scale precipitation estimates from the north and west. We will quantify this effect in subsequent sections.

7. Trend Analysis for Harris County

7.1 Trend magnitudes

Figure 7.1 shows the trend (1960 to 2020) for the extended data set across eastern Texas, while Fig. 7.2 shows the trend close-up around Harris County. Overall, trends are generally consistent with the regional analyses shown in Section 5. Positive trends dominate. In Harris County, the trends are larger than for almost any other county in the region.

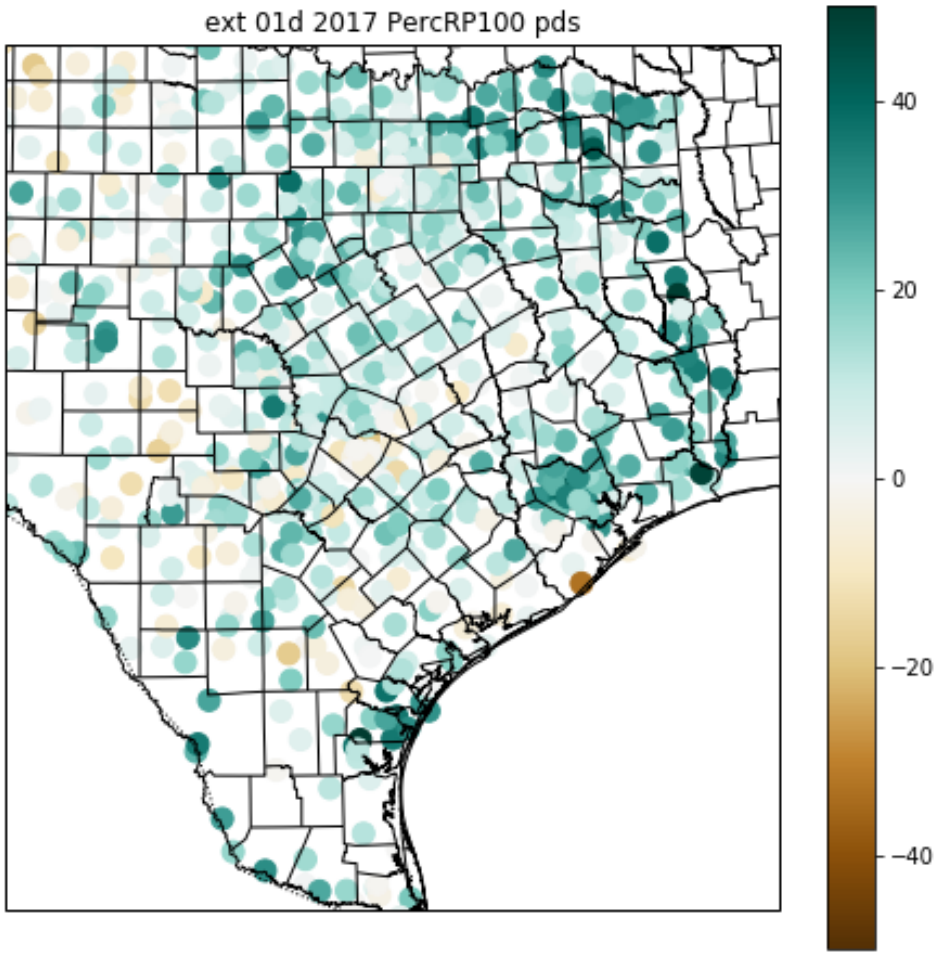

Figure 7.1: The trend in 1-day 100-year exceedance values, expressed as the difference between the 1960 value and the 2020 value, using ext data. Positive values imply an upward trend.

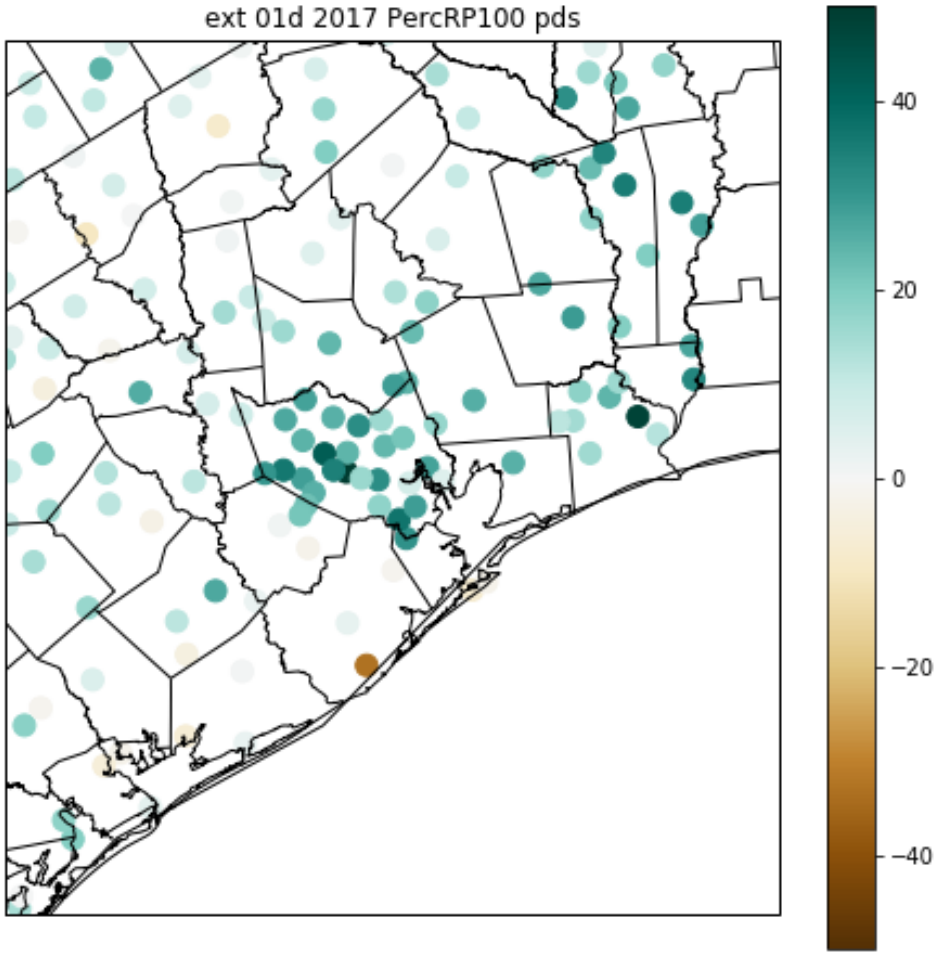

Figure 7.2: The trend in 1-day 100-year exceedance values, as in Fig. 7.1, but for southeast Texas.

The corresponding maps for 6-hour 100-year trend are given in Figs. 7.3 and 7.4. Since the nonstationary GEV model for individual stations uses a single nonstationary parameter and assume logarithmic precipitation dependence, the percentage trends in 2-year exceedance values are constrained to closely match the percentage trends in 100-year exceedance values, so they are not separately shown here.

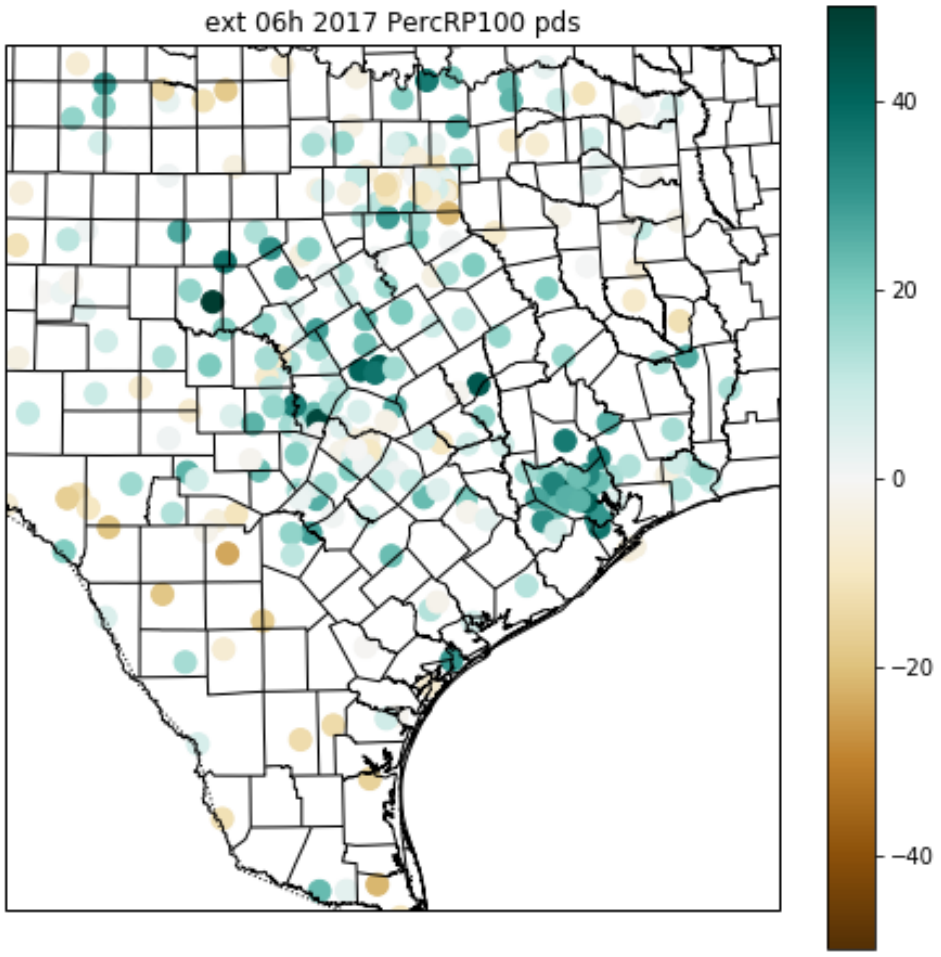

Figure 7.3: The trend in 6-hour 100-year exceedance values, expressed as the difference between the 1960 value and the 2020 value, using ext data. Positive values imply an upward trend.

In both Fig. 7.3 and Fig. 7.4, the unusual size of the trend in and around Harris County is readily apparent. No other area in central or eastern Texas features so many large positive trends. These trends reflect the long-term lived experience of Harris County residents: extreme precipitation has been more frequent and more intense in recent years.

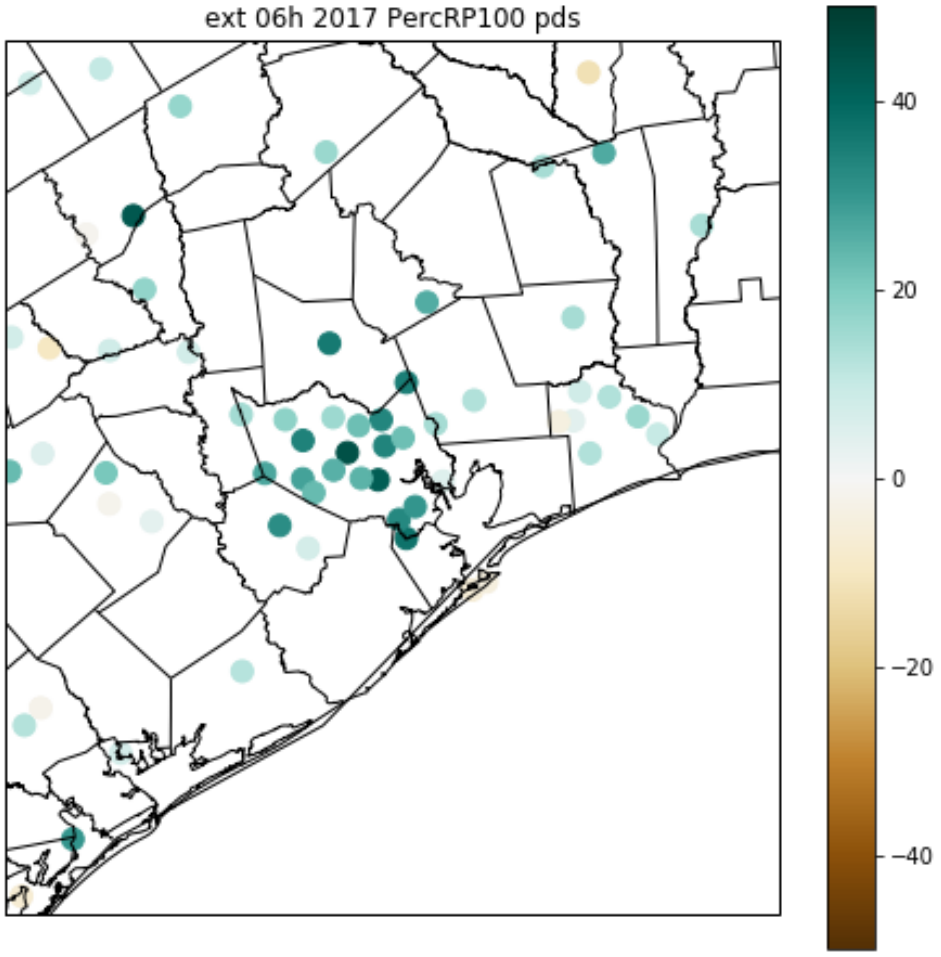

Figure 7.4: The trend in 6-hour 100-year exceedance values, as in Fig. 7.3, but for southeast Texas.

In summary, even with the ext data set, Harris County has a larger trend in the return values for extreme precipitation than any neighboring areas. Whether this trend should be expected to continue depends on the specific cause of the trends. Four possible causes for the enhanced Harris County trend will now be considered: coastal proximity, urbanization, climate change, and natural variability.

7.2 Analysis of relationship between coastal proximity and amounts/trends

Figure 6.2 illustrates that the highest 1-day 100-year return values are typically found within about one county of the coast, with Harris County intermediate between the coastal band with high values values farther inland. There appears to be nothing special about the return values at Harris County's distance from the coast in Harris County or in other areas.

Figure 7.1 shows the trend in 1-day 100-year return values. In this case and for trends in other return values, the trend in Harris County is larger than the trend both closer to the coast and farther inland. But Figure 7.1 shows that this pattern is unique to Harris County. Nowhere else along the Texas coast is there a maximum in the trend one or two counties inland from the coast. Indeed, the overall impression from Figure 7.1 is that of a random patchwork of larger and smaller trends overlaid on a general tendency for larger trends to the east and smaller trends to the west.

In summary, Harris County's proximity to the coast enhances its vulnerability to extreme rainfall, but there is no evidence that the effect of coastal proximity is changing over time or is contributing to the large trends in extreme rainfall experienced by Harris County.

7.3 Analysis of Relationship Between Urbanization and Amounts/Trends

Urbanization has been linked to extreme rainfall. For example, Yin et al. (2020) simulated a rainstorm over Guangzhou, China, that produced over 20 inches of rainfall in 12 hours, and found that the urban heat island and associated wind convergence was an important trigger for the event. So we now examine whether there is any consistent relationship between urbanization and extreme rainfall trends across Texas.

The same Figure 6.2 fails to provide any prima facie evidence that Harris County possesses anomalous return values due to urbanization. The return values in Harris County lie along a continuum from smaller values to the north and west and larger values to the south and east.

Figure 6.2 shows that the return values for other urban areas are a mixed bag. San Antonio lies along a gradient between smaller values to the south and larger values to the north, probably influenced by the local topography of the Balcones Escarpment. Austin has locally higher values, while Dallas-Fort Worth has locally lower values. Thus there is no direct evidence that urban areas are having an influence on the overall estimates of extreme return values in Texas.

Many previous studies have examined a possible urban influence on precipitation in Houston (such as Shepherd et al. 2010 and Orville et al. 2001), but few have investigated urban impacts on very extreme precipitation. Two recent Harvey-oriented studies examined this question, one directly and the other indirectly. Zhang et al. (2018) performed a baseline simulation of Harvey with a simple urban area parameterization and a second simulation with the urban areas replaced by cropland. Although the paper claims that urbanization enhanced the rainfall, a closer look at the results reveals that the rainfall was similar in magnitude but displaced

eastward in the simulation with the urban area. The model ensemble size (five members) may have been too small to robustly reveal the urban influence. Also, the urban parameterization would not have reflected the unique and varied urban cityscape of Houston. Pan et al. (2018) performed Harvey simulations with a giant offshore wind farm and found that the obstacle created by the wind farm enhanced precipitation offshore. The Houston urban core should similarly act as an obstacle and locally enhance precipitation during Harvey.

Urbanization might be more likely to manifest itself as an influence on trends, since urbanization has increased dramatically over the past several decades. But Figure 7.3 also presents a mixed bag. None of the other major cities in Texas have a localized, relatively high trend like Houston. Austin and Dallas-Fort Worth feature near-zero or even negative trends. The trends in Fig. 7.3 are organized neither by coastline nor urbanization.

7.4 Analysis of relationship between climate change, trends, and natural variability

As already noted, there is a robust upward trend in extreme rainfall across the southern and southeastern coastal United States. Section 4 reviewed the extensive evidence that such a trend is caused by global warming. But what about the specific trend in Harris County?

A classical analysis of the statistical significance of the Harris County trend would not settle the question. The trend in Harris County is higher than just about anywhere else in the southern and southeastern United States. Because 5% of all trends are expected to be statistically significant at the p=0.05 level, we can assume that the Harris County trend is statistically significant, but that tells us nothing since a few places are likely to be randomly statistically significant.

An alternative approach is to question whether the trend specific to Harris County can be caused by climate change. This is unlikely, since the same climate change processes that might hypothetically lead to an enhanced trend in Harris County ought to lead to an enhanced trend across most of the Gulf Coast. Figure 5.7 shows a smoothly varying trend along the Gulf Coast, but the spatial scale of even those variations seems too small to be robustly produced by global climate change, as discussed in Section 4.

We are aware of no research investigating the characteristic spatial scale of climate change trends in the absence of special topographic influences. The null hypothesis would be that the observed spatial variations are a consequence of natural variability: the specific history of extreme rainfall events in the area. If the weather of the past 125 years were to be re-started, the locations receiving extreme rainfall events such as Harvey and Imelda may well have been different, or the storms may not have existed at all. Given the absence of evidence that the spatial patterns of trends in extreme rainfall are deterministic, the appropriate minimum assumption is that the underlying trend is uniform across the entire region.

8. Estimation of Future Extreme Rainfall Likelihood

With the above analyses in mind, the report now considers likely return values for future extreme precipitation at the 6-hour and 1-day durations.

As an initial matter, if there were no trends in extreme rainfall and actual extreme rainfall events were evenly distributed in time, the NOAA Atlas 14 analyses would provide valid and accurate estimates of extreme rainfall risk. But the presence of an underlying positive trend and the additional clustering of extreme rainfall events near the end of the historical record in the Houston area, combined with the uneven distribution of periods of record of available stations, causes the NOAA Atlas 14 analysis to be suboptimal.

The remainder of this section makes quantitative estimates of the impact of various aspects of extreme rainfall in Harris County that were not fully considered in the NOAA Atlas 14 analysis. The starting point is the NOAA Atlas 14 analysis (Table 8.1); the three numbers in each cell correspond to regions 1, 2, and 3 of Yung (2019).

Table 8.1: NOAA Atlas 14 regional return values.

	2-YEAR RETURN PERIOD		100-YEAR RETURN PERIOD		500-YEAR RETURN PERIOD	
	6 HOUR	1 DAY	6 HOUR	1 DAY	6 HOUR	1 DAY
NOAA ATLAS 14	3.58	4.83	10.7	16.3	15.9	21.7
	3.75	5.11	11.3	16.9	16.7	22.9
	3.87	5.30	12.5	18.0	18.2	24.5

8.1 Adjustment for Short Record Lengths

At the county scale, the irregular and nonstationary distribution of historical precipitation and the use of shorter-duration stations in the Harris County area means that, for Harris County in particular, return values are unusually large because events are preferentially sampled from nearer the end of the data record when extreme rainfall happened to be plentiful. When data is extended back to 1895 by substituting nearby observations for missing values, the anomalously larger return values in Harris County disappear.

The changes in estimates (Table 6.1) were somewhat erratic from region to region within the county. NOAA Atlas 14 uses a larger spatial footprint to estimate return values. To more robustly estimate an adjustment for the extended record lengths, we average the three regional precipitation values before computing percent changes. We then compare those changes to changes relative to the original NOAA Atlas 14 values.

Table 8.2: Record length and MLE differences in return values

	2-YEAR RETURN PERIOD		100-YEAR RETURN PERIOD		500-YEAR RETURN PERIOD	
	6 HOUR	1 DAY	6 HOUR	1 DAY	6 HOUR	1 DAY
RAW REGIONAL	*3.67*	*4.90*	*10.66*	*16.21*	*15.39*	*24.73*
L-MOMENT	*4.07*	*5.12*	*11.36*	*15.52*	*15.94*	*22.57*
ESTIMATES	*4.17*	*5.50*	*14.01*	*18.75*	*22.19*	*29.29*
RAW AVERAGE	3.95	5.17	12.01	16.83	17.84	25.53
EXT REGIONAL	*3.58*	*4.63*	*9.58*	*15.03*	*13.29*	*23.02*
MLE ESTIMATES	*3.79*	*4.92*	*10.58*	*14.99*	*15.01*	*22.63*
	3.85	*5.10*	*11.09*	*16.73*	*16.12*	*25.89*
EXT AVERAGE	3.74	4.88	10.42	15.58	14.81	23.85
PCT CHANGE	**-5.3%**	**-5.6%**	**-13.2%**	**-7.4%**	**-17.0%**	**-6.6%**
NOAA ATLAS 14 AVERAGE	3.73	5.08	11.50	17.07	16.93	23.03
PCT CHANGE	**+0.2%**	**-3.9%**	**-9.4%**	**-8.7%**	**-12.5%**	**+3.5%**

The average percent difference from the raw L-moment values to the ext MLE values is -9.2%, whereas the average percent difference from the NOAA Atlas 14 values to the ext MLE values is -5.1%. The differences do not vary systematically across durations and return periods, so we identify a uniform best value to apply to all estimates. The spatial statistical smoothing applied during the NOAA Atlas 14 process probably contributed some of the statistical value provided by the ext approach. So -9.2% is an estimate of an upper bound of the adjustment that needs to be applied to the NOAA Atlas 14 data, while -5.1% is an estimate of the lower bound. We use as a best estimate the average of the two, which is -7.2%. The revised return values are given in Table 8.3.

Table 8.3: NOAA Atlas 14 regional return values with MLE/ext adjustment.

	2-YEAR RETURN PERIOD		100-YEAR RETURN PERIOD		500-YEAR RETURN PERIOD	
	6 HOUR	1 DAY	6 HOUR	1 DAY	6 HOUR	1 DAY
	3.58	4.83	10.7	16.3	15.9	21.7
NOAA ATLAS 14	3.75	5.11	11.3	16.9	16.7	22.9
	3.87	5.30	12.5	18.0	18.2	24.5
MLE/EXT ADJ			-7.2%			
RETURN VALUES	3.32	4.48	9.93	15.1	14.8	20.1
THROUGH	3.48	4.74	10.5	15.7	15.5	21.3
SECTION 8.1	3.59	4.92	11.6	16.7	16.9	22.7

8.2 Spatial Variations in Stationary Analyses

While Harris County itself doesn't stand out in the ext data, the southeastern Texas coast in general has what seems to be an anomalously large set of 100-year return values compared to neighboring locations. This issue was discussed in Section 5; here we examine this particular issue in more detail.

Figure 8.1 compares the 2-year and 100-year return values for durations of 1 day and 4 days. The specific coastal and inland (adjacent to coastal) regions are listed in Appendix B and are depicted in Fig. 5.11. The Florida Peninsula is excluded.

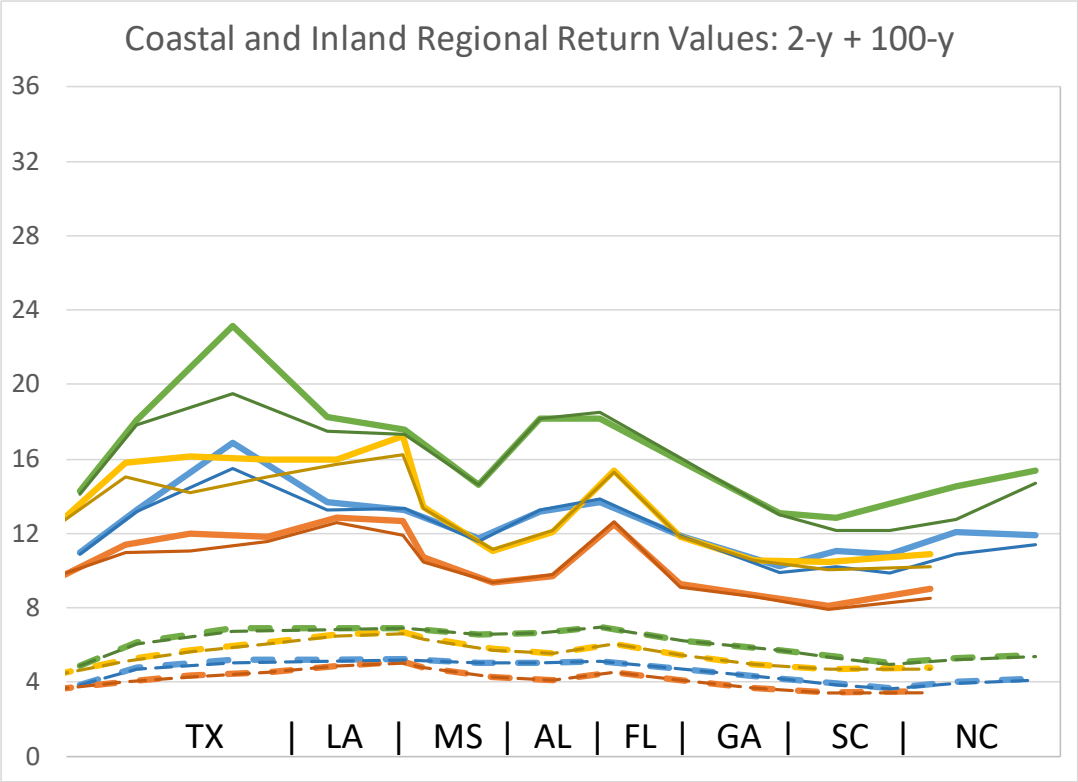

Figure 8.1: Stationary coastal and inland return values, qcd lumped data set, plotted left to right from southern Texas to northern North Carolina. In this and similar plots, the dashed lines correspond to 2-year return values while the solid lines correspond to 100-year return values. Blue and green represent coastal regions, with blue being 1-day accumulations and green being 4-day accumulations. Orange and yellow represent inland regions adjacent to coastal regions, with orange being 1-day accumulations and yellow being 4-day accumulations. The thick lines use the complete data set while the thin lines use data through 2014.

The 2-year return values are generally spatially smooth, with values increasing along the Texas coast to the northern Gulf Coast where they plateau at a high level. Lower values are found along the southeast Atlantic coast, although they rise toward North Carolina. Coastal and inland regions are generally consistent, rising and falling together as one progresses along the coast, with inland regions having lower return values.

The 100-year return values, being more sensitive to extreme events, are more spatially erratic than the 2-year return values. Nonetheless, the same overall pattern as in the 2-year return values is apparent: increasing along the Texas coast, generally high along the northern Gulf Coast, lower along the southeast Atlantic coast, and rising toward North Carolina.

The erraticness of the 100-year return values manifest themselves in two ways. First, each line tends to be less smooth. The mean percent difference between a given return value and that of adjacent regions along the same line is 4% for 2-year return values and 9% for 100-year return values. Second, the highest 1-day and 4-day return values are found in the southeast Texas coastal region, as already noted for 1-day values in Section 5, while the adjacent inland regions do not possess a sharp peak.

The thin lines on Fig. 8.1 show the stationary return periods calculated using data through 2014. Large differences are found at both coastal and inland locations in southeast Texas, illustrating how the recent very heavy rain events have substantially altered the return value estimates at long return periods throughout the region. At inland locations, this had the effect of smoothing the previous spatial variations in return values, while at the coastal region, this had the effect of amplifying a peak that was already there.

The other area with large return value updates is the Carolinas. The succession of hurricanes there has produced substantial fractional increases in return values, as noted in Section 5.

Figure 8.2 is similar to Figure 8.1, except it shows the 500-year return values along with the 2-year return values. The 500-year return values have a similar appearance as the 100-year values, except that they are even noisier (12% using the same metric as before). The southeast Texas coastal peak is even more dramatic, as is the change from the 2014 estimate.

The lack of consistency with inland return values, with return values for shorter periods, and with neighboring coastal return values all suggest that the southeast Texas coastal peak is a statistical aberration, a result of storms such as Hurricane Harvey that might have happened anywhere along the northern Gulf Coast striking southeast Texas. Such events should not be ignored, since they clearly can happen, but it does not seem appropriate to assign their probabilities entirely to southeast Texas rather than distributing their probabilities along the Gulf Coast.

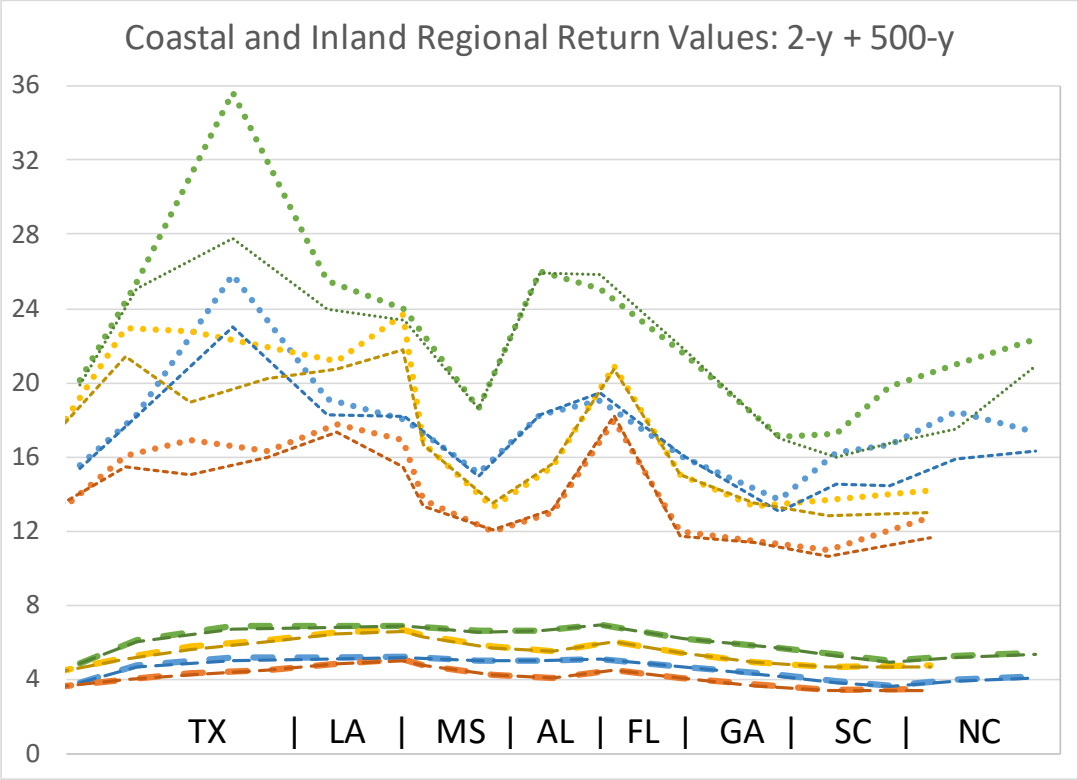

Figure 8.2: Stationary coastal and inland return values, qcd lumped data set, plotted left to right from southern Texas to northern North Carolina. Colors, line styles, and line widths are as in Fig. 8.1, except that the dotted lines show 500-year return values.

A rigorous analysis of this issue could be made by treating precipitation associated with tropical cyclones as being driven by tropical cyclone strike probabilities and envelopes of historic tropical cyclone motion rather than treating all tropical cyclone precipitation as location-specific. In the absence of such an analysis, we estimate regionally consistent return values for southeast Texas by taking averages of groups of lumped return values. One method uses the average of the southeast Texas coastal region and the two adjacent coastal regions, while the other also includes the other Louisiana coastal region, the Alabama coastal region, and the westernmost Florida coastal region. All of these regions are similarly situated with respect to exposure from weather arriving from the Gulf of Mexico.

The results are shown in Table 8.4. The differences at 2-year return periods are small, but the 100-year return period differences range from 13%-18% and the 500-year return period differences range from 18%-25%. The differences are only slightly larger at 4-day durations than at 1-day durations, suggesting that differences at 6-hour durations would be slightly smaller than at 1-day durations.

Table 8.4: Local coastal southeast Texas return values and average return values including nearby coastal regions (three and six regions in total), using lumped qcd data.

	2-YEAR RETURN PERIOD		100-YEAR RETURN PERIOD		500-YEAR RETURN PERIOD	
	1 DAY	4 DAYS	1 DAY	4 DAYS	1 DAY	4 DAYS
SE TX (REG. 3)	5.17	6.87	16.92	23.14	26.01	35.65
3-REG AVG	5.04	6.62	14.68	19.82	21.24	28.85
% DIFFERENCE	-2.5%	-3.6%	-13.3%	-14.3%	-18.3%	-19.1%
6-REG AVG	5.09	6.73	14.08	18.90	19.93	26.93
% DIFFERENCE	-1.5%	-2.0%	-16.8%	-18.3%	-23.4%	-24.5%

We conservatively choose the smaller adjustment of the two that are tested here, and assume that the difference between 6-hour adjustments and 1-day adjustments equals the difference between 1-day adjustments and 4-day adjustments. Table 8.5 shows the updated return values, taking into account both adjustments discussed so far.

Table 8.5: NOAA Atlas 14 regional return values with MLE/ext adjustment and adjustment for unrepresentative spike in southeast Texas coastal return values.

	2-YEAR RETURN PERIOD		100-YEAR RETURN PERIOD		500-YEAR RETURN PERIOD	
	6 HOUR	1 DAY	6 HOUR	1 DAY	6 HOUR	1 DAY
	3.58	4.83	10.7	16.3	15.9	21.7
NOAA ATLAS 14	3.75	5.11	11.3	16.9	16.7	22.9
	3.87	5.30	12.5	18.0	18.2	24.5
MLE/EXT ADJ				-7.2%		
RETURN VALUES	3.32	4.48	9.93	15.1	14.8	20.1
THROUGH	3.48	4.74	10.5	15.7	15.5	21.3
SECTION 8.1	3.59	4.92	11.6	16.7	16.9	22.7
SETX SPIKE ADJ	-1.0%	-1.5%	-12.3%	-13.3%	-17.7%	-18.4%
RETURN VALUES	3.29	4.42	8.71	13.1	12.1	16.4
THROUGH	3.45	4.67	9.20	13.6	12.8	17.4
SECTION 8.2	3.56	4.85	10.2	14.5	13.9	18.6

We note that the revised return values still include the influence of Hurricane Harvey, but that influence (and the influence of other storms) is distributed over a broader area. We also note that a similar region to the 6-region average was chosen by van Oldenborgh et al. (2017) for their estimates of return periods associated with Hurricane Harvey.

8.3 Nonstationary historical analysis

The same factors that make the NOAA Atlas 14 estimates too high as a stationary estimate invalidate the use of the revised stationary estimate for assessment of present-day or future

risk. To the stationary estimate it is necessary to apply an estimate of the long-term trend. Evidence presented in Section 4 suggests that a trend estimate calculated from the local Harris County values is unrepresentatively large and that long-term trends calculated over small geographical areas are unreliable in general.

In the absence of compelling evidence for robust long-term change-driven local trend enhancement, it seems prudent to choose a trend estimate based on precipitation over a broad region. Section 5 presented trend estimates using all 47 regions included in the lumped qcd data. However, it is possible that rainfall with large return periods may be influenced by climate driven trends in hurricane tracks, which tend to fluctuate between greater prevalence along the Gulf Coast and greater prevalence along the southeast Atlantic coast. So we also consider a smaller Gulf Coast region consisting of all regions from the Florida Panhandle and western Georgia westward.

The trends, expressed as the change between return values in the year 1960 and the year 2020, are shown in Table 8.6.

Table 8.6: Region-wide precipitation trends from 1960 to 2020. For 95% confidence intervals, twelve degrees of freedom are assumed for the Gulf Coast & Southeast region and eight degrees of freedom are assumed for the Gulf Coast region.

	2-YEAR RETURN PERIOD		**100-YEAR RETURN PERIOD**		**500-YEAR RETURN PERIOD**	
	GULF COAST AND SE	**GULF COAST ONLY**	**GULF COAST AND SE**	**GULF COAST ONLY**	**GULF COAST AND SE**	**GULF COAST ONLY**
MEAN TRENDS, 1-DAY DURATION	11.2% +/- 4.5%	12.2% +/- 5.5%	13.2% +/- 7.2%	13.4% +/- 8.5%	13.5% +/- 7.8%	13.6% +/- 9.1%
MS2, MS3, TX2, TXC, TXE (1-DAY)	12.4% (11.1% to 13.8%)		13.1% (8.7% to 15.6%)		13.3% (8.0% to 16.5%)	
MEAN TRENDS, 4-DAY DURATION	10.7% +/- 5.3%	11.6% +/- 6.5%	13.3% +/- 8.4%	14.0% +/- 9.3%	13.7% +/- 9.0%	14.5% +/- 9.8%
MS2, MS3, TX2, TXC, TXE (4-DAY)	11.8% (4.1% to 18.2%)		15.0% (5.2% to 25.0%)		15.5% (5.3% to 26.1%)	

The other rows of Table 8.6 shows the average trend and range of trends for five lumped regions in Texas and Mississippi that have been chosen to produce a similar average trend as the region-wide trends for 1-day durations. The average trends across these five regions are similar for 1-day and 4-day durations, though there is greater variability at 4 days.

The purpose of including these five regions is to be able to project percentage changes in Harris County return values using the nonstationary GEV fits of nearby regions that have historic trends similar to those inferred as appropriate for Harris County. Using these five regions, we

compute the percentage difference between the stationary fits and the 1960 values of the nonstationary fits and apply a similar percentage difference to the Harris County return values.

The 1960 2-year return value for 1-day durations is, on average across the five regions, 2.4% smaller than the stationary value. This is similar to the 2.1% stationary-nonstationary return value difference averaged across all 47 lumped regions. The 1960 100-year return values for the five regions average 3.0% smaller, compared to an overall average of 3.1%. For 500-year return values, the reductions are 3.2% and 3.4%, respectively. So the 5-region conversion factors are consistent and applicable.

After the adjustment from stationary to 1960, the percentage trends between 1960 conditions and present-day (2020) conditions for the Gulf Coast Only region are applied to the Harris County return values. The similarity between mean percentage changes at 1 day and 4 days, along with the lack of evidence of differences in regional-scale trends at shorter precipitation durations, justifies applying the 1-day percentage changes to 6-hour durations.

The results of the historical nonstationary analysis are given in Table 8.7.

Table 8.7: NOAA Atlas 14 regional return values with MLE/ext adjustment, adjustment for unrepresentative spike in southeast Texas coastal return values, and nonstationary analysis of return values for 1960 and 2020.

	2-YEAR RETURN PERIOD		100-YEAR RETURN PERIOD		500-YEAR RETURN PERIOD	
	6 HOUR	1 DAY	6 HOUR	1 DAY	6 HOUR	1 DAY
	3.58	4.83	10.7	16.3	15.9	21.7
NOAA ATLAS 14	3.75	5.11	11.3	16.9	16.7	22.9
	3.87	5.30	12.5	18.0	18.2	24.5
MLE/EXT ADJ			-7.2%			
RETURN VALUES	3.32	4.48	9.93	15.1	14.8	20.1
THROUGH	3.48	4.74	10.5	15.7	15.5	21.3
SECTION 8.1	3.59	4.92	11.6	16.7	16.9	22.7
SETX SPIKE ADJ	-1.0%	-1.5%	-12.3%	-13.3%	-17.7%	-18.4%
RETURN VALUES	3.29	4.42	8.71	13.1	12.1	16.4
THROUGH	3.45	4.67	9.20	13.6	12.8	17.4
SECTION 8.2	3.56	4.85	10.2	14.5	13.9	18.6
STATIONARY TO 1960 FACTOR	-2.4%		-3.0%		-3.2%	
1960	3.21	4.31	8.45	12.7	11.8	15.9
NONSTATIONARY	3.36	4.56	8.92	13.2	12.4	16.8
RETURN VALUES	3.47	4.73	9.87	14.0	13.5	18.0
1960 TO 2020 FACTOR	+12.2%		+13.4%		+13.6%	
2020	3.60	4.84	9.58	14.4	13.4	18.1
NONSTATIONARY	3.77	5.12	10.1	15.0	14.0	19.1
RETURN VALUES	3.89	5.31	11.2	15.9	15.3	20.4

8.4 Nonstationary future projections

Present-day nonstationary estimates are important, but what is most relevant is nonstationary estimates for the future because risk going forward is what must be mitigated. The historical analysis used the logarithm of carbon dioxide concentrations as a proxy for global warming intensity. Global mean surface temperature (or some other surface temperature) was not used because phenomena such as El Niño and volcanic eruptions were expected to affect surface temperatures and extreme rainfall differently than how long-term radiative forcing is expected to affect surface temperature and extreme rainfall. Carbon dioxide could be used because its long-term forcing is roughly similar to the total long-term forcing of all greenhouse gases and aerosols.

For future projections, it would be desirable to use projections of global mean surface temperature, since the warming itself, rather than the radiative forcing, is what is understood

to drive changes in extreme rainfall frequency. To do this, we scale future temperatures by the ratio of historic global warming and historic carbon dioxide changes and apply those scaled values to the nonstationary GEV results.

The historical global temperature change to date from around the beginning of the 20th century is approximately 1.0 °C to 1.2 °C (Fig. 8.3). We use a central estimate of 1.1 °C for warming to date, and project future return values for extreme rainfall corresponding to total global warming of 1.5 °C, 2.0 °C, 2.5 °C, and 3.0 °C. We do not adjust for the slight mismatch between observation-based global mean surface temperature and model-based global surface air temperature (Richardson et al. 2018). The Paris Accords call for global nations to keep global warming below 2.0 °C and to attempt to keep global warming below 1.5 °C.

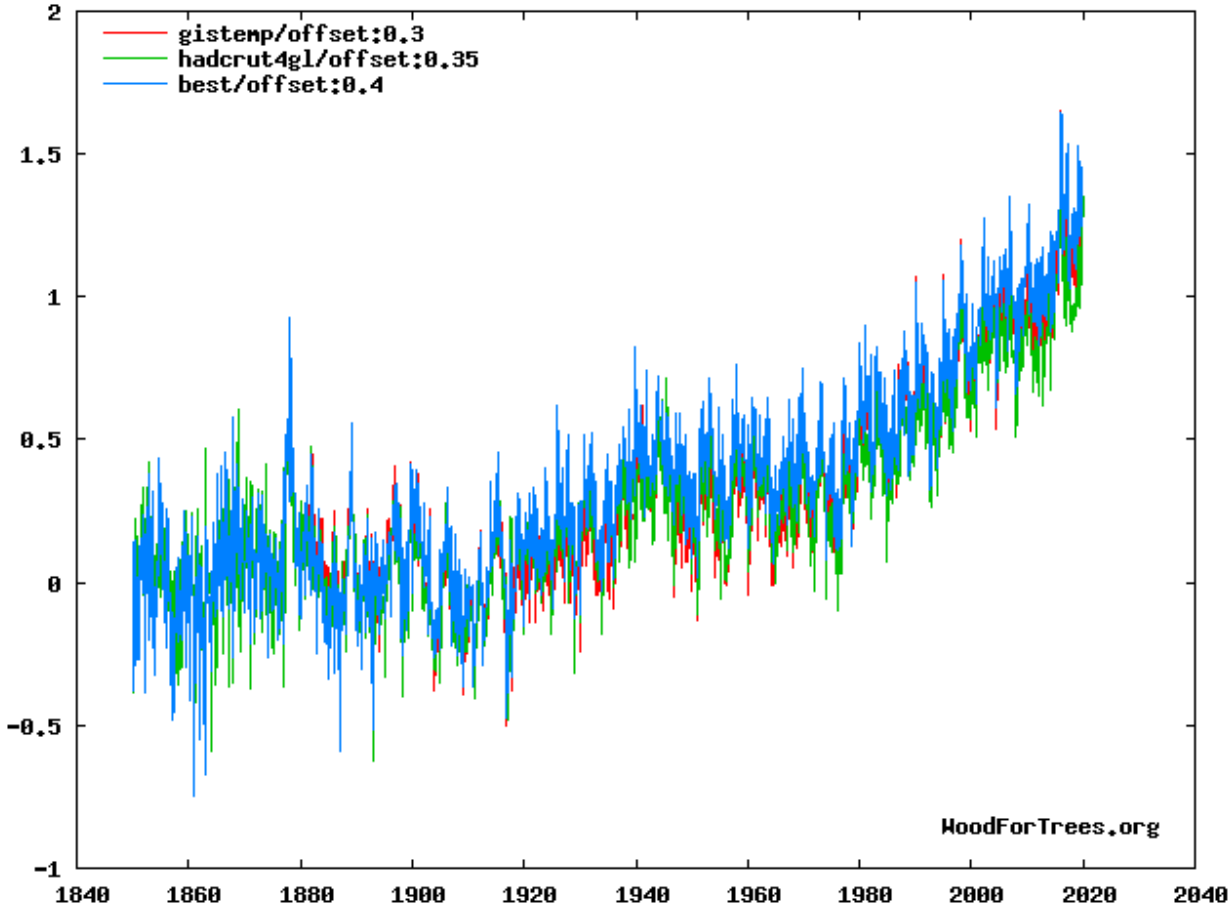

Figure 8.3: Global mean surface temperatures, with zero representing temperatures around the turn of the century (1850-1920). The three data sets are GISTEMP (red, Lenssen et al. 2019, GISTEMP Team 2020), HadCRUT4 (green, Morice et al. 2012), and BEST (blue, Rohde et al. 2012).

Here is an example of the calculation of a precipitation return value for a warming of 1.5 °C since the beginning of the 20th century. The present-day warming is 1.1 °C, so 1.5 °C corresponds to additional warming of 0.4 °C. The warming between 1960 and 2020 was about 0.8 °C, and that corresponded with an increase of ln(CO2) of 0.229. Additional warming of 0.4

°C would be a factor of (0.8 + 0.4)/0.8 = 1.5 increase since 1960, equivalent to a 0.229*1.5 = 0.435 increase of ln(CO2). We apply a ln(CO2) increase of 0.435 to each of the Gulf Coast regions and compute the fractional increase of return value in each region. We then apply the average fractional increase to the 1960 Harris County return values, thereby obtaining return values that correspond to a total global warming of 1.5 °C.

Table 8.8 presents the original NOAA Atlas 14 return values and the nonstationary return values for the present day and for total warming of 1.5-3.0 °C.

Table 8.8: NOAA Atlas 14 original return values and nonstationary analysis of return values for 1960, 2020, and temperatures of 1.5-3.0 °C above preindustrial (0.4-1.9 °C above present-day). Values larger than NOAA Atlas 14 are bolded.

	2-YEAR RETURN PERIOD		**100-YEAR RETURN PERIOD**		**500-YEAR RETURN PERIOD**	
	6 HOUR	**1 DAY**	**6 HOUR**	**1 DAY**	**6 HOUR**	**1 DAY**
	3.58	4.83	10.7	16.3	15.9	21.7
NOAA ATLAS 14	3.75	5.11	11.3	16.9	16.7	22.9
	3.87	5.30	12.5	18.0	18.2	24.5
	3.21	4.31	8.45	12.7	11.8	15.9
1960 VALUES	3.36	4.56	8.92	13.2	12.4	16.8
	3.47	4.73	9.87	14.0	13.5	18.0
1.1 °C INCREASE	12.2%		13.4%		13.6%	
	3.60	**4.84**	9.58	14.4	13.4	18.1
2020 VALUES	**3.77**	**5.12**	10.1	15.0	14.0	19.1
	3.89	**5.31**	11.2	15.9	15.3	20.4
1.5 °C INCREASE	18.0%		20.4%		20.8%	
	3.79	**5.09**	10.2	15.3	14.2	19.2
1.5 °C VALUES	**3.97**	**5.38**	10.7	15.9	14.9	20.3
	4.10	**5.58**	11.9	16.9	16.3	21.7
2.0 °C INCREASE	25.5%		30.1%		31.0%	
	4.03	**5.41**	**11.0**	**16.6**	15.4	20.8
2.0 °C VALUES	**4.22**	**5.72**	**11.6**	**17.2**	15.2	22.0
	4.36	**5.94**	**12.8**	**18.3**	17.6	23.5
2.5 °C INCREASE	33.4%		41.2%		42.7%	
	4.28	**5.75**	**11.9**	**18.0**	**16.8**	**22.7**
2.5 °C VALUES	**4.49**	**6.08**	**12.6**	**18.6**	**17.6**	**24.0**
	4.63	**6.31**	**13.9**	**19.8**	**19.2**	**25.6**
3.0 °C INCREASE	41.7%		54.0%		56.2%	
	4.55	**6.11**	**13.0**	**19.6**	**18.4**	**24.9**
3.0 °C VALUES	**4.77**	**6.46**	**13.7**	**20.3**	**1893**	**26.2**
	4.92	**6.70**	**15.2**	**21.6**	**21.0**	**28.1**

The return values in Table 4.8 are dependent on historic CO2 concentrations, historic temperatures, and observed extreme precipitation. To convert them into projections of future return values, it is necessary to project when the global mean temperature will attain those temperature values in a typical year. Such a projection depends on the scenario of future greenhouse gas emissions and other anthropogenic factors, the sensitivity of the climate to those changes, and variations in solar output, volcanic activity, and other forms of natural variability. Those projections will be refined over time as knowledge of the climate system improves and societal paths are laid out, but the return values in Table 8.8 are independent of those factors.

For reference, we provide the years at which these thresholds are achieved according to the average of CMIP5 model simulations for the RCP 2.6, RCP 4.5, and RCP 8.5 scenarios (Knutti and Sedlacek, 2013). RCP 8.5 is a high-end business-as-usual scenario, while RCP 2.6 would involve massive removal of carbon dioxide from the atmosphere. We consider something intermediate between RCP 4.5 scenario to be best for planning purposes: it reflects some action to constrain climate change but not nearly enough to meet the Paris targets. We label this projection 'Planning'. It projects a total global warming of 3.0 °C by the year 2100. Allowance is made in the Planning scenario for the fact that present-day temperatures are slightly lagging the model projections, which led the IPCC AR5 Report to project that temperatures over the next few decades were likely to continue to lag model projections (Kirtman et al. 2013).

Table 8.9: Years in which CMIP5 climate model consensus projects certain global temperature thresholds to be achieved. For thresholds that are never exceeded, the maximum achieved temperature is listed.

T ABOVE PREINDUSTRIAL	ACTUAL	RCP 2.6	RCP 4.5	RCP 8.5	PLANNING
1.1 °C	2020	2015	2015	2015	2020
1.5 °C	?	2035	2032	2028	2035
2.0 °C	?	max 1.65 °C	2052	2042	2052
2.5 °C	?	max 1.65 °C	2100	2052	2070
3.0 °C	?	max 1.65 °C	max 2.6 °C	2065	2100

As future scenarios and climate sensitivity become clearer and more precisely estimated, the years corresponding to the various temperature thresholds can be updated. For example, output from the newest generation of climate models (CMIP6) is becoming available, but the model output includes a wide range of potential future warming rates. Also, more data and improved methods will in the future permit better estimates of the dependence of local extreme rainfall on changing global temperatures.

8.5 Final comments

The assumptions in this analysis are many. For example, this analysis has lumped all forms of extreme precipitation together. There is evidence that tropical cyclone precipitation is

increasing in the United States at a faster rate than other forms of extreme precipitation (Kunkel et al. 2010; Dhakal and Jain 2019), so a more comprehensive assessment of future risk ought to treat the time-dependent risk from tropical cyclone rainfall separately from the time-dependent risk from other forms of extreme rainfall. Also, the assessment that local-scale trend variations are purely random needs greater statistical support. Analyses with different techniques for obtaining statistical fits to the data may yield different results. Lastly, some natural variability may be aliased onto the long-term trends, even when averaged across the entire Gulf Coast region.

According to this analysis, nonstationary 2-year return values in Harris County already slightly exceed the NOAA Atlas 14 design values, while more extreme return values still lag the NOAA Atlas 14 design values. Although it depends on the rate of future climate change, the 100-year return values are on track to exceed the current NOAA Atlas 14 design values around the middle of the 21st century, with 500-year return values exceeding the NOAA Atlas 14 design values a decade or two later.

While there is large uncertainty in these estimates, they are more comprehensive than those produced by a traditional stationary analysis in which additional uncertainty is hidden in the simplified structure of the statistical model.

Acknowledgements

This research was supported by Harris County via the Harris County Flood Control District. The opinions in this report are solely those of the author and do not necessarily represent those of the Harris County Flood Control District or Harris County. The author is grateful for the assistance of Judy Dickey, Savannah Jorgensen, Alex Smith, Brandon Gale, and Taylor Wells in the preparation of this report.

References

Aryal, Y. N., G. Villarini, W. Zhang, and G. A. Vecchi, 2018: Long term changes in flooding and heavy rainfall associated with North Atlantic tropical cyclones: Roles of the North Atlantic Oscillation and El Nino-Southern Oscillation. *Journal of Hydrology*, **559,** 698-710, 10.1016/j.jhydrol.2018.02.072.

Brown, V. M., B. D. Keim, and A. W. Black, 2020: Trend Analysis of Multiple Extreme Hourly Precipitation Time Series in the Southeastern United States. *Journal of Applied Meteorology and Climatology*, **59,** 427-442, 10.1175/jamc-d-19-0119.1.

Chen, G., J. Norris, J. D. Neelin, J. Lu, L. R. Leung, and K. Sakaguchi, 2019: Thermodynamic and Dynamic Mechanisms for Hydrological Cycle Intensification over the Full Probability Distribution of Precipitation Events. *Journal of the Atmospheric Sciences*, **76,** 497-516, 10.1175/jas-d-18-0067.1.

Chin, D. A., M. A. Jacketti, N. S. Karpathy, and P. J. Sahwell, 2019: Accounting for Tropical Cyclones in Extreme Rainfall Distributions in Florida. *Journal of Hydrologic Engineering*, **24,** 05019028, doi:10.1061/(ASCE)HE.1943-5584.0001858.

Dhakal, N., and S. Jain, 2019: Nonstationary influence of the North Atlantic tropical cyclones on the spatio-temporal variability of the eastern United States precipitation extremes. *Int. J. Climatol.,* 1-14, doi:10.1002/joc.6409.

Donat, M. G., A. L. Lowry, L. V. Alexander, P. A. O'Gorman, and N. Maher, 2016: More extreme precipitation in the world's dry and wet regions. *Nature Climate Change*, **6,** 508-513, 10.1038/nclimate2941.

Easterling, D.R., K.E. Kunkel, J.R. Arnold, T. Knutson, A.N. LeGrande, L.R. Leung, R.S. Vose, D.E. Waliser, and M.F. Wehner, 2017: Precipitation change in the United States. In: *Climate Science Special Report: Fourth National Climate Assessment, Volume 1* [Wuebbles, D.J., D.W. Fahey, K.A. Hibbard, D.J. Dokken, B.C. Stewart. and T.K. Maycock (eds.)]. U.S. Global Change Research Program, Washington, DC, USA, pp. 207-230, doi:10.7930/J0H993CC.

El Adlouni, S., T. B. M. J. Ouarda, X. Zhang, R. Roy, and B. Bobée, 2007: Generalized maximum likelihood estimators for the nonstationary generalized extreme value model, *Water Resour. Res.*, 43, W03410, doi:10.1029/2005WR004545.

Feng, X., C. Liu, F. Xie, J. Lu, L. S. Chiu, G. Tintera, and B. Chen, 2019: Precipitation characteristic changes due to global warming in a high-resolution (16 km) ECMWF simulation. *Quarterly Journal of the Royal Meteorological Society*, **145,** 303-317, 10.1002/qj.3432.

Fischer, E. M., and R. Knutti, 2016: Observed heavy precipitation increase confirms theory and early models. *Nature Climate Change*, **6,** 986-991, 10.1038/nclimate3110.

Giorgi, F., F. Faffaele, and E. Coppola, 2019: The response of precipitation characteristics to global warming from climate projections. *Earth Syst. Dynam*., 10, 73-89, doi:10.5194/esd-10-73-2019.

GISTEMP Team, 2020: *GISS Surface Temperature Analysis (GISTEMP), version 4.* NASA Goddard Institute for Space Studies. Dataset accessed via woodfortrees.org on 2020-04-12.

Hall, T. M., and J. P. Kossin, 2019: Hurricane stalling along the North American coast and implications for rainfall. *npj Climate and Atmospheric Science*, **2,** 17, 10.1038/s41612-019-0074-8.

Hershfeld, D.M., 1961: *Technical Paper No. 40: Rainfall Frequency Atlas of the United States for Durations from 30 Minutes to 24 Hours and Return Periods from 1 to 100 Years*. U.S. Department of Commerce, Washington, DC.

Hollebrandse, A.P., S. Gillespie, W. Asquith, and J.R.M. Hosking, 2015: lmoments3 Library documentation, Version 1.0. Revision d941a9a8, https://open-hydrology.readthedocs.io/projects/lmoments3/en/stable/ , accessed April 4, 2020.

Hosking, J.R.M., and J.R. Wallis, 1997: *Regional Frequency Analysis: An Approach Based on L-Moments.* Cambridge University Press, ISBN:0-521-43045-3.

Kirtman, B., and Coauthors, 2013: Near-term Climate Change: Projections and Predictability. *Climate Change 2013: The Physical Science Basis. Contribution of Working Group I to the Fifth Assessment Report of the Intergovernmental Panel on Climate Change*, T. F. Stocker, and Coauthors, Eds., Cambridge University Press.

Knutson, T., and Coauthors, 2019: Tropical Cyclones and Climate Change Assessment: Part I: Detection and Attribution. *Bulletin of the American Meteorological Society*, **100,** 1987-2007, 10.1175/bams-d-18-0189.1.

Knutson, T., and Coauthors, 2020: Tropical Cyclones and Climate Change Assessment: Part II: Projected Response to Anthropogenic Warming. *Bulletin of the American Meteorological Society*, **101,** E303-E322, 10.1175/bams-d-18-0194.1.

Knutti, R., and J. Sedlacek, 2013: Robustness and uncertainties in the new CMIP5 climate model projections. *Nature Climate Change*, **3,** 369-373, 10.1038/nclimate1716.

Kunkel, K. E., and S. M. Champion, 2019: An Assessment of Rainfall from Hurricanes Harvey and Florence Relative to Other Extremely Wet Storms in the United States. *Geophysical Research Letters*, **46,** 13500-13506, 10.1029/2019gl085034.

Kunkel, K.E., D.R. Easterling, D.A.R. Kristovich, B. Gleason, L. Stoecker, and R. Smith, 2010: Recent increases in U.S. heavy precipitation associated with tropical cyclones. *Geophys. Res. Lett,* 37, L24706 doi:10.1029/2010GL045164.

Kunkel, K. E., and Coauthors, 2013: Monitoring and Understanding Trends in Extreme Storms: State of Knowledge. *Bulletin of the American Meteorological Society*, **94,** 499-514, 10.1175/bams-d-11-00262.1.

Kunkel, K. E., T. R. Karl, M. F. Squires, X. Yin, S. T. Stegall, and D. R. Easterling, 2020: Precipitation Extremes: Trends and Relationships with Average Precipitation and Precipitable Water in the Contiguous United States. *Journal of Applied Meteorology and Climatology*, **59,** 125-142, 10.1175/jamc-d-19-0185.1.

Lenssen, N., G. Schmidt, J. Hansen, M. Menne, A. Persin, R. Ruedy, and D. Zyss, 2019: Improvements in the GISTEMP uncertainty model. *J. Geophys. Res. Atmos.*, **124**, no. 12, 6307-6326, doi:10.1029/2018JD029522.

Li, J., T. Y. Gan, Y. D. Chen, X. Gu, Z. Hu, Q. Zhou, and Y. Lai, 2020: Tackling resolution mismatch of precipitation extremes from gridded GCMs and site-scale observations: Implication to assessment and future projection. *Atmospheric Research*, **239,** 104908, doi:10.1016/j.atmosres.2020.104908.

Li, Z., X. Li, Y. Wang, and S.M. Quiring, 2019: Impact of climate change on precipitation patterns in Houston, Texas, USA. *Anthropocene,* 25, 100193, doi:10.1016/j.ancene.2019.100193.

Martins, E. S., and J. R. Stedinger, 2000: Generalized maximum-likelihood generalized extreme-value quantile estimators for hydrologic data. *Water Resour. Res.*, 36(3), 737–744, doi:10.1029/1999WR900330.

Mascioli, N. R., A. M. Fiore, M. Previdi, and G. Correa, 2016: Temperature and Precipitation Extremes in the United States: Quantifying the Responses to Anthropogenic Aerosols and Greenhouse Gases(,+). *Journal of Climate*, **29,** 2689-2701, 10.1175/jcli-d-15-0478.1.

Menne, M.J., I. Durre, R.S. Vose, B.E. Gleason, and T.G. Houston, 2012: An overview of the Global Historical Climatology Network-Daily database. *J. Atmos. Ocean. Tech*., 29, 897-910, doi:10.1175/JTEH-D-11-00103.1.

Morice, C. P., J. J. Kennedy, N. A. Rayner, and P. D. Jones, 2012: Quantifying uncertainties in global and regional temperature change using an ensemble of observational estimates: The HadCRUT4 data set. *Journal of Geophysical Research: Atmospheres*, **117**, 10.1029/2011jd017187.

Myhre, G., E. J. Highwood, K. P. Shine, and F. Stordal, 1998: New estimates of radiative forcing due to well mixed greenhouse gases. *Geophysical Research Letters*, **25,** 2715-2718, 10.1029/98gl01908.

Orville, R., and Coauthors, 2001: Enhancement of cloud-to-ground lightning over Houston, Texas. *Geophysical Research Letters*, **28,** 2597-2600, 10.1029/2001GL012990.

Paciorek, C.J., D.A. Stone, and M.F. Wehner, 2018: Quantifying statistical uncertainty in the attribution of human influence on severe weather. *Weather and Climate Extremes*, 20, 69-80, doi:10.1016/j.wace.2018.01.002.

Pan, Y., C. Yan, and C. L. Archer, 2018: Precipitation reduction during Hurricane Harvey with simulated offshore wind farms. *Environmental Research Letters*, **13**, 10.1088/1748-9326/aad245.

Pendergrass, A. G., and D. L. Hartmann, 2014: Changes in the Distribution of Rain Frequency and Intensity in Response to Global Warming. *Journal of Climate*, **27,** 8372-8383, 10.1175/jcli-d-14-00183.1.

Perica, S., S. Pavlovic, M. St. Laurent, C. Trypaluk, D. Unruh, O. Wilhite, 2018: *NOAA Atlas 14: Precipitation-Frequency Atlas of the United States, Volume 11 Version 2.0: Texas.* U.S. Department of Commerce, National Oceanic and Atmospheric Administration, National Weather Service, Silvers Spring, Maryland.

Pfahl, S., P. A. O'Gorman, and E. M. Fischer, 2017: Understanding the regional pattern of projected future changes in extreme precipitation. *Nature Climate Change*, **7,** 423, 10.1038/nclimate3287.

Requena, A. I., D. H. Burn, P. Coulibaly, 2019: Pooled frequency analysis for intensity–duration–frequency curve estimation. *Hydrological Processes*, 33, 2080–2094, 10.1002/hyp.13456.

Richardson, M., K. Cowtan, and R. J. Millar, 2018: Global temperature definition affects achievement of long-term climate goals. *Environmental Research Letters*, **13,** 054004, 10.1088/1748-9326/aab305.

Risser, M.D., and M.F. Wehner, 2017: Attributable human-induced changes in the likelihood and magnitude of the observed extreme precipitation during Hurricane Harvey. *Geophys. Res. Lett*., 44, 12457-12464, doi:10.1002/2017GL075888.

Rohde, R., R. A. Muller, et al. (2013) *A New Estimate of the Average Earth Surface Land Temperature Spanning 1753 to 2011*. Geoinfor Geostat: An Overview 1:1.. doi:10.4172/gigs.1000101

Russell. B.T., M.D. Risser, R.L. Smith, and K.E. Kunkel, 2019: Investigating the association between late spring Gulf of Mexico sea surface temperatures and U.S. Gulf Coast precipitation extremes with focus on Hurricane Harvey. *Environmetrics*, 31:e2595, doi:10.1002/env.2595.

Sanderson, B.M., C. Wobus, D. Mills, C. Zarakas, A. Crimmins, M.C. Sarofim, and C. Weaver, 2019: Informing future risks of record-level rainfall in the United States. *Geophys. Res. Lett.,* 46, 3963-3972, doi:10.1029/2019GL082362.

Shepherd, J. M., M. Carter, M. Manyin, D. Messen, and S. Burian, 2010: The impact of urbanization on current and future coastal precipitation: a case study for Houston. *Environment and Planning B-Planning & Design*, **37,** 284-304, 10.1068/b34102t.

van der Wiel, K., and Coauthors, 2016: The Resolution Dependence of Contiguous U.S. Precipitation Extremes in Response to CO2 Forcing. *Journal of Climate*, **29,** 7991-8012, 10.1175/jcli-d-16-0307.1.

van Oldenborgh, G.J., K. van der Wiel, A. Sebastian, R. Singh, J. Arrighi, F. Otto, K. Haustein, S. Li, G. Vecchi, and H. Cullen, 2017: Attribution of extreme rainfall from Hurricane Harvey, August 2017. *Env. Res. Lett.* 12, 019501, doi:10.1088/1748-9326/aa9ef2, *with corrigendum Env. Res. Lett*. 12, 124009, doi:10.1088/1748-9326/aaa343.

van Oldenborgh, G.J., K. van der Wiel, S. Philip, S. Kew, A. Sebastian, F. Otto, K. Haustein, R. Singh, J. Arrighi, and G. Vecchi, 2019: Rapid attribution of the extreme rainfall in Texas from Tropical Storm Imelda. World Weather Attribution, 16 pp. Accessed April 6, 2020 from https://www.worldweatherattribution.org/rapid-attribution-of-the-extreme-rainfall-in-texas-from-tropical-storm-imelda/ .

Villarini, G., and J. A. Smith, 2013: Flooding in Texas: Examination of temporal changes and impacts of tropical cyclones. *Journal of the American Water Resources Association*, **49,** 825-837, 10.1111/jawr.12042.

Vu, T. M., and A. K. Mishra, 2019: Nonstationary frequency analysis of the recent extreme precipitation events in the United States. *Journal of Hydrology*, **575,** 999-1010, https://doi.org/10.1016/j.jhydrol.2019.05.090.

Wang, S.-Y. S., L. Zhao, J.-H. Yoon, P. Klotzbach, and R.R. Gillies, 2018: Quantitative attribution of climate effects on Hurricane Harvey's extreme rainfall in Texas. *Env. Res. Lett*., 13, 054014, doi:10.1088/1748-9326/aabb85.

Westra, S., and Coauthors, 2014: Future changes to the intensity and frequency of short-duration extreme rainfall. *Reviews of Geophysics*, **52,** 522-555, 10.1002/2014rg000464.

Wright, D. B., C. D. Bosma, and T. Lopez-Cantu, 2019: U.S. Hydrologic Design Standards Insufficient Due to Large Increases in Frequency of Rainfall Extremes. *Geophysical Research Letters*, **46,** 8144-8153, 10.1029/2019gl083235.

Yin, J., D.-L. Zhang, Y. Luo, and R. Ma, 2020: On the Extreme Rainfall Event of 7 May 2017 over the Coastal City of Guangzhou. Part I: Impacts of Urbanization and Orography. *Monthly Weather Review*, **148,** 955-979, 10.1175/mwr-d-19-0212.1.

Yung, A.C., 2019: *Recommendations for: Rainfall Depths and Intensities in Harris County*. MAAPnext Modeling, Assessment & Awareness Project White Paper #1, Walter P. Moore and Associates, Inc., revised 5/31/2019, 14 pp.

Zhang, W., G. Villarini, E. Scoccimarro, and G. A. Vecchi, 2017: Stronger influences of increased CO2 on subdaily precipitation extremes than at the daily scale. *Geophysical Research Letters*, **44,** 7464-7471, 10.1002/2017gl074024.

Zhang, W., G. Villarini, G. A. Vecchi, and J. A. Smith, 2018: Urbanization exacerbated the rainfall and flooding caused by hurricane Harvey in Houston. *Nature*, **563,** 384-388, 10.1038/s41586-018-0676-z.

Zhu, L. Y., S. M. Quiring, and K. A. Emanuel, 2013: Estimating tropical cyclone precipitation risk in Texas. *Geophysical Research Letters*, **40,** 6225-6230, 10.1002/2013gl058284.

APPENDIX A: Creation of the ext Data Set

This appendix describes the process for creating the ext data set from the NOAA Atlas 14 data set. Examples are provided of the locations of observations that are used to extend the data record at particular locations.

The conventional approach for pooling stations involves the use of an index storm, a common reference storm whose differences across stations are used to adjust the station precipitation values when combining or pooling data among stations. This approach works when the (well-constrained) index storm values are applicable to the (poorly constrained) large return period rainfall values. We prefer not to make that assumption here, because (as recent storms such as Harvey and Imelda demonstrate) large return period rainfall values are often produced by individual tropical storms whose frequency and intensity are not reflected in common index storm types such as mean annual precipitation or median block maximum. The approach we follow here makes no such assumption, instead assuming that whatever processes control extreme rainfall amounts vary continuously and smoothly (small second derivatives) across the region from which data are drawn to extend a particular station.

The process proceeds chronologically from the starting year of the ext data set (1941 for less than 24-hour durations, 1895 for one day or longer). If data is missing at a particular year and target station, a search is made of all surrounding stations for non-missing data. At each such surrounding candidate station, a cost function is calculated. The cost function is defined as the average distance between the mean location of all observations used at the target station, including the candidate observation, and the actual target station location.
The observation that minimizes this cost function is added to the ext observation set for the target station.

The reason for using this algorithm, rather than simply using observations from the closest available station, is that typically the closest available station will be subject to extreme rainfall to a greater or lesser extent than at the target station. By choosing data whose average location is collectively as close as possible to the target station, the expected extreme rainfall is also as close as possible to that of the target station.

At the stations used to calculate the regional averages in the Harris County drainage areas, approximately half of the data points in the ext data are from neighboring stations. In other words, the nominal length of the data record is twice as long in the ext data as in the raw data.

Three stations, one from each region, are chosen to illustrate the use of data from multiple stations. At Waller (41-9448), the 6-hr data begins in 1987, making for 31 annual maxima. The other 36 annual maxima from 1941 through 1986 are drawn from surrounding stations. Figure A1 shows the station locations and the relative frequency of data used from them. Single annual maxima are used from stations as far away as Galveston and Wheelock; distant observations from the northwest and southeast are used with equal frequency, as are distant observations from the northeast and southwest.

Both Houston Independent Heights and Armand Bayou have closer stations available to draw from, so the footprint of their ext data is not as large (Figs. A2-A3). Both stations' ext data draw upon Houston WB City and Houston Intercontinental Airport frequently; Independent Heights balances them with data farther to the west, while Armand Bayou balances them with data farther to the southeast.

A somewhat different set of stations drawn upon for the 1-day ext data at these three stations (Figs. A4-A6). While the other stations have more than 70 years of annual maximum 1-day rainfall data, Armand Bayou only has 31 years of daily data and therefore its ext data includes 92 years of annual maxima from nearby stations. Nonetheless, there are several long-term stations nearby, so relatively little data needs to be drawn from more than 30 miles away.

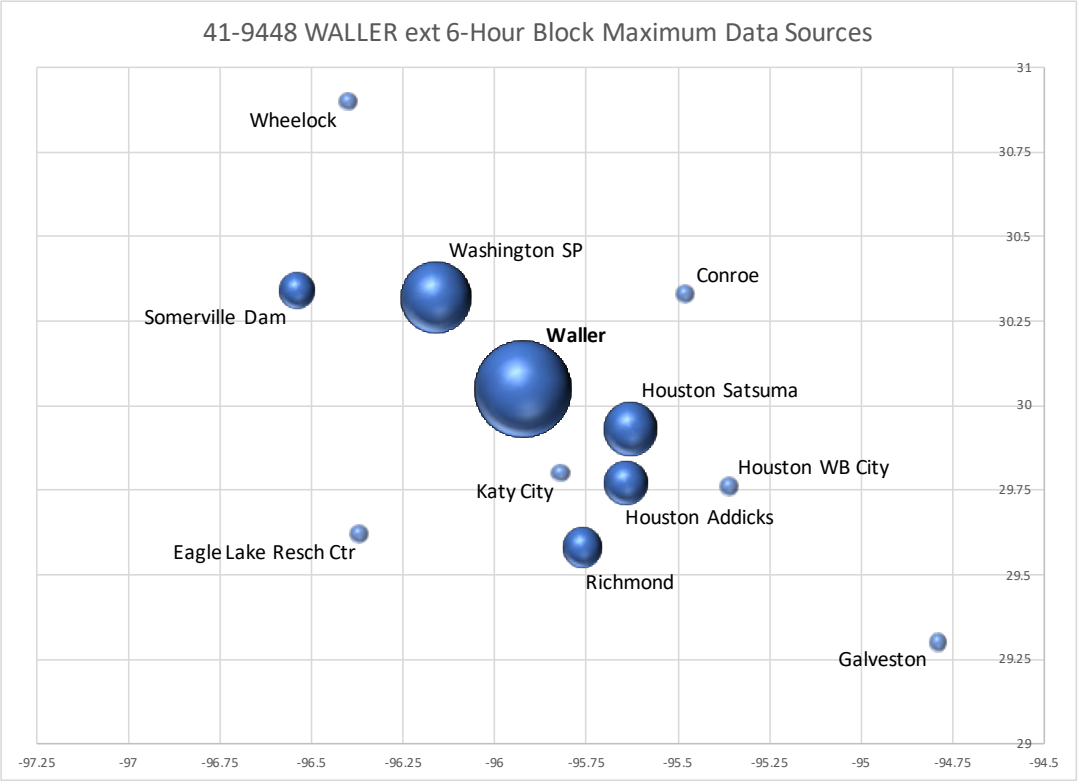

Figure A1: Locations of data used to create the Waller ext 6-hour annual maximum data set. The size of each circle is proportional to the number of observations used from each station.

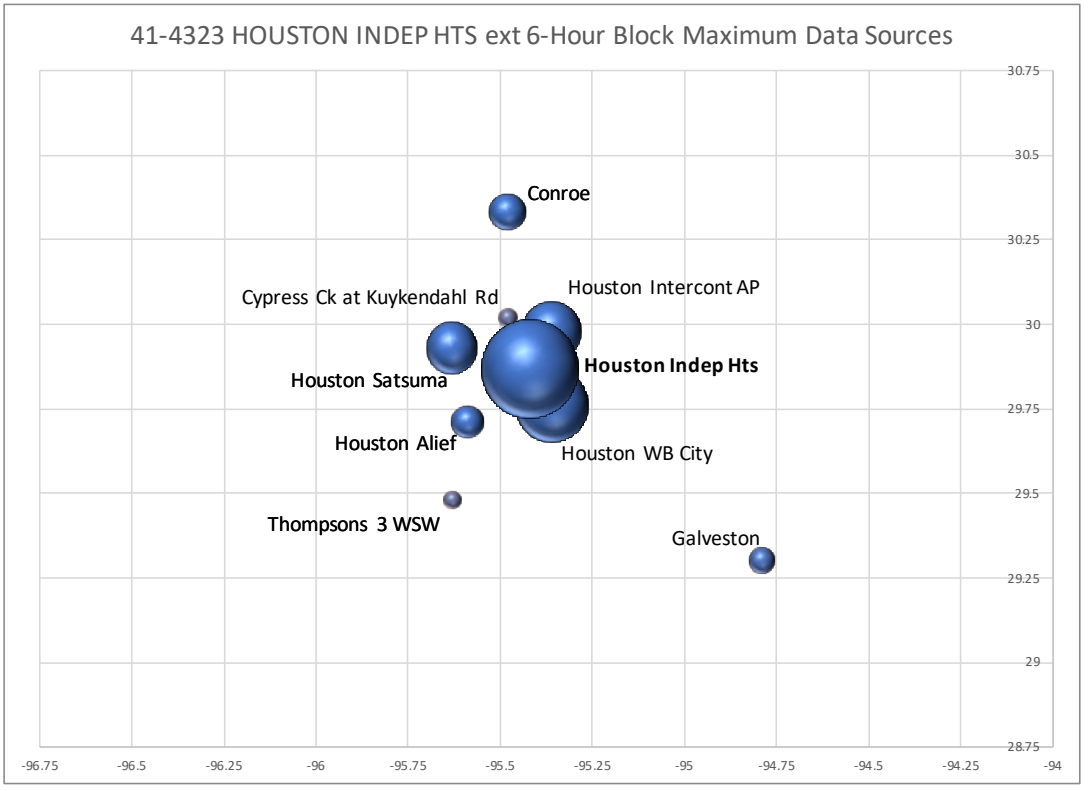

Figure A2: Locations of data used to create the Houston Indep Hts ext 6-hour annual maximum data set. The size of each circle is proportional to the number of observations used from each station.

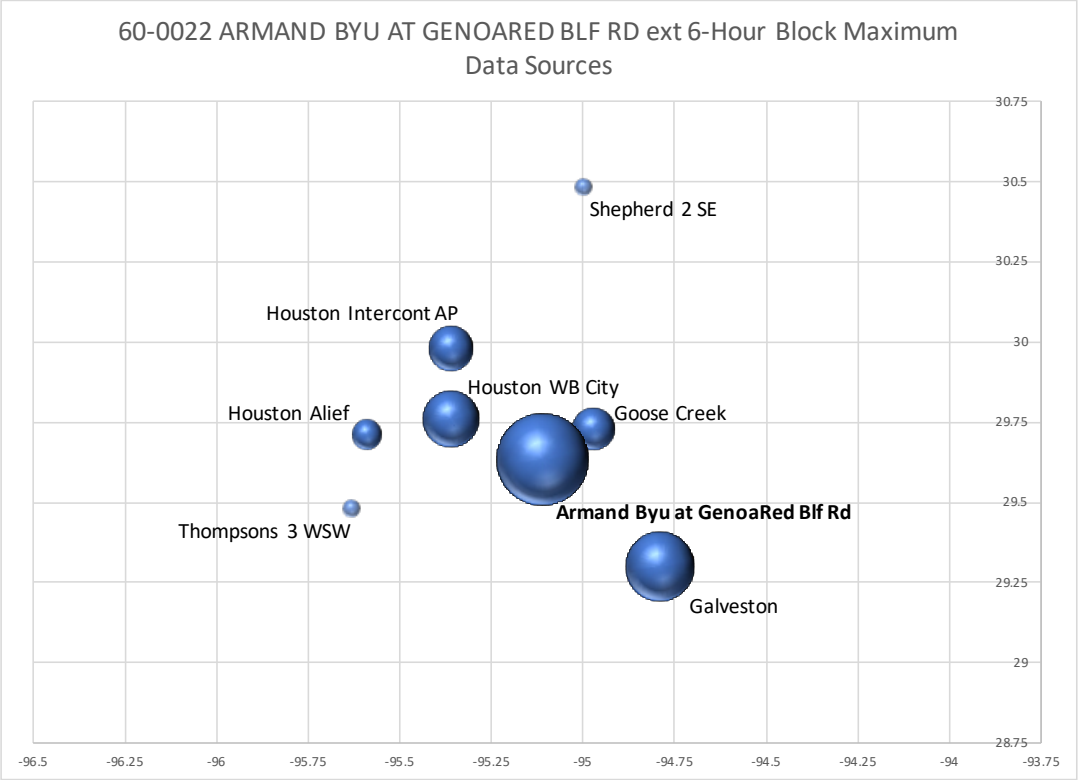

Figure A3: Locations of data used to create the Armand Bayou at Genoa-Red Bluff Rd ext 6-hour annual maximum data set. The size of each circle is proportional to the number of observations used from each station.

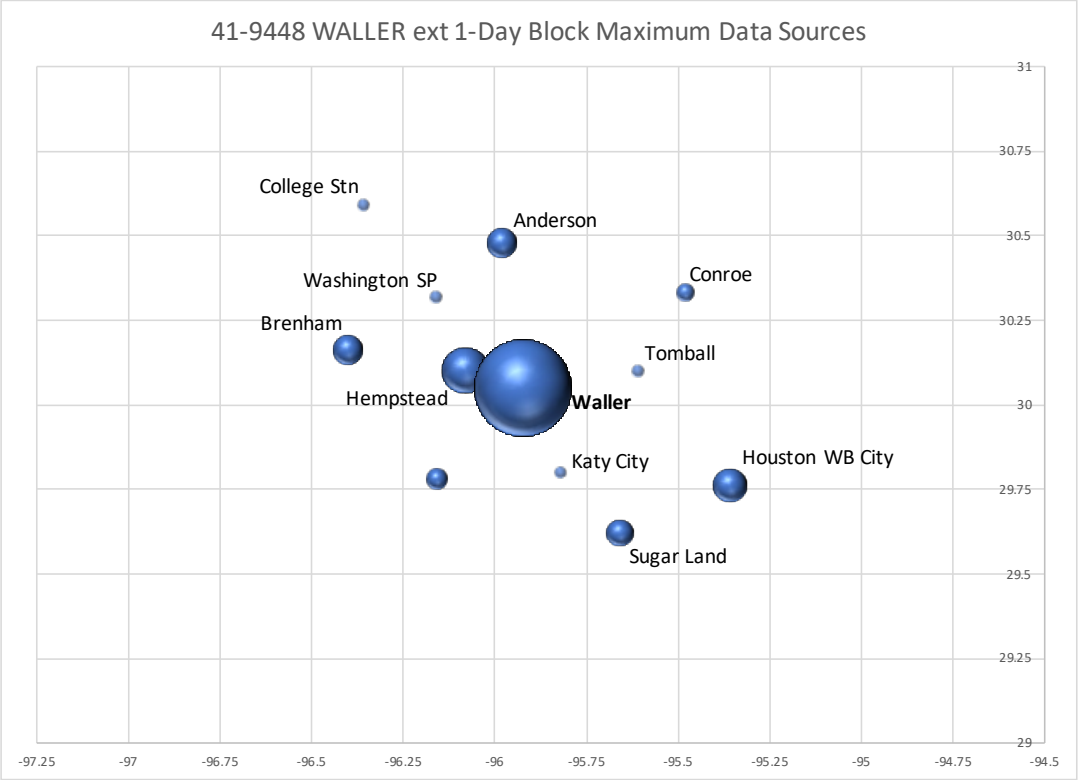

Figure A4: Locations of data used to create the Waller ext 1-day annual maximum data set. The size of each circle is proportional to the number of observations used from each station.

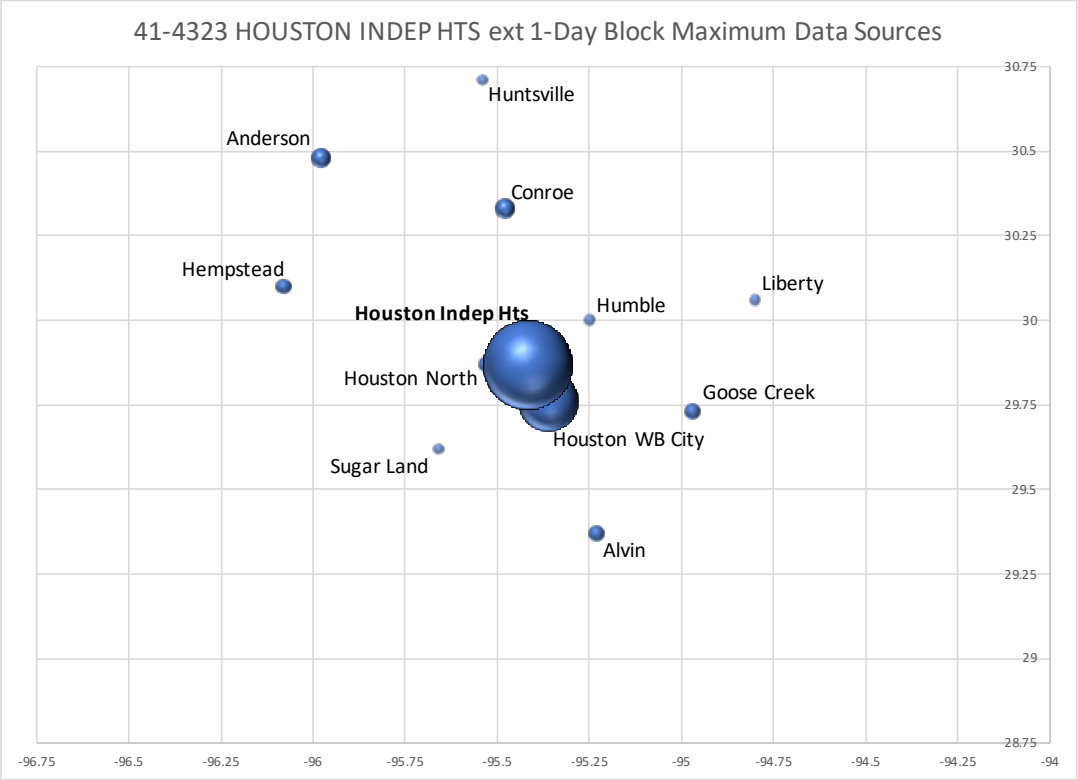

Figure A5: Locations of data used to create the Houston Indep Hts ext 1-day annual maximum data set. The size of each circle is proportional to the number of observations used from each station.

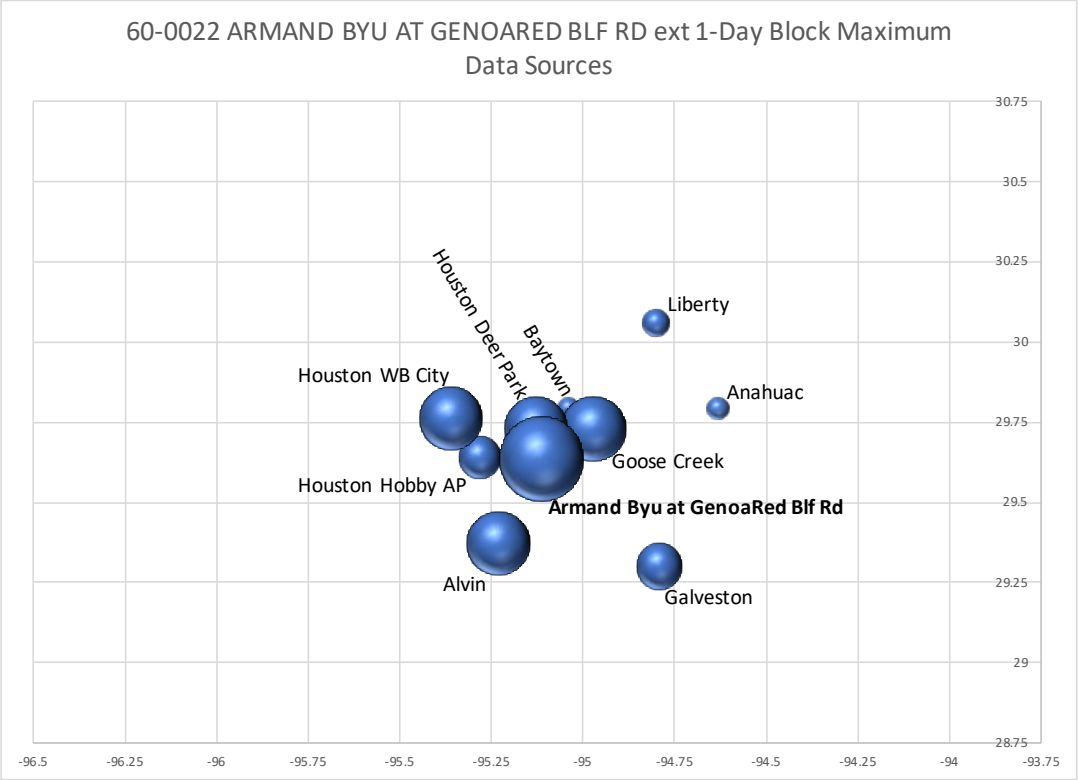

Figure A6: Locations of data used to create the Armand Bayou at Genoa-Red Bluff Rd ext 1-day annual maximum data set. The size of each circle is proportional to the number of observations used from each station.

APPENDIX B: Definition of Regions

Presented here is the state-by-state definition of counties comprising each region in the ful and qcd data sets, as it appears in the Jupyter Notebooks used for analysis. The regions designated 'coastal' and 'inland' in Section 8.2 are:

Coastal: TX9, TX5, TX3, LA1, LA2, MS2, AL1, FL1, FL2, GA3, SC1, SC2, NC2, NC3
Inland: TX8, TX4, TX2, TX1, LA4, LA3, MS1, MS4, AL3, AL2, GA1, GA2, SC3, NC1

```
regions['AL'] = {'Region 1':['Washington','Clarke','Monroe','Conecuh',
                             'Mobile','Baldwin','Escambia'],
                 'Region 2':['Butler','Crenshaw','Pike','Barbour','Covington',
                             'Coffee','Dale','Henry','Geneva','Houston'],
                 'Region 3':['Sumter','Greene','Hale','Perry','Bibb',
                             'Choctaw','Marengo','Wilcox','Dallas'],
                 'Region 4':['Chilton','Coosa','Tallapoosa','Autauga','Elmore','Macon',
                             'Lee','Lowndes','Montgomery','Bullock','Russell']}

regions['FL'] = {'Region 1':['Escambia','Santa Rosa','Okaloosa','Walton','Holmes','Jackson',
                             'Washington','Bay','Calhoun','Gulf'],
                 'Region 2':['Franklin','Liberty','Gadsden','Leon','Wakulla','Jefferson',
                             'Madison','Hamilton','Taylor','Lafayette','Suwannee','Dixie'],
                 'Region 3':['Columbia','Baker','Nassau','Duval','Union','Bradford',
                             'Clay','Gilchrist','Alachua','Putnam','Levy','Marion'],
                 'Region 4':['Citrus','Sumter','Hernando','Pasco','Pinellas',
                             'Hillsborough','Polk','Manatee','Hardee','Sarasota'],
                 'Region 5':['DeSoto','Highlands','Charlotte','Glades','Lee','Hendry','Collier','Monroe'],
                 'Region 6':['Indian River','Okeechobee','St. Lucie','Martin',
                             'Palm Beach','Broward','Miami-Dade'],
                 'Region 7':['St. Johns','Flagler','Volusia','Lake','Orange',
                             'Seminole','Osceola','Brevard']}

regions['GA'] = {'Region 1':['Quitman','Randolph','Terrell','Lee','Worth','Clay','Calhoun',
                             'Dougherty','Tift','Early','Miller','Baker','Mitchell','Colquitt',
                             'Cook','Seminole','Decatur','Grady','Thomas','Brooks','Lowndes','Echols'],
                 'Region 2':['Turner','Irwin','Ben Hill','Telfair','Wheeler','Montgomery','Treutlen',
                             'Emanuel','Jenkins','Berrien','Coffee','Jeff Davis','Toombs','Candler',
                             'Lanier','Atkinson','Bacon','Appling','Tattnall','Evans','Bulloch','Screven','Burke'],
                 'Region 3':['Clinch','Ware','Pierce','Charlton','Brantley','Wayne','Long','Liberty',
                             'Bryan','Effingham','Camden','Glynn','McIntosh','Chatham'],
                 'Region 4':['Troup','Meriwether','Pike','Lamar','Harris','Talbot','Upson','Monroe',
                             'Muscogee','Chattahoochee','Marion','Taylor','Crawford','Bibb',
                             'Schley','Macon','Peach','Houston','Stewart','Webster',
```

```
                'Sumter','Dooly','Pulaski','Crisp','Wilcox'],
            'Region 5':['Jones','Baldwin','Hancock','Taliaferro','Wilkes','Lincoln',
                'Warren','McDuffie','Columbia','Twiggs','Wilkinson','Washington',
                'Glascock','Jefferson','Richmond','Bleckley','Dodge','Laurens','Johnson']}

regions['LA'] = {'Region 1':['Cameron Pari','Vermilion Pari','Calcasieu Pari','Jefferson Davis Pari',
                 'Acadia Pari','Lafayette Pari','Beauregard Pari','Allen Pari',
                 'Evangeline Pari','St. Landry Pari'],
            'Region 2':['Iberia Pari','St. Martin Pari','St. Mary Pari','Assumption Pari',
                'Terrebonne Pari','Lafourche Pari','St. Charles Pari','Jefferson Pari',
                'Orleans Pari','St. Bernard Pari','Plaquemines Pari'],
            'Region 3':['Iberville Pari','Ascension Pari','St. James Pari',
                'St. John the Baptist Pari','Washington Pari','Pointe Coupee Pari',
                'West Feliciana Pari','West Baton Rouge Pari','East Feliciana Pari',
                'East Baton Rouge Pari','St. Helena Pari','Livingston Pari',
                'Tangipahoa Pari','St. Tammany Pari'],
            'Region 4':['Sabine Pari','Natchitoches Pari','Winn Pari','Grant Pari',
                'La Salle Pari','Vernon Pari','Rapides Pari','Avoyelles Pari'],
            'Region 5':['Caddo Pari','De Soto Pari','Bossier Pari','Red River Pari',
                'Webster Pari','Claiborne Pari','Bienville Pari','Union Pari',
                'Lincoln Pari','Jackson Pari','Ouachita Pari'],
            'Region 6':['Morehouse Pari','West Carroll Pari','East Carroll Pari',
                'Richland Pari','Madison Pari','Caldwell Pari','Franklin Pari',
                'Tensas Pari','Catahoula Pari','Concordia Pari']}

regions['MS'] = {'Region 1':['Jefferson','Adams','Wilkinson','Franklin','Amite','Lincoln',
                 'Pike','Lawrence','Walthall','Jefferson Davis','Marion'],
            'Region 2':['Covington','Jones','Wayne','Lamar','Forrest','Perry','Greene',
                'Pearl River','Stone','George','Hancock','Harrison','Jackson'],
            'Region 3':['Issaquena','Sharkey','Yazoo','Madison','Warren',
                'Hinds','Rankin','Claiborne','Copiah','Simpson'],
            'Region 4':['Leake','Neshoba','Kemper','Scott','Newton',
                'Lauderdale','Smith','Jasper','Clarke']}

regions['NC'] = {'Region 1':['Union','Stanly','Anson','Montgomery','Richmond','Moore',
                'Chatham','Lee','Harnett','Wake','Johnston','Franklin',
                'Nash','Wilson','Edgecombe'],
             'Region 2':['Scotland','Hoke','Cumberland','Sampson','Wayne','Greene',
                'Robeson','Bladen','Duplin','Lenoir','Columbus',
                'Brunswick','New Hanover','Pender','Onslow','Jones'],
             'Region 3':['Pitt','Craven','Beaufort','Pamlico','Carteret','Hyde',
                'Martin','Washington','Tyrrell','Dare','Bertie','Hertford',
                'Gates','Chowan','Perquimans','Pasquotank','Camden','Currituck']}
```

```
regions['SC'] = {'Region 1':['Barnwell','Orangeburg','Calhoun','Allendale','Bamberg',
                    'Hampton','Jasper','Beaufort','Colleton','Dorchester',
                    'Berkeley','Charleston'],
            'Region 2':['Sumter','Lee','Darlington','Marlboro','Clarendon','Florence',
                   'Dillon','Williamsburg','Marion','Georgetown','Horry'],
            'Region 3':['McCormick','Edgefield','Saluda','Newberry','Fairfield','Lancaster',
                    'Aiken','Lexington','Richland','Kershaw','Chesterfield']}

regions['TX'] = {'Region 1':['Shelby','Nacogdoches','San Augustine','Trinity',
                     'Angelina','Sabine','Polk','Tyler','Jasper','Newton'],
            'Region 2':['Lee','Burleson','Brazos','Madison','Grimes','Walker',
                    'San Jacinto','Montgomery','Washington','Austin','Waller'],
            'Region 3':['Orange','Jefferson','Hardin','Liberty','Chambers',
                    'Harris','Galveston','Fort Bend','Brazoria'],
            'Region 4':['Guadalupe','Caldwell','Bastrop','Wilson','Gonzales',
                    'Fayette','Karnes','DeWitt','Lavaca','Colorado'],
            'Region 5':['Bee','Goliad','Victoria','Jackson','Wharton','San Patricio',
                    'Refugio','Aransas','Calhoun','Matagorda'],
            'Region 6':['Llano','Burnet','Williamson','Gillespie','Blanco','Kerr',
                    'Bandera','Kendall','Comal','Hays','Travis'],
            'Region 7':['Kinney','Uvalde','Medina','Bexar','Maverick',
                    'Zavala','Frio','Atascosa','Dimmit'],
            'Region 8':['La Salle','McMullen','Live Oak','Webb','Duval','Zapata','Jim Hogg'],
            'Region 9':['Jim Wells','Nueces','Kleberg','Brooks','Kenedy',
                    'Willacy','Starr','Hidalgo','Cameron'],
            'Region A':['Wood', 'Upshur', 'Marion', 'Harrison', 'Smith',
                    'Gregg','Cherokee', 'Rusk', 'Panola'],
            'Region B':['Falls', 'Limestone', 'Freestone', 'Anderson',
                    'Milam', 'Robertson', 'Leon', 'Houston'],
            'Region C':['San Saba', 'Mills', 'Hamilton', 'Bosque', 'Hill',
                    'Lampasas', 'Coryell', 'McLennan', 'Bell'],
            'Region D':['Lamar', 'Red River', 'Bowie', 'Delta', 'Hopkins',
                    'Franklin', 'Titus', 'Camp', 'Morris', 'Cass'],
            'Region E':['Fannin', 'Collin', 'Hunt', 'Rockwall', 'Rains',
                    'Dallas', 'Kaufman', 'Van Zandt', 'Ellis', 'Navarro', 'Henderson'],
            'Region F':['Montague', 'Cooke', 'Grayson', 'Wise', 'Denton',
                    'Parker', 'Tarrant', 'Hood', 'Somervell', 'Johnson']}
```